CARDIFF UNIVERSITY
PRIFYSGOL CAERDYDD

ORCA – Online Research @ Cardiff

This is an Open Access document downloaded from ORCA, Cardiff University's institutional repository:https://orca.cardiff.ac.uk/id/eprint/96285/

This is the author's version of a work that was submitted to / accepted for publication.

Citation for final published version:

Morgan, A. M., Howard, A. D., Hobley, Daniel , Moore, J. M., Dietrich, W. E., Williams, R. M. E., Burr, D. M., Grant, J. A., Wilson, S. A. and Matsubara, Y. 2014. Sedimentology and climatic environment of alluvial fans in the Martian Saheki Crater and a comparison with terrestrial fans in the Atacama Desert. Icarus 229 , pp. 131-156. 10.1016/j.icarus.2013.11.007

Publishers page: http://dx.doi.org/10.1016/j.icarus.2013.11.007

Please note:
Changes made as a result of publishing processes such as copy-editing, formatting and page numbers may not be reflected in this version. For the definitive version of this publication, please refer to the published source. You are advised to consult the publisher's version if you wish to cite this paper.

This version is being made available in accordance with publisher policies. See http://orca.cf.ac.uk/policies.html for usage policies. Copyright and moral rights for publications made available in ORCA are retained by the copyright holders.

Sedimentology and Climatic Environment of Alluvial Fans in the Martian Saheki Crater and a Comparison with Terrestrial Fans in the Atacama Desert

A. M. Morgan[a,*], A. D. Howard[a], D. E. J. Hobley[a,g], J. M. Moore[b], W. E. Dietrich[c], R. M. E. Williams[d], D. M. Burr[e], J. A. Grant[f], S. A. Wilson[f], and Y. Matsubara[a]

[a]Department of Environmental Sciences, P.O. Box 400123, University of Virginia, 22904-4123, United States

[b]NASA Ames Research Center, M.S. 245-3, Moffett Field, CA 94035-1000, United States

[c]Department of Earth and Planetary Science, University of California, Berkeley, CA 94720-4767, United States

[d]Planetary Science Institute, 1700 E. Fort Lowell, Suite 106, Tucson, AZ 85719, United States

[e]Earth and Planetary Sciences Department, University of Tennessee-Knoxville, 1412 Circle Drive, Knoxville, TN 37996-1410, United States

[f]Center for Earth and Planetary Studies, National Air and Space Museum, Smithsonian Institution, MRC 315, 6th Street at Independence Avenue, SW, Washington, District of Columbia 20013, United States

[g]now at Department of Geological Sciences, University of Colorado Boulder, UCB 399, 2200 Colorado Ave., Boulder, CO 80309-0399, United States

[*]Corresponding Author: E-mail: amm5sy@virginia.edu, 650-766-4169

Highlights

- **Wind erosion reveals Saheki crater fan stratigraphy**
- **A distributary network of fluvial channels fed extensive mudflow overbank deposits**
- **The fans are up to 850 m thick and contain 550 km^3 of sediment**
- **Fan-forming discharges derived from annual or episodic melting of crater rim snow**
- **Thousands of years were required to deposit the fans**

Abstract. The deflated surfaces of the alluvial fans in Saheki crater reveal the most detailed record of fan stratigraphy and evolution found, to date, on Mars. During deposition of at least the uppermost 100 m of fan deposits, discharges from the source basin consisted of channelized flows transporting sediment (which we infer to be primarily sand- and gravel-sized) as bedload coupled with extensive overbank mud-rich flows depositing planar beds of sand-sized or finer sediment. Flow events are inferred to have been of modest magnitude (probably less than ~60 m^3/s), of short duration, and probably occupied only a few distributaries during any individual flow event. Occasional channel avulsions resulted in the distribution of sediment across the entire fan. A comparison with fine-grained alluvial fans in Chile's Atacama Desert provides insights into the processes responsible for constructing the Saheki crater fans: sediment is deposited by channelized flows (transporting sand through boulder-sized material) and overbank mudflows (sand size and finer) and wind erosion leaves channels expressed in inverted topographic relief. The most likely source of water was snowmelt released after annual or epochal accumulation of snow in the headwater source basin on the interior crater rim during the Hesperian to Amazonian periods. We infer the Saheki fans to have been constructed by many hundreds of separate flow events, and accumulation of the necessary snow and release of meltwater may have required favorable orbital configurations or transient global warming.

1. Introduction

An alluvial fan is a semi-conical landform that develops where a channel exits a confined valley, and through avulsions and channel branching spreads sediment across the unconfined terrain (Blair and McPherson, 2009). The combination of slope reduction and lateral spreading reduces the carrying capacity and forces progressive sediment deposition. Martian alluvial fans have been identified ranging in scale from sub-kilometer (Williams and Malin, 2008) to a few kilometers (Burr et al., 2009) to tens of kilometers (Moore and Howard, 2005; Kraal et al., 2008; Anderson and Bell, 2010; Grant and Wilson, 2011, 2012). The well-preserved, mid-latitude fans of the Hesperian (and perhaps even younger) (Grant and Wilson, 2011; Kraal et al., 2008; Moore and Howard, 2005, Morgan et al., 2012a,b) are of particular interest because they, along with deltas (e.g., Malin and Edgett, 2003; Moore et al., 2003; Lewis and Aharonson, 2006; Pondrelli et al., 2008,2011; Mangold et al, 2012b; Wilson et al., 2013) and small valleys in the mid-latitude regions (e.g., Hynek et al., 2010; Fassett et al., 2010; Howard and Moore, 2011; Mangold, 2012), may represent a widespread episode of large-scale fluvial landform construction and modification on Mars occurring well after the Late-Noachian to Early Hesperian epoch of valley network incision (Grant and Wilson, 2011; Howard and Moore, 2011). This later period of fluvial activity occurred in an environment thought to be characterized by a relatively thin atmosphere and global cryosphere (Carr and Head, 2010; Fassett and Head, 2011; Lasue et al, 2013). Although difficult to decipher, the effects of water (both fluid and ice) on a paleo-landscape are the most unambiguous markers of past climatic environment and have significant potential to further our understanding of the climate evolution and potential late-stage habitability of Mars.

Almost all mapped martian alluvial fan systems have been found to be enclosed within basins (craters) and source from deeply incised crater rim alcove basins (Moore and Howard, 2005; Kraal et al., 2008; Wilson et al., 2013)., which strongly constrains both the hydrological and sedimentary environments. The association between the sediment and water source areas in the dissected crater wall and the fan system is short and direct. The presence of a large alluvial fan in an enclosed basin limits the possible range of the hydrologic regime; on the low end it is constrained by the necessity to erode and transport sediment from the headwater source and on the high end by the apparent absence of coincident deep lakes within the crater. Previous work on the larger equatorial fans has concluded that they formed during periods of enhanced precipitation (probably as snowfall) primarily through hundreds of flow events over tens of thousands (to perhaps millions) of years (Armitage et al., 2011; Grant and Wilson, 2011, 2012; Moore and Howard, 2005).

This study focuses on Saheki crater (85 km-diameter, 21.7°S, 73.2°E), one of several fan-bearing craters along the northern rim of the Hellas basin (Figs. 1 and 2). Fans in this crater are among the largest catalogued by Kraal et al. (2008) and Moore and Howard (2005) and contain the clearest exposed stratigraphy yet identified on Mars (Table 1). The studies of alluvial fans in southern Margaritifer Terra (Grant and Wilson, 2011, 2012) revealed that the fans and fan-deltas of this region date to the Late Hesperian to Early Amazonian rather than being coeval with the extensive valley networks of Late Noachian to Early Hesperian, which had been suggested by Howard et al. (2005). The exquisite alluvial fan stratigraphy exposed in craters of the Hellas north rim (Fig. 1), and Saheki crater in particular (Fig. 2), permits a comprehensive assessment of several unresolved issues concerning martian alluvial fans, including the mode of sedimentation (e.g., fluvial versus debris flows), the magnitude, frequency and duration of

formative flows, the age of the alluvial fans and the associated climatic environment. We address these issues through a detailed stratigraphic analysis, crater count-derived ages, quantitative interpretation of the flows (velocity and discharge) forming the fans, and a comparison with a terrestrial analog fan system in the Chilean Atacama Desert. This is followed by our synthesis of the fan sedimentology, geologic history of fan deposition, and the associated hydrologic and climatologic environment. We conclude that the Saheki crater fans were deposited by a combination of channelized fluvial and muddy overbank flows by many separate flow events numbering in the hundreds to thousands over an extended time period around the Hesperian-Amazonian boundary. Snowmelt sourced from upper crater walls is found to be the most tenable water source.

2. Observations and Interpretations

2.1 Geologic Setting and Data Used

Six fan-bearing craters, labeled "G", "K" (since named Saheki by the IAU), "L", "M" (since named Harris by the IAU), "P", and "X" (Fig. 1) have been identified in the far western Terra Tyrhenna (Moore and Howard, 2005; Kraal et al., 2008; Williams et al., 2011). As part of a new global inventory of alluvial fans (Wilson et al., 2013), several additional fan-hosting craters have been identified in the north Hellas rim region ("@" symbols in Fig. 1). Our morphologic and stratigraphic study primarily focuses on the fans within Saheki.

Saheki crater is superimposed onto a larger ~100 km crater to the east and an elongated elliptical basin measuring 90 km by 45 km to the northwest. It contains two prominent fans (K1 and K2 in Fig. 2) sourcing from its western rim and one much smaller fan sourcing from the southeastern rim. The Saheki fans are of shallow gradient (~0.03) and large size (greater than

750 km^2) (Table 1), comparable to dimensions of other alluvial fans in the region. Localized fluvial dissection occurs on the craters' ejecta as well as within the main cavity and is of an uncertain age relationship to the fans. The southern rim of Saheki features large slumps presumably formed by failure of the steep transient crater wall shortly after the crater itself was formed. These slumps have been modified by mass wasting and fluvial erosion and based on their superposition must pre-date the fan deposits discussed (Fig. 3). All of the large fans in this region are sourced from steep-walled, sharply defined alcoves carved into the crater rim that act as the sole sediment source region and drainage basin supplying the fan.

The Saheki fans have been completely imaged by the Mars Reconnaissance Orbiter's (MRO) CTX camera (Context Camera, resolution ~6 meters/pixel (Malin et al., 2007)) and have varying degrees of HiRISE coverage (High Resolution Imaging Science Experiment, resolution ~30 cm/pixel (McEwen et al., 2007)). We have produced digital elevation models (DEMs) from select HiRISE and CTX stereo pairs with the Ames Stereo Pipeline software package (Morato et al., 2010). MOLA topographic data (Zuber et al., 1992) was used for areas not covered by our DEMs. Spectral data from the Thermal Emission Imaging System (THEMIS) and the Compact Reconnaissance Imaging Spectrometer for Mars (CRISM) datasets (Murchie et al., 2007) were not useful in this investigation; two CRISM images covering the fans indicated the presence of hydrated minerals but did not resolve any spatial pattern that could be correlated with visible features.

2.2. Fan Morphology and Stratigraphy

The fans in Saheki, particularly the more southern of the two principal fans (K2, Fig. 3) exhibit surface texture and erosion-accentuated bedding at hectometer scale (Moore and Howard,

2005) that is far more pronounced than observed on other martian fans. Both the K1 and K2 fans (Fig. 2) form typical conical morphology and are sourced from deeply dissected source basins on the northwestern and western crater rim. The K1 and K2 fans merge concordantly at their lateral boundaries, but no clear superposition relationship was identified and they likely formed simultaneously, resulting in interfingered deposits. The two fans are of similar size, surface gradient and source basin characteristics (Table 1). The surface of the upper parts of the K1 fan is relatively featureless at the decameter scale except for superimposed impact craters and a 650 m wide valley extending about 10 km into the fan from the apex. Several indistinct shallow valleys radiate from this incised valley. The eastern, distal 10 km of the K1 fan has been wind-dissected into linear ridges similar to those on the K2 fan (discussed below). In contrast, the upper portion of the K1 fan appears to be relatively unaffected by wind erosion, but meter to decameter features of the original fan surface have been obscured by post-fan impact gardening and modest aeolian deposition, largely occurring as scattered transverse aeolian ripples (TARs) (Wilson and Zimbelman, 2004; Balme et al., 2008; Berman et al., 2011). As a result, fluvial morphology and stratigraphy is poorly exposed, so this study emphasizes the better exposures on the K2 fan.

The K2 fan surface features prominent ridges radiating from the fan apex (Fig. 3). These ridges have the greatest relief and continuity on the southern and eastern distal portions of the fan. Clear exposures of layered deposits on the sides of the inverted ridges indicate that winds keep exposures free of dust and that wind is the likely erosional agent inverting the ridges (Fig. 4). TARs with a dominant E-W orientation mantle much of the depressed inter-ridge surfaces, although whether winds were northerly or southerly is uncertain. Layer exposures on the south side of the dominantly E-W trending ridges are generally clearer than on the north side,

161 suggesting that the strongest winds are southerly. Consistent with this interpretation, composite
162 IRB HiRISE images (composites with the near-IR, red, and blue–green images displayed in red,
163 green, and blue channels, respectively) indicate a distinct bluish cast on the north side of some
164 ridges indicative of a different composition, which, when coupled with obscuration of layers,
165 suggests aeolian accumulation on the sheltered side (Fig. 4). The TARs suggest a high
166 availability of sand-to-granule size sediment (our terminology for grain size is summarized in
167 Table 2) to aid aeolian scour, and because the TARs are concentrated on the fan surfaces rather
168 than on the exposed crater floor, the fan deposits are a likely sediment source.

169 Thicknesses of the Saheki fans were estimated by comparing topographic profiles of the
170 nearly flat eastern half of the crater floor to profiles through the fans (Fig. 5), so that the fans are
171 likely 800-850 m thick near the apices and approximately 300 m thick where they impinge upon
172 the central peak. The volume of the fan deposits was estimated in two ways. The first method
173 gives an order of magnitude estimate by multiplying an assumed average fan thickness (400 m)
174 by the combined surface area of K1 and K2 fans (1563 km^2) giving 525 km^3. Another estimate is
175 based on circular projection of the profiles A through E in Fig. 5 to produce the estimated basal
176 fan topography and calculating the volumetric difference with the modern DEM, giving 586 km^3.
177 This second value is likely a slight underestimate because valley fill deposits above the fan apex
178 were not accounted for. Unfortunately, the MOLA DEM has insufficient resolution to estimate
179 the eroded volume of the source basin, and higher resolution stereo imaging was not available
180 there.

181 Three distinct geomorphic and associated sedimentary features are associated with the
182 Saheki fans, each of which is described below: 1) linear ridge and broad platform features and
183 associated deposits that locally broaden into nearly flat benches with rough-textured surfaces; 2)

fine-textured layered deposits largely exposed on side-slopes beneath ridges and platforms; and 3) level benches at distinct elevations bordering the fan deposits at their southern and eastern margin.

2.2.1. Linear and Platform Features

We broadly define this class of features as downslope-oriented ridges or depressions radiating from the fan apex and traceable over kilometer or longer distances (Figs 6-8). These features occur as four subtypes. The dominant morphology occurs as linear to modestly sinuous (<1.2), narrow (10s of meters in width) ridges that stand up to 70 m above the surrounding terrain. With distance downslope, ridges often become narrower, discontinuous, and higher relative to their surroundings, although the ridge tops define an accordant, sloping surface. A second, less common morphology consists of two parallel ridges that are separated by a few 10s of meters. A third morphology comprises linear depressions generally 100 m or more across. In a few cases, a systematic down-fan transition from a depression through parallel ridges to a single ridge is observed, although unequivocal examples are rare (Fig. 6). Individual linear features can locally be traced 15 km or more down-fan, but none of the features extends from the fan apex to the distal fan margin (Fig. 3). A fourth morphology occurs as broad, nearly level platforms that display a ridge and swale topography, generally with the long axis oriented downstream although sometimes displaying a curved pattern (Fig. 7). Ridges are typically spaced a few 10s of meters apart and platforms commonly connect to linear ridges upslope or downslope (Fig. 3). In the mid-section of the fan, these platforms mostly occur as isolated features, often widening downstream in small flared forms (Fig. 8) that are usually dissected at their downstream ends (black arrows in Fig. 8). About 10 km from the distal end of the fan, the platforms become broader, more numerous, and interfinger at different stratigraphic levels (e.g., Figs. 7 and 9).

Comparing the actual elevations of the lower fan surface to a virtual conic surface projected from the upper fan suggests that as much as 120 m of sediment may have been wind-eroded from low regions between ridges (Fig. 9).

Onlap and superposition relations are visible locally all over the fan surface (Fig. 3, 7, 9). In almost every case, each linear ridge projects downstream to a higher elevation than ridges originating farther downstream. Although superposition relationships are evident locally, correlations across the entire fan surface are not possible. Essentially all of the linear ridges and depressions are oriented downslope, but ridges at different levels occasionally cross at acute angles. Definitive examples of ridge intersections at an accordant level are sparse. Where they occur, they generally exhibit downslope branching, although rare braiding patterns occur.

The top surface of the linear ridges typically has a scalloped appearance at decameter scales (Figs. 3 and 10). Blocks up to several meters in diameter are visible locally on the ridge surfaces, and in numerous locations the surface shows occasional ~1 m blocks interspersed with a characteristic mottling or speckling (Fig. 10 inset) that appears to be limited in occurrence to the ridge surfaces. Elsewhere, the ridge crests are relatively smooth at meter to sub-meter scales. To establish the distribution and setting of the blocks, we mapped occurrences by careful examination of three HiRISE images covering the K2 fan surface (Fig. 11). Concentrations of blocks occur almost exclusively on the tops of linear ridges or as exposures on the top few meters of side-slopes at the edge of the ridges. Block exposures are generally elongated along the direction of the ridge crests and often occur in close association with mottled/speckled surfaces. Both blocks and mottling become less frequent towards the distal end of the K2 fan, so that ridge crests are smooth at meter scale (although frequently scalloped at decameter scale).

2.2.2. Interpretation of Linear and Platform Features

230 The linear and platform features radiate from the apex, trend downslope, and generally
231 exhibit nearly uniform widths downstream. Consistent with channelized flow, we interpret these
232 features as fluvial distributaries constituting the sediment dispersal backbone of the alluvial fans
233 (Grant and Wilson, 2012; Moore and Howard, 2005; Williams et al.,2011) and the fact that most
234 of these linear features are exposed as ridges to indicate they have been inverted by differential
235 aeolian erosion. The channelized distributaries must have been embedded within finer and/or
236 more poorly cemented deposits that were preferentially stripped. The characteristics of these
237 easily-eroded deposits are discussed in Section 2.2.4.

238 Boulders on the Saheki fan surface might have originated through a variety of processes,
239 such as fluvial deposition, through cementation of a deposit and its subsequent weathering into
240 blocks, or as impact ejecta. We, however, interpret the visible blocks exposed on the ridges (Fig.
241 10) to be fluvially transported and deposited boulders ranging from 0.25 – 4 m in diameter.
242 Blocks are largely absent in the depressions between ridges, although the frequent mantling by
243 TARs could obscure some deposits. Exposures of coarse-grained material occur primarily from
244 the K2 fan apex to about 10 km from the distal margin of the fan (Fig. 11), and are positively
245 correlated with an apparent increase in total incision into the fan surface (Fig. 9). This
246 observation is consistent with a downstream fining of channel bed sediment, with boulders
247 giving way to finer gravel and sand as the distance from the fan apex increases, as sometimes
248 observed in terrestrial fluvial fans (Stock et al., 2008; Stock, 2013). On terrestrial fans dominated
249 by debris flows, systematic downstream changes in grain size would not be expected, reinforcing
250 our interpretation that these Saheki fans are not debris flow fans (Blair and McPherson, 2009).
251 The observation that fluvial conglomerates are present on an alluvial fan in Gale crater (Williams

et al, 2013) supports the interpretation that runoff on Martian alluvial fans was capable of transport of gravel.

On portions of the distributary deposits near the downstream end of areas with visible boulders, the ridge tops are commonly mottled or speckled at 30 cm/pixel HiRISE resolution (Fig. 10). Mottling in images could result from a variety of surface morphologies, including wind ripples and patterned ground, but the association of these mottled surfaces with visible coarser-grained material in nearby exposures suggests that they are gravels below the limit of HiRISE resolution (see section 3.5). Distributary ridges that do not display either visible boulders or a mottled surface are presumably deposits finer than a few tens of cm in diameter.

Distributary ridges are often discontinuous (Fig 7), implying that ridges can be eroded, either by direct removal by wind erosion and/or by lateral backwasting of hillslope scarps. The resistance of the fluvial distributaries to wind erosion that results in their topographic inversion could be due either to diagenetic cementation or to a component of the fluvial sediment being coarser than a few mm in diameter (the effective limit to wind transport (Greeley et al., 1976; Zimbelman et al., 2009; Gillies et al., 2012;). Sand and gravel in fluvial deposits, being permeable, often become cemented from percolating groundwater, whereas interbedded and largely impermeable fine deposits are not (Spötl and Wright, 1992). The decameter-scale fluting on the surface of many of the inverted channels suggests a loose component of the sediment that can be deflated; in such locations cementation is probably less important than the presence of a component of coarse sediment that can form a wind-resistant pavement. Similar wind fluting occurs on fine, apparently modestly cemented deposits in Terby crater (Ansan et al., 2011; Wilson et al., 2007) and on fine-grained deposits on Atacama Desert fans (discussed in section

3.2.1). The local presence of fluvially-deposited boulders (Fig. 10) suggests that mass wasting must dominate ridge backwasting at least locally because wind cannot strip such coarse debris.

The pattern shown in Figs. 3 and 6 in which distributaries emerge from beneath stratigraphically higher deposits, increase in relative height and height of inversion downslope, and terminate before reaching the distal fan edge indicate that the degree of aeolian stripping increases systematically towards the distal end of the K2 fan. Near the apex of the K2 fan, distributaries are in low relative relief and difficult to differentiate. This muted topography would be expected near a fan apex, where distributaries shift frequently (thereby covering a greater area with coarser material) and where deposition would likely be dominated by coarse-grained channel deposits.

Occasionally the K2 fan surface has eroded into two parallel ridges which typically transition down-fan into raised ridges of similar width (black arrows in Fig 6 and red arrows in Fig. 7) but which often become indistinct hollows when traced upstream (Fig. 6). We interpret these parallel ridges to be narrow natural levees that would be the first coarse-grained component of an overbank channel deposit to emerge during wind scour, with the finer distal overbank deposits being preferentially removed. Likewise, the interiors of such channels were presumably filled with finer, more readily-eroded sediment after abandonment.

The wider platform features mapped in Fig. 3 are interpreted as fluvial deposits created either by multiple, braided channels (Fig. 8) or by a single, slightly sinuous channel that migrates laterally, leaving scroll-bar ridges (Fig.7), as suggested by Moore and Howard (2005). Similar inverted features interpreted as scroll bars occur on the Eberswalde crater delta (Malin and Edgett, 2003; Moore et al., 2003) and sinuous channels in the Aeolis-Zephyria region (Burr et

al., 2009, 2010). It is likely that flow did not occupy the entire width of these broad expanses at any given time.

The isolated platform deposits in the mid-section of the K2 fan (Figs. 3 and 8) might form by two processes, one related to avulsion and the other to autogenic processes. The avulsion scenario would accompany distributary shifts into a new course. As fans aggrade, the inactive portions of the fan become relative depressions. When an avulsion penetrates into a depression, splay-like bedload deposition may occur until the depression becomes filled and material can be transported further down-fan. Subsequent fluvial erosion downstream from the relative depression can result in entrenchment of the splay deposits or abandonment due to an avulsion. The second scenario involves local flow expansion, transverse gravel bar deposition, infilling of the resultant upstream depression, and eventual breaching and trenching of the bar (Field, 2001; Stock, 2013).

The broad band of overlapping platform deposits about 5-10 km upstream from the distal end of the fan might have resulted from the effects of a rising temporary lake (playa) base level at the fan terminus which would encourage enhanced deposition and a spreading flow pattern. The high relief on the distal end of the fan suggests that wind erosion has stripped at least 70 m and perhaps up to 120 m of fan and basin-floor deposits, indicating a higher base level when the uppermost fan deposits were laid down (Fig. 9). As discussed in section 2.2.7, benches along the southern margin of the fan also suggest a higher base level was present during deposition of the youngest fan deposits. It is also possible that decreasing grain size downstream simply led to reduced formation of levees around the channels, resulting in more sheet-like and laterally unconstrained flow and deposition.

2.2.3. Distributary Widths

319 Information on distributary widths is important for analysis of flow discharges. The
320 aeolian erosion that inverts the distributaries serves to expose the channels, but may also narrow
321 them as a result of lateral backwasting of the channel edges by mass wasting triggered by aeolian
322 erosion of weaker surrounding layers. Burr et al. (2010) conclude that many inverted meandering
323 channels in the Aeolis Dorsa/Zephyria Plana region have been significantly narrowed because of
324 an observed meander wavelength to preserved ridge width that significantly exceeds the typical
325 terrestrial value of about 10-14 (Knighton, 1998, p. 215). In some environments, however,
326 wavelength/width ratios can reach 20-25, as along the low gradient, mud-bank Quinn River in
327 Nevada (Matsubara et al., 2012). If the interpretation of the meander pattern in Fig. 7 is correct,
328 the wavelength of about 750 m divided by an average distributary width of 40 m gives a meander
329 wavelength/width ratio of about 19. Although we suspect large observational variance and
330 perhaps some bias in resolving distributary width, a best estimate will serve to calculate
331 approximate formative discharges. Width measurements of 68 inverted channel segments on the
332 K2 fan where ridge tops are flat with well-defined margins with consistent widths over
333 reasonable (> 500 m) distances (Fig. 7) yielded no systematic spatial trend with position on the
334 fan. The distribution of these widths has a sharp, well-defined peak at 38 m (Fig. 12), though
335 with a significant positive skew of apparently wider channels. This tail may be in part due to
336 misidentification of wider platforms as single-thread instead of braided channels or to lateral
337 migration of meandering channels. In the few cases where ridges measured for width can be
338 traced upstream to parallel ridges (presumed to be levees), the ridge spacing is approximately
339 equal (within several meters) to the ridge width. Limited HiRISE coverage over other fans in the
340 vicinity of Saheki (Fig. 1) and the lack of additional well-preserved flat-topped ridges in other

fan systems prevents a thorough assessment of channel widths elsewhere, though channel widths appear to be qualitatively similar (Burr et al., 2010; Grant and Wilson, 2012).

2.2.4. Fine-Textured, Layered Fan Deposits

The topographic inversion of the distributary fluvial deposits and the presence of broad depressions between individual distributaries imply that wind erosion has excavated extensive deposits of erodible sediment interbedded with the channel deposits. In most locations, exposures of these deposits are largely obscured by the TAR bedforms mantling inter-ridge depressions. However, at the distal end of the K2 fan, the extensive wind erosion has inverted the fluvial ridges into as much as 70 m of relative relief. Exposures of layered deposits are common on the sideslopes below the ridges (Figs. 4, 10, 13). These sideslopes are generally smoother at multi-meter scales than the scalloped ridge crests and typically the slopes exposing the layers incline close to the angle of repose for loose sediment (~30°). Resolvable layers are typically 2-3 m thick, although image resolution may limit detection of finer-scale bedding. The beds are commonly massive in appearance and contain no blocks visible at HiRISE resolution (Fig. 13). Beds are often separated by thin light layers that appear to be slightly more resistant to wind erosion and are less continuous, possibly nodular or upward-scalloped (Figs. 13 and 14). Well-exposed individual layers can be traced for several hundred meters but with subtle pinching out occurring locally (Fig. 13b). Thick layered sequences of very similar beds are exposed on the interior walls of several craters that are superimposed onto the K1 and K2 fans. A ~300 m thick section of the distal fan exposed in a crater wall near Saheki's central peak indicates the finest resolvable layers are ~2 m thick, and many individual layers can be traced several kilometers

363 along the crater wall (Fig. 15). This exposure reveals no resolvable meter-scale blocks except at
364 the base of the section where probable central peak materials appear to be exposed.

365 The beds exposed on the slopes below the inverted ridges are largely conformable in their
366 dip to the gradient of the ridges (e.g., Fig. 13c). Individual beds cross-cut elevation contours
367 along the trend of the ridge seen in Fig. 13c, with an interpreted gradient of about 0.021 to the
368 southeast following the general dip of the fan using individual prominent beds crossing multiple
369 mapped contours. Similar measurements of bed dips at eight locations elsewhere on the portion
370 of the fan covered by the HiRISE DEM yielded dips ranging from 0.025 to 0.041; the mean for
371 the nine total measurements is 0.032, very close to the ~0.03 gradient of the entire K2 fan surface
372 as measured from MOLA tracks.

373 **2.2.5 Interpretation of Fine-Textured Deposits**

374 The ease by which wind can erode the layered deposits and the near absence of exposed
375 blocks (save for the thin interbeds) suggests that these deposits are sand size or smaller in
376 dominant grain size. If the deposits were loose sand, however, wind erosion would probably
377 readily sculpt the deposits into dunes. Also if sand were the principal component of the layers,
378 appreciable accumulation of sand dunes might be expected within the Saheki crater, but are not
379 found. The observed TARs comprise a small volume of material compared to the total wind-
380 eroded volume. This proportionality suggests an appreciable component of silt and possibly clay
381 within the layered deposits that can be removed in suspension.

382 The observation that the fine-textured layers dip concordantly with the superjacent ridges
383 eliminates the possibility that they are exposures of layering pre-dating the fluvial fan ridges,
384 e.g., lacustrine deposits. Rather, the finer-textured deposits must be a distinct facies generally
385 coeval to the channel deposits. We interpret the layered sediment to be deposited by overbank

386 flows sourced from flows within distributary channels that are sufficiently deep to spread across
387 the adjacent fan surface, analogous to overbank deposits on floodplains. Such deposits are likely
388 to be continuous over long distances downstream and to border the source distributaries, but thin
389 laterally. The subtle pinch-outs of layers shown in Fig. 13b may reflect the limited lateral extent
390 of deposition from an individual distributary channel. The apparent thickness of 2-3 m for
391 individual layers could indicate deep, long-duration flows through individual distributaries with
392 large concentrations of suspended sediment. Because of limited image resolution, however,
393 individual visible beds may be composed of many thin layers from multiple smaller flow events.
394 Because exposed layers are stratigraphically lower than the superjacent channel deposit capping
395 the ridges (e.g., Figs 4, 10, 13), we infer they are would have been sourced from a different
396 channel at the same stratigraphic level as the exposed layer rather than being related to the
397 superjacent ridge.

398 The thin, light-toned, and possibly nodular layers that separate the smoother, darker, and
399 thicker (~2-3m) units in layered exposures (Figs. 13 and 14) may result from processes occurring
400 on the fan surface in the time intervals between overbank flooding events, or possibly are some
401 form of graded bedding. However, their thinness compared to the more massive units, the
402 sharpness of their expression and lack of gradual transitions to the overlying or underlying
403 massive beds argues against graded bedding. If, as we postulate, the character of the beds
404 represents post-depositional modification, this alteration likely occurred during times when
405 depositional activity has shifted to other parts of the fan, or during periods of fan inactivity
406 associated with quasi-cyclical climatic variations orbital variations (Laskar et al., 2004; Ward,
407 1979). Such processes could include wind erosion and surface concentration of granule layers,
408 surface cementation, wetting and drying events, or cold-climate processes. The concave

scalloping of some of the light-toned layers has an apparent spatial scale of 2-5 m (Fig. 14), and might be the result of desiccation-crack development, which occurs at spatial scales ranging from centimeters to tens of meters (El Maarry et al., 2012; Harris, 2004; Neal et al., 1968; Weinberger, 1999), teepee structures from chemical precipitates (Dixon, 2009; Shaw and Thomas, 1989), or patterned ground from thermal cycling or ice-related processes (Chan et al., 2008; Korteniemi and Kreslavsky, 2012; Levy et al., 2009; Mangold et al., 2004; Mellon, 1997). There are no obvious vertical structures in the sediment beneath the scalloped layer edges, however, so that direct evidence for any of these mechanisms is lacking.

The clearest exposures of layered deposits occur on 25-35° side slopes of flanking ridges capped by fluvial deposits. No interbedded boulders are visible at HiRISE scale. The exposure of layering indicates the slopes are not deeply mantled with debris. Gradients close to the angle of repose of loose sediment (~32-35°) and the smoothness of the side slopes, however, suggest that the exposures may be shallowly, and possibly discontinuously, mantled by debris mass-wasted from the ridge-capping fluvial deposits plus sediment derived from the beds themselves. Such threshold slopes are common on terrestrial badlands (e.g., Howard, 2009). Despite the shallow mantling, indurated beds are often exposed in outcrop, helping to define the stratigraphic relationships. The thin, light-toned layers visible in Figs. 10, 13, and 14 are probably such examples. In some situations the apparent mantling obscures expression of the layering (e.g., the northerly slope of the hill near (a) in Fig. 13), but it is likely that at least discontinuous mantling occurs on the southwest-facing slope in Figs. 10 and 13 to account for the uniformity of the slope. The sediment may be friable and thus easily eroded, although some weathering of the layered deposits, forming a thin regolith similar to that observed in terrestrial badlands, might be necessary prior to their erosion by wind.

2.2.6. Benches

A vertically-stacked series of nearly horizontal benches border the southern margin of the K2 fan against the Saheki crater interior wall (Figs. 3 and 16). HiRISE stereo imaging of part of this bench complex (Fig. 9) demonstrates that the individual bench surfaces are essentially flat-lying with a slope of less than 0.5%. At meter to decameter scales, the surfaces of the benches are quite rough, with numerous quasi-circular depressions (Fig. 17). The surface is littered with numerous angular, meter-scale blocks and the outer edges of the benches form abrupt scarps with irregular outlines. Angular blocks that apparently mass-wasted from the bench surface often discontinuously mantle the steep sideslopes of the benches. Where not mantled by debris, the subjacent slopes are smooth and express subtle layering that appears to be conformable with the overlying terraces (Fig. 17). This layering is very similar to the fine-textured layers exposed on the sides of inverted fan distributary ridges upslope (Fig. 13). The highest bench within the HiRISE DEM is about 85 m above the similarly-textured basin floor surface, although a slightly higher bench lies just to the south of the DEM. Along the southern margin of the K2 fan some linear ridges interpreted as distributary channels appear to overlie or to merge accordantly with the rough-textured benches, and in such locations the ridges take on the rough texture of the benches. Fine-textured layered deposits also locally superpose the benches. Similar surfaces appear elsewhere, including the lowest point of the eastern half of the nearby “L” crater where a rough, flat-lying surface occurs at the terminus of four large fans (Fig. 18). Part of the Saheki crater floor immediately adjacent to the fan deposits also has a similar flat surface at 100+ meter scale that is rough at decameter scale, although it has not been eroded laterally to form a bench

(Fig. 3). Similarly rough-textured surfaces also occur in small depressions along channels dissecting the southwestward flank of Saheki crater.

2.2.7. Interpretation of Benches

We interpret the benches to be underlain by playa and/or possibly shallow lacustrine sediments sourced by runoff from the adjacent fans. Their level surface implies they are probably composed of fine sediment deposited from suspension. Alluvial fans in enclosed basins typically terminate in nearly level playas that receive fine suspended sediment that is carried beyond the end of the fan (Shaw and Thomas, 1989). Although the higher benches in Saheki crater are spatially limited to bordering the southern crater rim (Fig. 3), and are thus largely isolated from the fan system, the similar-appearing bench in "L" crater clearly occupies a basin-central position where playa or lacustrine sedimentation would be expected (Fig. 18).

The bench surfaces appear to be thin, nearly horizontal resistant layers that have been laterally eroded, shedding boulders onto subjacent slopes. The numerous rounded depressions (Figs. 17 and 18) suggest that the roughness of the surface is due to impact gardening forming a blocky regolith. The resistant layers are underlain by apparently conformable layers that are more easily eroded by wind. We interpret the benches and other rough-textured level surfaces in the region to be chemically-cemented layers that have been subsequently broken up. They occur at topographic lows, or, where the benches occur at higher levels, what might have been low points prior to aeolian stripping.

Being the endpoint for both suspended and dissolved loads, playa sediments are commonly rich in salts concentrated from evaporation of ephemeral shallow lakes or delivered by groundwater (Dixon, 2009; Langer and Kerr, 1966; Shaw and Thomas, 1989; Yechieli and Wood, 2002). Solute-cemented playa deposits are common in the southwestern United States and

in the salars of the Atacama Desert. In the Atacama and similar desert settings elsewhere, the segregation of mineral precipitates within the sediments often results in volumetric expansion and small-scale deformation of the surface sediments, resulting in chaotic surface topography at meter to decameter scales (e.g., the "Devil's Golf Course" in Death Valley National Park (Hunt et al., 1966; Smoot and Castens-Seidel, 1995) and similar forms in Atacama salars (Stoertz and Ericksen, 1974). The roughness of the Saheki bench surfaces may thus be a combination of chemical cementation, small-scale deformation associated with playa sedimentation, and disturbance by impact gardening.

In terrestrial enclosed basins, the fan and playa deposits interfinger during basin infilling (e.g., Shaw and Thomas, 1989). The stratigraphy of terminal deposits in enclosed basin centers often alternates between playa and lacustrine sediments, with varying degrees of interbedded and co-deposited chemical precipitates (Pueyo et al., 2001; Smith, 1957, 1974). This complex stratigraphy reflects climatic changes and the simplest explanation to account for the multiple planar benches in Saheki crater would be that the successively higher playa surfaces formed sequentially as the center of the basin became infilled. Episodes of playa cementation alternated with periods of sediment input without appreciable chemical co-deposition (creating the less-indurated layers revealed below the erosional edges of the terraces, Fig. 17). Subsequent aeolian deflation would have had to remove at least 100 m of basin fill sediments in the vicinity of the benches based upon their relief relative to the present basin floor (Fig. 9). By this interpretation the highest benches have experienced greater erosion and backwasting than lower benches as a result of undermining by erosion of the non-indurated finer interbeds, and the lower, younger indurated playa deposits would have extended beneath the remnant higher benches. Note that this implies an age sequence with the highest bench being youngest, inverse to the usual sequence of

fluvial terraces increasing vertically in age. The "L" crater basin floor (Fig.18) would presumably resemble the basin floor at the south end of Saheki crater prior to the period of intense aeolian deflation. More complicated scenarios are also possible involving declining or varying basin floor levels in which fan and playa deposition alternate with episodes of aeolian erosion or in which the bench-forming deposits did not extend across the basin floor.

2.3 Source Basins

The large alluvial fans in the southern highlands on Mars are generally sourced from steep dendritic valley networks incised into the interior crater walls of large, deep, relatively fresh martian craters (Mangold et al., 2012b; Moore and Howard, 2005). This is clearly the case for fans in Saheki and "L" craters (Fig. 2). Within individual craters, the largest drainage networks and largest associated fans are generally sourced from the highest portions of the hosting crater rim. The only exception to this pattern is that the K1 source basin occurs along a low rim section contiguous with a degraded elliptical basin beyond the NW rim of Saheki. Source basin and corresponding fan and gradients areas for the K1 and K2 fans are summarized in Table 1, with comparative average statistics for all of the fans surveyed by Moore and Howard (2005).

We find no evidence for valleys incised into the Saheki fans from runoff sourced on the fan itself. The deep aeolian erosion on the K2 fan could have erased evidence for such local runoff, but the relatively pristine K1 fan surface shows all distributaries radiating from the fan apex. Likewise, other large martian fans appear to have received little runoff directly on the fan surface because the surfaces exhibit no channelized erosion initiating from mid-fan sources– the basin headwaters (fan-hosting crater walls) were overwhelmingly the source of runoff (Grant and Wilson, 2012; Moore and Howard, 2005).

523 **2.4 Age Relationships**

524 Crater density counts are a standard method of determining the relative ages of planetary
525 surfaces. Absolute model ages can then be estimated by comparing these counts to the lunar
526 surface, which has been radiometrically dated. The fan-bearing craters in the region lie on terrain
527 that has been mapped as Noachian (Greeley and Guest, 1987; Irwin et al., 2013). Using a CTX
528 basemap within ArcGIS, our crater count analysis incorporated craters with a diameter of larger
529 than 200 meters to avoid complications arising from the preferential erosion of smaller craters
530 and the increasing influence of secondaries with decreasing diameter (McEwen et al., 2005;
531 McEwen and Bierhaus, 2006). Central peaks, obvious secondary craters, and the interior rims of
532 the host crater were excluded from the analysis. Crater statistics were compiled using CraterStats
533 software (Michael and Neukum, 2010), using the production function of Ivanov (2001) and the
534 chronology function of Hartmann and Neukum (2001). When using craters to derive ages, the
535 surface area over the feature of interest must be large enough to obtain a sufficient sample of
536 craters, and there are inherent accuracy issues with deriving ages when using craters smaller than
537 D<1km (McEwen et al., 2005), although recent studies largely confirm the use of smaller craters
538 (Hartmann, 2007; Hartmann et al., 2008; Hartmann and Werner, 2010; Michael and Neukum,
539 2010; Werner et al., 2009).

540 These limitations considered, the fan surfaces in Saheki and "L" crater date to the Mid to
541 Late Hesperian, and in the case of fan K2, as late as the Early Amazonian (as defined by Tanaka
542 (1986) and Werner and Tanaka (2011)) (Fig. 19). In fitting ages to the cumulative frequency
543 curves in Fig. 19, we utilized craters greater than 500 m in diameter to minimize effects of crater
544 degradation and we did not include the three large (>1.4 km diameter) craters with large error
545 bars. These ages are indistinguishable from those obtained for fans in Margaritifer Terra (Grant

546 and Wilson, 2011). The K2 fan surface has a crater retention age (Early Amazonian) that is
547 notably younger than that of K1, which is probably due to the different degrees of aeolian
548 erosion. Ridges on the K2 fan rise as much as 70 m above the surrounding fan surface. If we
549 assume a crater depth/diameter ratio of 1:5 (Garvin et al., 2003), we conservatively infer that
550 craters smaller than 350 m in diameter would be completely erased from the surface record. If
551 the estimate of ~100 m of stripping from Fig. 9 is accurate, this erosion could eradicate craters
552 up to diameters of ~0.5 km; deposition of dust would cause further infilling and obliteration of
553 potentially even larger craters. In a number of places, stratigraphically higher surfaces that have
554 not been eroded preserve significantly higher densities of craters than the underlying eroded fan
555 surfaces (e.g., Fig. 18), confirming qualitatively that this effect is important, and that the
556 apparent age difference is due to subsequent amount of erosion of the fan. We have detected no
557 craters embedded in layer exposures, so that wind-exhumed craters probably contribute little to
558 inferred ages.
559

560 **3. Discussion**

561 The Saheki K2 fan has a strongly bimodal character, comprising a radiating network of
562 long distributaries and broader platforms capped by coarse (sand and cobble) fluvial bedload
563 (possibly indurated) interspersed with finer, wind-erodible layered sediment. The strong
564 component of fine sediment deposition in the Saheki fan complex contrasts with the types of
565 terrestrial alluvial fans most discussed in the literature, which emphasizes steep fans in high-
566 relief terrain. On these fans, sedimentation most frequently occurs either as coarse-grained
567 bedload deposited by wide, often braided or sheetflood distributaries or as equally coarse debris
568 flows (e.g., Blair and McPherson, 2009; Harvey, 1999; Stock, 2013). In such settings, the

associated fine sediment is primarily deposited either in a debris flow matrix or in basin-center playas. In neither case would wind erosion be capable of creating the characteristic inverted distributary system seen in Saheki and several other craters.

The intense aeolian deflation that has affected the K2 fan at the southern end of Saheki crater must have resulted in removal of a vast volume of sediment. We conservatively estimate this volume to be about 10 km^3, assuming 25 m of deflation over the distal 400 km^2 of the K2 fans surface. A small fraction of this sediment remains trapped in the numerous TARs covering the fan surface. Because there are no major dune fields within Saheki crater, we infer that the majority of the eroded sediment must be composed of grains fine enough (sand size or smaller) to have been swept by winds out of the crater. This inference underscores our interpretation that the majority of the layered sediment in the Saheki fans is composed of fine sediment deposited from overbank sedimentation and in playa deposits. Some of this sediment appears to have been redeposited in the source basins on the crater walls, which appear to be partially infilled with fine-grained sediment.

The deflated material from the ridges and to some degree from the finer layered interbeds is interpreted to be the sediment source for the widespread TAR megaripples present between ridges (Figs 4, 6-8). By analogy with megaripples observed by both of the MER rovers (Jerolmack et al., 2006; Sullivan et al., 2008), we interpret them to contain a significant granule-sized component. We have also observed similar local sourcing of granules to form aeolian ripples occurring in our analogue field site in the Atacama Desert (see section 3.2.1).

3.2. Possible Terrestrial Analog Fans

In only a few cases have terrestrial fans with sedimentary characteristics similar to those inferred for the Saheki K2 fan been discussed. Bull (1962, 1963) describes fan sedimentation in

592 the western Central Valley of California sourced from headwaters underlain by sandstone, shale
593 and siltstone bedrock. Both fluvial and mudflow deposits occur on these fans. Mudflow deposits
594 are unsorted, typically containing 54% mud (clay and silt), 40% sand, and 6% gravel. Clay
595 percentages range from 12-76%, averaging 31%. Mudflow deposits generally decrease in
596 thickness downstream from 0.5 m to 0.1 m, with abrupt terminal edges that range from 0.3 cm to
597 2.5 cm in thickness. Mudflows are transported through a channelized fluvial system. In upstream
598 portions of the fan, the mudflow deposits occur as lobate overbank deposits thicker on outside
599 channel bends, but they terminate downstream as sheet-like deposits. Mudflows develop
600 polygonal shrinkage cracks upon drying. Some flows across the fan have a more fluvial
601 character, creating well-sorted, thin deposits dominated by sand with typically less than 10%
602 mud and less than 10% gravel. Fluvial flows are typically up to 0.15 m deep and occur as braided
603 channels or sheetflows.

604 Blair (2003) discusses the sedimentology of the Cucomungo Canyon fan in California as
605 characterized by both fluvial and mudflow deposits. The dimensions of this fan approach that of
606 the Saheki crater fans, being 15 km in length, with an areal extent of 119 km^2, a concave profile,
607 and an average fan gradient of 0.03. The fan is sourced from strongly weathered granitic
608 bedrock. Mudflow deposits are typically 10% mud, 70% sand, and 20% gravel (Table 3).
609 Mudflow deposits on this fan are thicker than those described by Bull, ranging from 10-100 cm
610 thick with 10-40 cm high abrupt, rounded lateral edges and terminations. Mudflows source from
611 feeder channels and are typically 50-300 m wide but extend the length of the fan. The mudflows
612 surfaces are smooth and develop narrow polygonal shrinkage cracks. Feeder channels are
613 typically 5-30 m wide (width decreasing down-fan) and 2-6 m deep (also decreasing depth
614 down-fan), with smaller secondary channels. Such channels cover less than 10% of the fan

surface, and deposit well-sorted deposits ranging from pebbly sand to cobbly pebble gravel. Fluvial and mudflow facies are interbedded in the fan deposits, with the proportion of fluvial gravels decreasing down-fan. A field reconnaissance conducted by the authors in 2012 on the Cucomungo Canyon fan suggests, however, that fluvial deposits are volumetrically more important than mudflow deposits on this fan, particularly on the downstream portions of the fan.

A third potential analog for the Saheki fans is a suite of fans in the Atacama Desert of Chile. These fans contain similar bimodal fluvial and mudflow deposits but also display the relief inversion due to aeolian deflation that is characteristic of the Saheki K2 fan. Because of this close morphologic analogy, the Atacama fans are described in detail below, and used to better understand the formative processes of the Saheki fans.

3.2.1. A Chilean Terrestrial Analog

The alluvial fans of the Pampa del Tamarugal region of the Chilean Atacama Desert (Fig. 20) appear to constitute a close analog in morphology and formative processes to the Saheki crater fans in the following ways:

1. The fan gradients, areas, and concavity of two representative Atacama fans fall within the range of martian fans, although the Atacama fans are somewhat smaller, steeper, and more concave that the K1 and K2 fans (Table 1).

2. The Atacama fans in the area of study have channels ranging from sand to boulder beds, with mud-rich overbank deposits (Figs. 21, 22, and Table 3), mirroring what we have inferred for the Saheki fans.

3. Inactive parts of the Atacama fans are wind eroded (Fig. 23), resulting in 1-2m of inverted channel relief (Fig. 24), consistent with the erodibility of the fine-grained

638 overbank deposits. The Saheki fans are likewise inverted, although surface relief is
639 greater (as much as 70m).

640 4. Overbank deposits on the Atacama fans exhibit no evidence for fluvial reworking
641 by local runoff subsequent to deposition.

642 5. The Atacama fans terminate in mixed playa/lake "salars" (salt-rich enclosed
643 basins) (Amundsen et al., 2012); the K2 Saheki crater distributaries terminate at
644 possibly analogous flat-lying deposits (Sections 2.2.6 and 2.2.7).

645 Because of these similarities, analysis of sedimentary processes and landforms on the
646 Atacama fans has the potential to yield insights into the mechanics and environment forming
647 large martian fans. The fans are located along a ~140 km transect of the western slopes of the
648 Andes centered at about 21°S, 69°W (Fig. 20), radiating westward from the Andean mountains
649 onto a hyperarid upland plateau. The fans experience only a few millimeters of direct
650 precipitation annually and almost no locally-generated runoff (Amundson et al., 2012). Despite
651 the hyperaridity of the immediate fan environment, flood events sourced from the superjacent
652 Andes occur with appreciable frequency as evidenced by disruption of vehicle tracks, footprints
653 on recent deposits, and sediment deposition on roads and railroad tracks (Houston, 2006) (see
654 also Fig. 26).

655 Our study of the Atacama fans is based on a combination of reconnaissance field
656 investigations plus remote sensing interpretation. During a field season in 2012, we surveyed fan
657 cross-sections and longitudinal profiles using differential Global Positioning Satellite
658 observation, excavated pits and streambank exposures, collected sediment samples, and made

659 Ground Penetrating Radar transects across portions of the fans. Sediment grain size distributions
660 (Table 3) are based on laser diffraction analysis of dispersed samples.

661 The fine sediment comprising these Atacama fans is originally derived from erosion of
662 fine-grained deposits including mudstones, sandstones and volcanic ash, exposed on the flanks of
663 the Andes to the east of the fans (Servicio Nacional de Geologia y Mineria, 2003). A
664 representative canyon (Quebrada de Guatacondo) heading in the Andean foothills (location 25
665 and upstream in Fig. 20) that feeds a fan gives evidence of a spectrum of flows with markedly
666 different properties (Fig. 25). The channel bed exposes clean sub-meter gravels and cobbles
667 indicating that normal fluvial floods are common. The channel walls, however, are plastered with
668 remnants of at least three recent mudflows that occurred in early 2012. The mudflows are
669 typically nearly 50% mud (clay and silt), 30% sand, and 20% pebbles (Table 3). The same event
670 in 2012 deposited an extensive deposit on another fan (Fig. 21) that is likewise characterized by
671 both channelized and overbank flows. As in the canyon flows shown in Figure 25, later (waning
672 stage?) deposits were lighter colored and more confined to distinct channels.

673 Where flows spread onto the aggrading fan, a distinctive and repeated pattern of
674 deposition occurs. The differences in color resulting from variations in sediment color and
675 darkening by aeolian erosion suggest that during an individual flow event only a few distributary
676 channels are active, with widths typically in the range of 3-10 m and depths of up to a meter. The
677 channel bed deposits consist of a mixture of grain sizes, dominated by pebble and finer sediment
678 but containing occasional cobble and boulder bars with median grain size of about 100 mm.
679 Undercut banks of distributaries expose layered sediment averaging about 45% mud, 45% sand,
680 and 10% pebbles (Table 3). However, beds of well-sorted sand or pebbles are interbedded with
681 the muddier layers. Individual layers range from a few centimeters to 20 cm in thickness. A

682 similar facies association of channel gravels and overbank mudflows has been described for
683 other fans in the Pampa del Tamarugal region (Kiefer et al., 1997; Houston, 2002).

684 Large flow events through distributaries spread overbank, depositing sheet-like mud
685 deposits extending a few meters to 150 m bilaterally around the distributary (Figs. 21, 22, 26).
686 Locally, however, these mudflows may extend several hundred meters to a kilometer or more
687 across the surrounding fan surface as broad depositional lobes (Figs. 22, 26). The overbank
688 deposits typically contain 60% mud and 40% sand, although a few beds contain granules and
689 fine pebbles (Fig. 27). These deposits harden to adobe-like consistency typically with well-
690 developed mudcracks. Individual deposits are nearly homogeneous and range up to 25 cm in
691 thickness. The beds generally thin away from the distributary, generally with abrupt, rounded
692 edges a few cm high. Repeated flows gradually develop broad natural levees extending >150 m
693 to either side of the distributary (Fig. 28). Deposits from individual overbank events are
694 generally easily distinguished by sharp flow margins and, often, color differences between
695 deposits from different events (Fig. 26). We have described the formative flows as mudflows
696 because they have abrupt, rounded lateral and downstream boundaries. Also, vertical surfaces
697 inundated by the mudflows retain coatings several millimeters thick. Both observations indicate
698 the flows displayed finite yield strength. However, the flows have low viscosity relative to many
699 terrestrial mudflows as indicated by their thin terminal edges.

700 Locally the distributaries exhibit modest sinuosity, although vertical aggradation
701 probably dominates over lateral shifting. As with fluvial channels in general, distributary widths
702 are determined by the balance of erosion and deposition of the fine-grained deposits forming the
703 channel banks. Their width is remarkably constant downstream despite the significant lateral
704 leakage of flow that must accompany the mudflows that deposit the overbank deposits. This

consistency of width suggests that formative discharges may consist of a sediment-laden early peak flow overflowing to form lateral deposits followed by slowly receding flow largely contained within the channel and responsible for determining channel width.

As channels and their natural levees aggrade though multiple flow events, the channel floor may rise ~1 m above the fan surface within a 150-200 m radius (Fig. 28). This resultant relief can lead to avulsions, trenching of a new flowpath through the natural levee, a new distributary channel on the fan surface, and infilling of the abandoned distributary below the avulsion point. The stratigraphy resulting from multiple such events is characterized by gradually tapering layers separated by diastems (minor hiatuses).

The net result of multiple avulsions is a fan surface consisting of a complex network of active and abandoned channel segments (Figs. 26). Avulsions may lead to reoccupation of abandoned distributary channels that have gradually become topographically low relative to adjacent actively aggrading distributaries. Other inactive channel segments become buried by subsequent deposition.

Although the overbank deposits harden to such consistencies that blocks must be excavated by pickaxe, they are easily eroded on a grain-by-grain basis by wind-driven saltating grains (Fig. 23). These grains, up to a few millimeters in size, are derived from the eroding overbank deposits, and over a period of time lag layers and megaripples of granules create a thin (0-10 cm) pavement away from the fluvially active areas, progressively covering the overbank deposits. Burial by later overbank deposits can create diastems demarcated by granule layers.

On the Atacama fans, the granules forming the pavement are dark colored relative to the bulk overbank deposits. Thus recently active portions of the fan systems are light-colored, but inactive portions gradually become darker as the percentage cover by granules increases (Figs.

728 23 and 26). This natural color-coding permits easy recognition of the relative ages of sections of
729 fan surfaces (Fig. 26). Satellite imagery of the fans show that deposition is typically active
730 (lacking dark sediment cover) over zones 1-5 km wide (measured normal to the flow direction)
731 of the 10-20 km width of individual fan complexes, and within these zones of recent activity
732 individual flood deposits occupy a cumulative width of a few hundred meters or less. The
733 channels range from 3 to 10 m wide. The spatial relationship of these features indicates that fans
734 are built though hundreds or thousands of individual flow events often separated by several
735 years.

736 Inactive portions of the fan complex become modified by aeolian deflation, resulting in
737 inverted topography as the channels containing gravel resist erosion, whereas sand saltation
738 readily abrades the muddy overbank sediments (Figs. 23 and 24). Granules deflated from the
739 channel and coarser overbank deposits are swept into megaripples less than 10 cm high that form
740 a distributed pavement limiting the rate of aeolian erosion. On the Atacama fans, the inverted
741 channel relief is generally limited to 2 meters or less, set by the depth of erosion of overbank
742 deposits required to generate a coherent granule pavement and possibly by the duration of wind
743 erosion.

744 The strong sedimentological and morphological similarity between the Atacama and
745 Saheki crater fan complexes are used to formulate several working hypotheses for the Saheki
746 fans:

747 1. The Saheki fans are formed through many hundreds of flow events, often with
748 long intervals between flow events.

749 2. Only a small portion of a fan complex receives flow and sedimentation during any
750 event.

751 3. The bulk of the deposited sediment consists of fine-grained overbank deposits.

752 4. Individual overbank deposits may extend long distances downslope but likely thin
753 and feather out laterally.

754 5. Avulsions are common as channels and natural levees aggrade, and individual
755 distributary segments may be reoccupied during later flow events, resulting in a
756 complex intertwining of channel deposits.

757 6. Flows vary in intensity and fine sediment content. Gravel and boulder deposits in
758 distributaries may only be transported during the largest flow events whereas
759 overbank mudflow deposition may occur during more frequent flows.

760 As with any terrestrial analog to martian landforms, there are limits to the process,
761 material, and morphological similarities:

762 1. The strong tonal contrast between bright recent overbank deposits and the darker
763 granule pavement that develops during wind erosion is much less obvious on the
764 TARs partially mantling the wind-eroded Saheki fan than for the Atacama fans.
765 This difference in tonal contrasts may be due to lithologic differences, smaller
766 clay content on the martian fans, possible biofilms on the terrestrial granules, or a
767 smaller component of granule-sized overbank sediment on Mars. A lower granule
768 component in the Saheki deposits would limit pavement formation and promote
769 deeper deflation of fan surfaces as observed.

770 2. Distributaries on the Atacama fans are narrower than estimates of the Saheki
771 crater inverted channels (3-10 m for the Atacama fans (Fig. 25, 26) versus an
772 average of ~38m for Saheki; (Fig. 12)). This dissimilarity could be due to greater

discharges on the martian fans, to less sediment concentration in formative flows, or to a smaller proportion of cohesive clays contributing to deposition on channel banks.

3. Individual overbank layers deposited on the Atacama fan are generally less than 25 cm thick and generally much thinner near flow margins, whereas observed layering in Saheki crater deposits is typically 2-3 m thick. The degree to which this thickness difference is due to freshness of exposures or to image resolution limitations is uncertain.

3.2.2. Summary of Terrestrial Fan Analogs

The terrestrial fans described above are relatively unusual relative to the total population of alluvial fans in having a combination of gravel-bedded distributaries with fine-grained overbank sediments deposited by mudflows. This is inferred to also characterize the Saheki crater fan sediments. Mudflows are characterized by finite yield strength, and imply an appreciable mud fraction (silt and clay). Unlike more viscous debris flows, however, they normally do not transport sediment coarser than pebbles. The mudflow deposits of the Atacama and those described by Bull (1962, 1963) contain an appreciable fraction (>10%) of clay, whereas the Cucomungo Canyon fan deposits (Blair, 2003) typically have about 1% clay and only 10% total mud, indicating that a high concentration of clay and silt is not necessary to support mudflow overbank transport. While the fine sediment composition of the Saheki crater overbank deposits is uncertain, it likely falls within the range of the terrestrial mudflow fans.

3.3. Interpretation of Saheki Fan Stratigraphy and Evolution

795 The observations in section 2 and on possible terrestrial analogs indicate that the Saheki
796 crater fans are composed of a network of fluvial distributaries formed by channelized flows with
797 associated fine overbank mudflow deposits, and, at the fan terminus, playa or shallow lake
798 sediments with some chemically-cemented interbeds. The coexistence of fluvial distributaries
799 with gravel beds and mudflow-dominated overbank deposits might seem contradictory because
800 debris-flow dominated terrestrial alluvial fans typically are largely composed of unsorted matrix-
801 supported deposits with lobate flow terminations (Blair and McPherson, 2009). The flows on the
802 terrestrial analog channels discussed earlier, however, have aspects of both fluvial and mass
803 flows. Debris flows and presumably the finer grained mudflow events commonly occur as deep,
804 viscous noses followed by long, more watery terminal flows (Costa, 1984, 1988; Johnson, 1984)
805 that are more channelized and winnow fine material from the bed. In addition, large discharge,
806 deep mudflows are commonly interspersed with more frequent, lower magnitude fluvial flows.
807 Either trailing or subsequent-event fluvial flows could be responsible for the relatively clean
808 gravel bed of the Atacama channel shown in Fig. 25.
809 In the next two sections, we interpret the stratigraphy of the Saheki crater fans and their
810 erosion by the wind in a simplified cross-sectional model, followed by a discussion of the
811 formative hydrological and climatic environment.
812

813 **3.3.1. Interpretive Model of Saheki Fan Surface Erosion**

814 An interpretive, semi-quantitative 2D cross-sectional model detailing the inferred fan
815 stratigraphy undergoing aeolian deflation in Saheki (Fig. 29) is used to evaluate the viability of
816 our interpreted fan history and material properties of the fan sediment (see Appendix A for full
817 details of model). The model was developed to illustrate three aspects of our interpretation of the

818 alluvial fan composition and subsequent fan erosion: 1) the fan deposits can be interpreted as the
819 two facies of resistant channel deposits and wind-erodible overbank deposits; 2) the erosional
820 processes include interacting processes of aeolian stripping, shallow mass wasting, and
821 undermining of the caprock; and 3) the surface area covered by exposed channel deposits
822 considerably exceeds their volumetric proportion within the fan deposits. The model takes as its
823 starting condition an idealized hypothetical cross-section of the lower part of fan K2, comprising
824 a randomly distributed set of rectangular "channel bodies" (blue) composed of fluvial sands and
825 gravels scattered through a more easily eroded muddy overbank stratigraphy (uncolored).
826 Aeolian inversion is mimicked by a set of rules for the vertical removal of the overbank material
827 at a rate in part dependent on the local surface curvature (convex-upwards surfaces erode more
828 easily due to greater exposure to the wind), but the channel bodies containing coarser sediment
829 cannot be directly wind-eroded. Instead, they can erode only by hillslope mass wasting, with the
830 resulting material being transferred diffusively down sideslopes. This mass wasting exposes the
831 overbank deposits and moves material into the adjacent topographic lows as well as becoming
832 covered by TARs, both of which decrease the rate of wind erosion (idealized by having the rate
833 of wind erosion diminish in concave upwards locations).

834 The initial surface is the horizontal black line at the top of the cross section in Fig. 29.
835 The colored and dashed curves show the surface profile at successive times during the
836 simulation. The model indicates that, as would be expected, erosion of channel gravels lags
837 behind lowering of the adjacent overbanks until eroded laterally by mass wasting. Exposure of
838 the overbank deposits occurs primarily on slopes subjacent to the gravel ridges and on low-relief
839 surfaces in between ridges. An important effect of wind erosion is to magnify the fraction of
840 gravel on the surface relative to its volumetric fraction. In this simulation, channel deposits

841 occupy 25-36 % of the land surface (locations where the land surface is in the blue deposits in
842 Fig. 29) in the later stages of wind erosion compared to the 5% volumetric fraction proscribed at
843 the start of the run. This change of proportionality over time due to the exposure of buried
844 channels is likely true for the wind-eroded portions of the Saheki fans. We suggest that the
845 present pattern of inverted ridges gives a false impression of what the density of channels on the
846 active fan may have been, possibly overestimating it several-fold.

847 **3.3.2. Interpreted Hydrological Environment of Saheki Fans**

848 In this section, we use observations and measurements of the fan slopes and channel
849 widths with inferences about likely channel bed grain sizes and sediment loads to quantitatively
850 interpret the discharges and flow velocities in the distributary channels at peak discharge. This
851 information allows us to discriminate between the various possible environments of formation
852 for the fans. We then employ these estimates to assess formation timescales for the fans,
853 addressing in particular whether the fans could have formed by one or a few, long-duration
854 flows, or alternatively would have required many cycles of sedimentation over perhaps
855 thousands or tens of thousands of years.

856 The estimated age of the Saheki crater fans (Mid to Late Hesperian) is a time period
857 when both the atmospheric pressure and temperature are thought to be too low to support
858 precipitation other than as snow (Carr, 2006; Forget et al., 2013; Wordsworth et al., 2013).
859 Groundwater discharge has been considered to be a possible water source for martian valley
860 networks as well as modern gullies (Malin and Carr, 1999; Malin and Edgett, 2000; Harrison and
861 Grimm, 2009; Goldspiel and Squyres, 2000, 2011). The dendritic structure of the source basins,
862 and especially the stream heads descending from narrow ridge spurs away from the walls of the
863 craters, argues strongly for a spatially distributed surface water source. In addition, with the

exception of the K1 fan, which has an elevated degraded crater behind the crater rim source basin, all of the source basins in the Saheki and "L" crater fans are eroded into the highest parts of the crater rim with negligible potential groundwater source areas beyond the head of the incised basins. Therefore in our analysis we assume that flows eroding the source basins and delivering sediment to the fans derives from melting of ice and snow by solar insolation at the surface, a conclusion also reached by Grant and Wilson (2012).

Our method mirrors the approach of Kleinhans (2005), in that we explicitly model the effects of channel bed roughness into our discharge calculations. We assume that the flow during fluvial transport is primarily contained within the distributary channels. Because flows clearly become overbank when depositing the fine-grained inter-channel deposits, this assumption provides a minimum estimate of formative flow magnitude. In addition, we also incorporate additional constraints based on a critical Shields stress in the channels, assuming that the coarsest sediment is transported primarily by the high flows responsible for creating the observed channel geometry. This approach yields internally consistent flow velocities and discharges commensurate with what we know of terrestrial coarse bed alluvial streams.

We aim to model discharges on a single fan (K2) in Saheki crater where we have a high density of HiRISE observations from which to draw data, and where we can adequately constrain the drainage basin structure feeding the fan. Flow velocity, u, in streams can be modeled based on channel hydraulic radius, h, channel slope, S, and some measure of channel bed roughness. From these velocities discharges, Q, can be derived by conservation of mass,

$$Q = uhW \quad (1)$$

where W is the channel width.

886 The local splaying (Figs. 7 and 8) suggests wide channels that are close to the threshold
887 of braiding, so we assume that channels are much wider than they are deep. Under this
888 assumption, the hydraulic radius converges with the channel depth, and we use the terms
889 interchangeably. We also demonstrate below the channels likely have large width-to-depth
890 (aspect) ratios (>20). Even for narrow channels, making this assumption introduces only a few
891 percent bias. A large number of formulations exist in the literature describing calculations of
892 flow velocity. Most follow either the form of the Manning equation,

893 $$u = \frac{h^{0.67} S^{0.5}}{n} \quad (2)$$

894

895 where n is an empirically determined channel roughness; the Chezy equation,

896 $$u = C\sqrt{hS} \quad (3)$$

897

898 where C is another empirically determined channel roughness term; or the Darcy-Weisbach
899 equation,

900 $$u = \sqrt{\frac{8ghS}{f}} \quad (4)$$

901

902 where f is the Darcy-Weisbach friction factor, and g the gravitational acceleration. Following
903 Kleinhans (2005) and Wilson et al. (2004), we work only with the Darcy-Weisbach formulation.
904 This equation makes explicit the dependence of the flow velocity on g, thus allowing more
905 reliable extrapolation of terrestrial calibrations to Martian conditions (though we note by
906 comparison of 2, 3, and 4, that n and C can also be expressed as functions of g).
907 Determining the friction factor f under various conditions has occupied many researchers
908 over the years, as summarized by, e.g., Ferguson (2007) and Rickenmann and Recking (2011).

909 This parameter integrates the interaction of flow turbulence with channel roughness across all
910 length scales, and thus shows variability under differing hydrological conditions and fluvial
911 environments. In particular, it incorporates both skin and form roughness, i.e., roughness of the
912 bed at both grain scale and bedform scale (although the latter is neglected in many laboratory
913 calibrations of *f*). The most recent forms of these equations (e.g., Ferguson, 2007; Rickenmann
914 and Recking, 2011) seek to incorporate the effects of very high form drag throughout the flow
915 from the largest clasts on a mixed grain size fluvial bed when flow is shallow, but recognize that
916 flow follows logarithmic laws progressively more closely as the flow deepens and the topology
917 of the boundary becomes less important. When compared to existing databases of terrestrial flow
918 data, these formulations perform at least as well as the best of the older, heuristic approaches –
919 although Ferguson (2007) notes that a factor of two error in predicted discharge should be
920 expected in all cases.

921 We adopt Ferguson's favored equation for this scale-dependent roughness, which uses a
922 power law to describe the transition zone between the "deep" and "shallow" ($h/D_{84} < 4$) flow
923 regimes, because of both its physical basis and superior performance in terrestrial datasets. This
924 choice is further justified by the fact that our calculated Shields stresses (see below) tell us that
925 the relative roughness of these Martian channels falls in the shallow flow regime poorly
926 described by older approaches. The Ferguson (2007) equation is

927
$$\sqrt{\frac{8}{f}} = 17.7\left(\frac{h}{D_{84}}\right)\left[56.25 + 5.5696\left(\frac{h}{D_{84}}\right)^{5/3}\right]^{-0.5} \quad (5)$$

928

929 The equation has been calibrated across a range of gravel to boulder bed streams, with slopes
930 0.0007 to 0.21. These ranges bracket the measurements taken for our Martian channels (see
931 below).

To solve equation (4) for cross-sectional average velocity requires as inputs the channel slope, S, depth relative to the bed grain size, (h/D_{84}), width, and absolute channel depth. We constrain channel widths by examining and measuring the inverted ridges of the fan surface, as described in section 2.3.2. From these data, we take W = 38 m as the average width of these channels on the well-constrained fan K2. Channel slope can be determined directly from MOLA digital terrain models of the fan, having established that the channels and associated overbank sediments are subparallel to the exposed fan surface, and that the channel sinuosity is negligible (Fig. 3; <5% increase in channel length compared to a straight line). Slopes were measured along the same segments used to obtain widths, and were found to be consistent with S = 0.029 in the upper part of the K2 fan.

The relative depth of these channels, (h/D_{84}), can be constrained by assuming a critical Shields stress, τ_c^*, for the channel bed:

$$\tau_c^* = \frac{S}{r}\left(\frac{h}{aD_{84}}\right), \quad r = \frac{\rho_s - \rho_f}{\rho_f} \tag{6}$$

where r is the relative submerged specific gravity of the sediment clasts, and ρ_s and ρ_f are the densities of the clasts themselves and the transporting fluid respectively. The parameter a represents the sorting of the sediment (i.e., $D_{50} = aD_{84}$), and is very poorly constrained on Mars. We here assume a = 0.5, a fairly typical value for coarse grained alluvial systems on Earth. Note that equation (6) is not sensitive to g, making it appropriate to apply to martian conditions. This expression was originally derived by considering the force balance on a single particle in a sediment bed, and it semi-empirically describes the threshold of motion for particles in a clast bed. Terrestrial gravel channels typically transport bed sediment at discharges just slightly exceeding the threshold of motion of the D_{50} grain size (Andrews, 1984; Dade and Friend, 1998; Howard, 1980; Parker, 1978; Talling, 2000), so that the dominant (channel-forming, bankfull)

discharge corresponds to the threshold of motion, and we assume the same is true of the Martian channels. The value of τ_c^* applicable to a given channel varies somewhat, and is a complex function of bed structure, grain size magnitude and distribution, and flow characteristics. However, in almost any fluvial channel it falls in the range $0.03 < \tau_c^* < 0.1$, and much of the variability in the value can be folded into the variability with channel slope (e.g., Lamb et al., 2008):

$$\tau_c = 0.15 S^{0.25} \quad (7)$$

We adopt this relation, which indicates that on our fan (S=0.029), $\tau_c^* = 0.062$. We take ρ_s = 3000 kg/m^3, the approximate density of basalt. We treat ρ_f as a variable, taking ρ_f = 1000 kg/m^3 for assumed clear water flow as a reference case, but allowing the value to rise to represent more realistic turbid flows. Flows can retain many of the bedload transport characteristics of fluvial flows while the sediment concentration remains $\sim<$ 40% (e.g., Costa, 1988), and we adopt this value as a fairly arbitrary upper limit for the fluid density. Hence, using these values and following equation 6, (h/D_{84}) = 2.1 for clearwater flow, decreasing as the flow becomes more turbid, reaching (h/D_{84}) = 0.7 when 40% of the flow by volume is basalt.

The only remaining variable to constrain is the flow depth, which we can calculate by constraining the bed grain size. HiRISE imagery of the fans at 0.25 m/pixel scale indicates that a high proportion of the flat-topped ridges which were measured for channel width are studded with occasional boulders up to a few times the pixel width, and that the rest of the surface has a speckled appearance. This texture is qualitatively suggestive of clasts close to or slightly below the resolution limit of the camera. We place this estimate on a more quantitative footing by resampling imagery of terrestrial river bed sediment with known D_{84} to varying relative

978 resolutions (i.e., pixel resolution/D_{84}) and comparing it to the texture seen in the HiRISE images
979 (Fig. 30). We infer that the speckled texture seen on the ridges (Fig. 10) corresponds to a grain
980 size in the range $12.5 < D_{84} < 25$ cm (i.e., 1-2 D_{84} grains/pixel), and most probably towards the
981 higher end of that range. Using our value of (h/D84), we obtain $0.25 < h < 0.5$ m for clear water
982 flow (and channel aspect ratios $70 < W/h < 150$, confirming our approximation that the channel
983 depth equals the hydraulic radius). Such cobble-grade grain sizes are also consistent with our
984 model for the fan inversion process, as described in section 3.2, as the coarse sediment on the
985 bed of the channel will not be transportable by wind.
986 Combining equations 1 and 4-7, we calculate the flow velocities and corresponding
987 dominant discharges in each of these channels (Fig. 31). Under the range of appropriate sediment
988 concentration and grain size values, we derive flow velocities between ~0.4 and 2.5 m/s and
989 dominant discharge ranged from 0.5-21 m^3/s. Note that these values are also dependent on the
990 value chosen for the sorting parameter a above; however, even if $a = 1$, (i.e., $D_{50} = D_{84}$, the
991 theoretical maximum value where there is no size variation at all amongst the coarser fraction of
992 the sediment), the maximum values we could obtain are only $u = 2.0$ m/s and $Q = 95$ m^3/s.
993 It is uncertain how many channels on the fan were active at any given time, and it may be
994 necessary to multiply these channel discharges by some factor to arrive at the total discharge
995 from the source catchment per event. However, the scarcity of bifurcations seen on the channel
996 ridges suggests that this factor should be low, probably ≤ 3 as is observed in the Atacama analog
997 (Fig. 25). Assuming three active channels, the coarsest possible grain sizes, a=1, and clearwater
998 flow, maximum total discharge across the fan could be up to 285 m^3/s. Much more likely total
999 discharges are probably in the range ~30-60 m^3/s, allowing for a small percentage of sediment in
1000 the fluid, and a grain size in the middle of our suggested range, a plausible particle size

distribution, and 2-3 active channels (Fig. 31). We also reemphasize (following Ferguson, 2007) that a factor of two error in these figures should be assumed.

We constrain the area of the source catchment of this fan as 793 km^2. In order to produce the maximum (i.e., very optimistic) discharges of 285 m^3/s, the source catchment would have to supply water at the rate of 1.3 mm/hr. Our preferred, lower discharges ~30-60 m^3/s would result in proportionally lower supply rates of ~0.1-0.2 mm/hr. These estimates are probably somewhat conservative, as we cannot account quantitatively for refreezing, evaporation, or infiltration in the system. However, if discharge is sourced from an overlying wet snowpack over permafrost, the contributions of all three loss mechanisms are likely to be relatively minor. Such discharges would have to be sustained for at least a timescale comparable with the time taken for water to move through the catchment system, to allow the discharge to integrate across the whole drainage area. For the ~20 km length K2 basin, and assuming flow velocities as seen on the fan are typical of flow velocities higher in the catchment (a conservative assumption, $u \sim 1$ m/s), then discharge across the catchment would have to be sustained for at least several hours.

We can however test snow or ice ablation as a mechanism for sourcing the discharges based on our data, a hypothesis for the water source for fans and deltas in the Margaritifer Terra region (Grant and Wilson, 2012), and also suggested for contemporaneous shallow channels in Newton and Gorgonum basins (Howard and Moore, 2011). Ablation of ice is fundamentally limited by the energy balance of the icepack itself, including incoming solar flux, reflection at the surface and in the atmosphere, re-radiation from the ice itself, downwelling longwave heat flux from the atmosphere (e.g., from clouds), and potentially complex effects from convection (e.g., winds), advection (e.g., water drainage, dust movements), and secular changes in the driving parameters (e.g., day/night, seasons, obliquity changes). Were all the incoming solar flux

to be converted into latent heat to melt ice, we acquire a hard (and physically implausible) upper limit for water supply rates of 5.4-7.5 mm/hr, assuming solar insolation of 500-700 W under the modern orbital eccentricity of Mars (c.f., Laskar et al., 2004). Other authors have used more sophisticated energy balances to investigate the melt rates and total discharges expected from melting snow on Mars. Williams et al. (2008a, 2009a) concluded runoff > 1 mm/h at spatially averaged rates exceeding 0.25 mm/h would be readily possible in the Martian midlatitudes over the past 5 Ma, and their data suggests occasionally somewhat higher rates and discharges may also be possible. Kite et al. (2013) suggest that in general across Mars' history, maximum snow melt rates should be 2-3 mm/h, with melt occurring in widely spaced discrete temporal windows, promoted by either orbital parameter variation or by transient darkening of snow surfaces by ash or ejecta.

Our estimates of runoff production rates in the catchment for the K2 fan are comparable to Williams and colleagues' (2009a) estimates for "typical" snow melt events for recent Mars, and comfortably below Kite and colleagues (2013) long term maxima for melt production rates. We thus conclude that melt by ablation of snow deposits on the crater walls is a viable mechanism for the production of the flows that built the K2 fan, and by inference, the other fans in Saheki and crater L that have relief characteristics to the K2 fan (Moore and Howard, 2005). This analysis cannot address the physics of melt production beneath a snowpack, which is likely complex and nonlinearly dependent on the timing of warming of the pack in the solar year (e.g., Williams et al., 2008a), but indicates that the flux magnitude is not sufficient to reject the snow melt hypothesis.

Large terrestrial alluvial fans form over thousands of years of seasonal or rarer flows (such as for the Atacama Desert fans discussed above). Scenarios have been proposed that

martian fan-deltas (Jerolmack et al., 2004; Mangold et al., 2012b) and some small channel systems (Morgan and Head, 2009; Mangold, 2012) have been created over a short time period by relatively continuous flows resulting from thermal anomalies created, for example, by energy resulting from by bolide impacts. Here we evaluate whether the Saheki fans could have formed from one or a few relatively continuous flow events. Our analysis suggests maximum flow rate to the K1 and K2 fans was unlikely to be more than ~100 m^3/s. The K1 and K2 fan volume is about 586 km^3. Assuming a generous sediment concentration of 20% of water flow volume, a continuous flow could create the fans in a minimum of ~500 Mars (~1000 Earth) years. The primary issue, however, is in generating the flows. As discussed previously, groundwater flow is an unlikely source, so precipitation on the crater walls (almost certainly as snow) would have been required. For the 20% sediment concentration across the known headwater area a total runoff depth of 3.57 km of water would be required. Given sublimation losses and the high porosity of snow, a total snow accumulation several times that figure would have been required. If, say, 10 km of snowfall were required of the headwater areas to form the fan in 500 martian years, this would require an annual snow accumulation of ~20 m. A more reasonable scenario would be seasonal snowmelt occurring for 6 hours per day, 100 days per Mars year, requiring ~3600 martian years to form the fan and an annual snow accumulation rate of ~3 m/yr. This is still a very optimistic scenario given the high average sediment loads assumed.

Another check on a minimum timescale comes from the observed layer stratigraphy. If the ~2 m-thick beds observed in HiRISE images (Figs. 13 and 15) represent annual accumulations and we take an average fan thickness of ~400 m, then approximately 200 deposition events are recorded at any given location. If as much as 10% of the fan surface were active during any given year, then 2000 martian years would have been required. It is likely,

1070 however, that higher resolution imaging of clean layer exposures would reveal finer-scale
1071 layering than observed. Thus we conclude that at least a few thousand martian years was
1072 required to form the alluvial fans. More likely, given the probability of lower sediment load
1073 percentages, less frequent flow events, and thinner annual bed thickness, the fans may have
1074 required a few tens of thousands of martian years to form at a minimum. These years need not
1075 have been sequential. A fan lifetime with a small number of annual events during favorable
1076 obliquity may have been separated by long inactive periods through multiple obliquity cycles.
1077 We do note, however, that we have seen no evidence for impact cratering having disturbed
1078 visible bedding during deposition, although appreciable cratering has occurred subsequent to fan
1079 deposition.
1080
1081 **3.4 Comparison with Other Martian Fans**
1082 Large alluvial fans on Mars have morphological characteristics that vary through a
1083 narrow range of fan gradients, ratios of gradient to contributing area, and ratios of fan area to
1084 contributing basin area (Moore and Howard, 2005) (Table 1). These characteristics suggest very
1085 similar hydrological and sedimentary processes and materials characterized most martian fans.
1086 The "L" crater 25 km southeast of Saheki crater hosts fans that are of similar size and
1087 morphology as those of Saheki crater. The major differences appear to be the multiple fans in
1088 "L" sourcing from all quarters of the rim, and lesser aeolian stripping of the fan surface
1089 (although, as in Saheki crater, the greatest wind erosion has occurred on the southern fans).
1090 Recent high-resolution imaging, however, reveals differences in fan morphology and geologic
1091 context among other fan-bearing craters. In Harris crater (Fig. 1), the fans show pronounced
1092 distributary patterns like Saheki, but the fan in the northeast quadrant exhibits an isolated, rough–

surfaced, bouldery deposit crossing the fan with a wide, lobate planform morphology that has been interpreted as a debris flow deposit (Williams et al., 2011). The fans on the west side of this same crater overlie a light-toned, layered deposit not found in Saheki crater. The fan surfaces in Runanga crater (Fig. 1) exhibit inverted distributaries, but the interbedded layered deposits are light-toned and are broken by meter to decameter polygonal fracturing, which might be explained by either more coherent sediment or a different weathering environment. Most of the fans in Margaritifer Terra studied by Grant and Wilson (2012a) exhibit radiating distributary patterns similar to those in Saheki and "L" craters, but one set of fans terminates in steep-fronted lobes that could be explained by their deposition into a concomitant lake (with the fan-delta in Eberswalde crater being a prominent case of interaction with a lake (Malin and Edgett, 2003; Moore et al., 2003)). Finally, Holden crater features a more complicated history of successive fan development than has been proposed for Saheki crater (Grant and Wilson, 2012).

These observations illustrate a range of fan stratigraphic patterns across martian fans, perhaps reflecting local climate or differences in source materials. Nonetheless, the general pattern seen in Saheki and "L" craters -- of radiating distributaries composed of wind-resistant sediment interbedded with finer, layered sediments -- characterizes most martian fans which have been sufficiently exposed by aeolian erosion to reveal their stratigraphy.

4.0 Conclusions

The Hesperian Period is generally thought of as a cold and dry period dominated by extensive volcanism, canyon formation, and large outflow channels. Recent studies have suggested that fluvial activity was widespread though probably sporadic on Mars well into Hesperian and perhaps occurring as late as the Hesperian/Amazonian transition (Fassett et al.,

2010; Grant and Wilson, 2011, 2012; Howard and Moore, 2011; Mangold et al., 2012a). Widespread post-Noachian fluvial features which require precipitation (probably as snow) as their water source are indicative of a global climate favorable to surface water transport as suggested by Grant and Wilson (2011, 2012) and Howard and Moore (2011).

The precipitation and discharge of water is the premier question in understanding the climatic implications to fan formation. Our calculated discharges and the origin of runoff being the highest portions of hosting crater rims effectively rule out the possibility of groundwater as a source of water feeding the fans, leaving atmospheric precipitation as the likely candidate. Given the constraints imposed by the martian climate during the Hesperian as well as the lack of fluvial channel heads on the fan surface, torrential rain is very unlikely. Our hydrological analysis (section 3.3.2) shows that snowmelt appears to be adequate to drive the required discharges.

One of the most enigmatic observations of the alluvial fan systems on Mars is their highly localized distribution. On a global scale, large fans are limited to within mid-latitude band craters (Kraal et al., 2008; Moore and Howard, 2005; Wilson et al., 2012), and even within craters fans are limited in their spatial distribution. Despite being just several tens of kilometers apart, “L” crater contains seven fans sourcing from all sides of the crater rim while Saheki contains only three, one of which is too small to be of much significance. The high crater rims of the relatively young craters hosting fans may have helped to create a microclimate that could trigger appreciable snow accumulation. Restriction of fans to certain portions of crater rims may also be attributed to crater rims containing deposits susceptible to erosion by modest runoff rates, that is, predominantly fine-grained and unconsolidated materials. Both of the main Saheki fans source from a region that intersects both the western rim of a larger adjacent crater as well as the

elongated basin to the northwest (Fig. 2), both of which could be potential sites of antecedent sediment accumulation.

Fans on Mars exhibit vastly different levels of subsequent aeolian erosion. The two fans within Saheki crater have slightly different crater-derived surface ages, yet interfingering of distributaries along their border is suggestive that the fans formed at the same time and that the apparent age difference is due to the subsequent amount of erosion of the fan surface. The amount of aeolian erosion is thus not solely a function of surface age, but rather a product of other factors including sediment composition and wind direction and intensity. However, while different fans have undergone varying levels of erosion, they mostly share the same morphological characteristics. We propose many of the large fans in this latitude belt formed from similar hydrologic processes and conditions as the Saheki fans. Therefore, even though Saheki crater was chosen for detailed study due to the high amount of information revealed from surface aeolian erosion, other fans have formed through similar processes, albeit with some variations in processes, materials, and setting as indicated in Section 3.6.

Evidence from the fans in Saheki crater and elsewhere represent significant fluvial activity relatively late in martian history and contribute to our ever-changing understanding of the fate of Mars' climate. These fans could not have formed in a single event; their formation requires many years and multiple periods of snow accumulation and subsequent runoff. Moreover, for snow to preferentially accumulate on local topographic highs, the atmospheric pressure had to be higher during this time than at present (Wordsworth et al., 2013). The sedimentological characteristics of the Saheki and "L" crater fans indicate that flows during at least the final stages of fan activity were fluvial flows with occasional overbank mudflows, so that volumes of sediment that could be transported during individual flow events would be

limited to a fraction of the discharge volumes. The modest discharges that would be available from the source basins suggests that only a few distributaries were active in any given flow event. The lack of evidence for deep lakes occupying Saheki crater during the time of fan formation indicates formative flows were of limited volume and duration, requiring many flow events to construct the fans. The thin, light-toned beds in the fine-grain deposits may relate to modifications occurring during depositional hiatuses (Figs. 13 and 14). Flow events did not necessarily follow a yearly cycle; rather, there may have been epochal periods of snow accumulation followed by periods of release during favorable orbital configurations or transient aperiodic but repeated global warming events such as volcanic eruptions. In addition, occurrence of snowfall may have been tied to availability of source water, possibly related to phreatomagmatic eruptions or flood events in outflow channels.

Appendix A: Idealized Model for Aeolian Inversion of Saheki Fans

The starting conditions are a hypothetical cross-section of the lower part of fan K2, with the cross-section being taken normal to the dominant flow direction with a 1000 m section taken across the fan perpendicular to the downslope direction and a 100 m vertical extent (Fig. 29). In this model the uncolored area is envisioned to consist of fine-grained overbank deposits. Interbedded with the overbank deposits are gravel channel deposits scattered randomly within the cross section. The width of each channel is randomly sampled from a uniform distribution from 30 to 80 m, and each channel deposit is 2 m thick. Coordinates for channel deposits are selected randomly within the cross-section, and deposits are added (blue boxes in Fig. 29) until 5% of the total cross-sectional area (an arbitrary number) is channel gravel. The stack of channel and overbank deposits is then wind-eroded, with the initial surface being a flat surface at the top of the stack (black line). The channel deposits are assumed to be inerodible by wind, but the overbank deposits on a flat surface are eroded at a rate z_{wf} of 5.0 m/t (time, t, and the erosion rate z_{wf} are in arbitrary but consistent units relative to other simulation parameters). Wind erosion is also assumed to be more rapid on convex slopes due to greater exposure. The wind erosion rate, z_w (m/t) relative to a flat surface rate z_{wf} is given by:

$$z_w = z_{wf} \exp(-K_w \nabla^2 z) \tag{A1}$$

where K_w is a scale constant and has the value 40 m and z is the surface elevation. The value of K_w was selected to rapidly scour ridges no longer capped by gravels, because uncapped hills of layered sediment are rare on the K2 fan.

As time progresses and wind vertically erodes sediment (which is assumed to be entirely removed from the cross-section), diffusive mass wasting occurs using a non-linear relationship (Hanks and Andrews, 1989; Roering et al., 1999, 2001):

$$q_m = -\frac{K_m S}{\left[1-\left(S/S_c\right)^2\right]} \quad \text{(A2)}$$

where q_m is the vector mass wasting flux (volume per unit width of slope in m^2/t) S is slope gradient (as a vector in the numerator), S_c is a critical slope gradient (the angle of repose for loose sediment, set to 0.6 here), and K_m is diffusivity. For these simulations K_m was set at 10.0 m^2/t. Net erosion or deposition rate is given as:

$$z_m = -\nabla \bullet q_m. \quad \text{(A3)}$$

Erosion of the channel gravels is assumed to occur only through mass wasting. The majority of the eroding slope surface is underlain by the overbank deposits. We assume that the gravels make up a minor component of the slope mantle and have no effect upon mass wasting rates or aeolian deflation of the portions of the slope on overbank deposits. Note that we consider the aeolian erosion and the mass wasting to be independent, additive processes. Additive processes are commonly assumed in landform evolution models, such as in modeling drainage basin evolution by mass wasting and fluvial erosion (e.g., Howard, 1994). The net rate of surface change, z , is the sum of z_w plus z_m.

The absolute values of the rate constants in the model are arbitrary. Their relative values were chosen to reproduce the topographic patterns observed on the wind-eroded surface of the southern Saheki K2 fan (e.g., Figs. 3 and 6 through 9). We view the model to be an illustrative portrayal of the pattern of wind erosion and layer exposure pattern, rather than being quantitatively accurate.

Acknowledgements

This study was partially supported by the NASA Graduate Student Researchers Program, NASA grants NNX08AE47A, NNX08AM91G, NNX09AM02G, and NNX12AM73H, and by an award to Y. Matsubara by the Department of Environmental Sciences, University of Virginia.

References

Amundson, R., et al., 2012. Geomorphologic evidence for the late Pliocene onset of hyperaridity in the Atacama Desert. Geological Society of America Bulletin 124**,** 1048-1070.

Anderson, R., Bell, J. F. I., 2010. Geologic mapping and characterization of Gale Crater and implications for its potential as a Mars Science Laboratory landing site. The Mars Journal 5**,** 76-128.

Andrews, E. D., 1984. Bed-material entrainment and hydraulic geometry of gravel-bed rivers in Colorado. Geological Society of America Bulletin 95**,** 371-378.

Ansan, V., et al., 2011. Stratigraphy, mineralogy, and origin of layered deposits inside Terby crater, Mars. Icarus 211**,** 273-304.

Armitage, J. J., Warner, N. H., Goddard, K., Gupta, S., 2011. Timescales of alluvial fan development by precipitation on Mars. Geophysical Research Letters 38**,** L17203, doi:10.1029/2011GL048907.

Balme, M., Berman, D. C., Bourke, M. C., Zimbelman, J. R., 2008. Transverse Aeolian Ridges (TARs) on Mars. Geomorphology 101**,** 703-720.

Berman, D. C., Balme, M. R., Rafkin, S. C. R., Zimbelman, J. R., 2011. Transverse Aeolian RIdges (TARs) on Mars II: Distributions, orientations, and ages. Icarus 213**,** 116-130.

Blair, T. C., 2003 Features and origin of the giant Cucomungo Canyon alluvial fan, Eureka Valley, California. In: M. A. Chan, A. W. Archer, (Eds.), Extreme Depositional Environments: Mega End Members in Geologic Time. Geological Society of America, Denver, CO, pp. Special Paper 370, 105-126.

1243 Blair, T. C., McPherson, J. G., 2009. Processes and forms of alluvial fans. In: A. J. Parsons, A.
1244 D. Abrahams, (Eds.), Geomorphology of Desert Environments. Springer
1245 Science+Business Media B. V., pp. 413-466.
1246 Bull, W. B., 1962. Relation of textural (CM) patterns to deposition environment of alluvial-fan
1247 deposits. Journal of Sedimentary Petrology 32**,** 211-216.
1248 Bull, W. B., 1963. Alluvial-fan deposits in western Fresno County, California. Journal of
1249 Geology 71**,** 243-251.
1250 Burr, D. M., Enga, M.-T., Williams, R. M. E., Zimbelman, J. R., Howard, A. D., Brennand, T.
1251 A., 2009. Pervasive aqueous paleoflow features in the Aeolis/Zephyria Plana Region,
1252 Mars. Icarus 200**,** 52-76.
1253 Burr, D. M., Williams, R. M. E., Wendell, K. D., Chojnacki, M., Emery, J. P., 2010. Inverted
1254 fluvial features in the Aeolis/Zephyria Plana region, Mars: Formation mechanism and
1255 initial paleodischarge estimates. Journal of Geophysical Research 115**,** E07011,
1256 doi:10.1029/2009JE003496.
1257 Carr, M. H., 2006, The Surface of Mars, 2nd Ed., Cambridge, Cambridge University Press
1258 Carr, M. H., Head, J. W., 2010. Geologic history of Mars. Earth and Planetary Science Letters
1259 294**,** 185-203.
1260 Chan, M. A., Yonkee, W. A., Netoff, D. I., Seiler, W. M., Ford, R. L., 2008. Polygonal cracks in
1261 bedrock on Earth and Mars: Implications for weathering. Icarus 194**,** 65-71.
1262 Costa, J. E., 1984 Physical geomorphology of debris flows. In: J. E. Costa, P. J. Fleisher, (Eds.),
1263 Developments and applications of geomorphology. Springer-Verlag, pp. 268-317.

1264 Costa, J. E., 1988 Rheologic, geomorphic, and sedimentologic differentiation of water floods,
1265 hyperconcentrated flows, and debris flows. In: V. R. Baker, et al., (Eds.), Flood
1266 geomorphology. Wiley-Interscience, pp. 113-122.
1267 Dade, W. B., Friend, P. F., 1998. Grain-size, sediment-transport regime, and channel slope in
1268 alluvial rivers. Journal of Geology 106**,** 661-675.
1269 Dixon, J. C., 2009 Aridic soils, patterned ground, and desert pavements. In: A. J. Parsons, A. D.
1270 Abrahams, (Eds.), Geomorphology of Desert Environments. Springer Science+Business
1271 Media B. V., pp. 101-122.
1272 El Maarry, M. R., Kodikara, J., Wijessoriya, S., Markiewicz, W. J., Thomas, N., 2012.
1273 Desiccation mechanism for formation of giant polygons on Earth and intermediate-sized
1274 polygons on Mars: Results from a pre-fracture model. Earth and Planetary Science
1275 Letters 323-324**,** 19-26.
1276 El Maarry, M. R., Markiewicz, W. J., Mellon, M. T., Goetz, W., Dohm, J. M., Pack, A., 2010.
1277 Crater floor polygons: Desiccation patterns of ancient lakes on Mars? Journal of
1278 Geophysical Research 115, E10006, doi:10.1029/2010JE003609.
1279 Fassett, C. I., Dickson, J. L., Head, J. W., Levy, J. S., Marchant, D. R., 2010. Supraglacial and
1280 proglacial valleys on Amazonian Mars. Icarus 208**,** 86-100.
1281 Fassett, C. I., Head, J. W., 2011. Sequence and timing of conditions on early Mars. Icarus 211**,**
1282 1204-1214.
1283 Ferguson, R., 2007. Flow resistance equations for gravel- and boulder-bed streams. Water
1284 Resources Research 43**,** W05427, doi:10.1029/2006WR005422.
1285 Field, J., 2001. Channel avulsion on alluvial fans in southern Arizona. Geomorphology 37**,** 93-
1286 104.

1287 Forget, F., Wordsworth, R., Millour, E., Madeleine, J.-B., Kerber, L., Leconte, J., Marcq, E.,
1288 Haberle, R. M., 2013. 3D modelling of the early martian climate under a denser CO2
1289 atmosphere: Temperatures and CO2 ice clouds. Icarus 222, 81-99.
1290 Garvin, J. B., Sakimoto, S., Frawley, J. J., 2003. Craters on Mars: Global geometric properties
1291 from gridded MOLA topography. Sixth Intern. Conf. Mars, Pasadena, Ca. Abstract 3277.
1292 Gillies, J. A., Nickling, W. G., Tilson, M., Furtak-Cole, E., 2012. Wind-formed gravel bed
1293 forms, Wright Valley, Antarctica. Journal of Geophysical Research 117**,** F04017,
1294 doi:10.1029/2012JF002378.
1295 Goldspiel, J. M., and Squyres, S. W., 2000, Groundwater sapping and valley formation on Mars
1296 Icarus, 148, 176-192.
1297 Goldspiel, J. M., and Squyres. S. W., 2011, Groundwater discharge and gully formation on
1298 martian slopes. Icarus 2011, 238-258.
1299 Grant, J. A., Wilson, S. A., 2011. Late alluvial fan formation in southern Margaritifer Terra,
1300 Mars. Geophysical Research Letters 38**,** L08201, doi:10.1029/2011GL046844.
1301 Grant, J. A., Wilson, S. A., 2012. A possible synoptic source of water for alluvial fan formation
1302 in southern Margaritifer Terra, Mars. Planetary and Space Science 72**,** 44-52.
1303 Greeley, R. White, B., Leach, R., Iversen, J. Pollack, J., 1976. Mars: Wind friction speeds for
1304 particle movement, Geophysical Research letters. 3, 417-420.
1305 Greeley, R., Guest, J. E., 1987. Geologic Map of the Eastern Equatorial Region of Mars. U. S.
1306 Geological Survey Miscellaneous Investigations Series Map. I-1802-B.
1307 Hanks, T. C., Andrews, D. J., 1989. Effect of far-field slope on morphologic dating os scarp-like
1308 landforms. Journal of Geophysical Research 94**,** 565-573.

1309 Harris, R. C., 2004. Giant dessication cracks in Arizona. Arizona Geological Survey. Open-File
1310 Report 04-01**,** 1-93.
1311 Harrison, K. P., and Grimm, R. E., 2009. Regionally compartmented groundwater flow on Mars.
1312 Journal of Geophysical Research 114, E04004, doi: 10.1029/2008JE003000.
1313 Hartmann, W. K., 2007. Martian cratering 9: Toward resolution of the controversy about small
1314 craters. Icarus. 189**,** 274-278.
1315 Hartmann, W. K., Neukum, G., 2001. Cratering chronology and the evolution of Mars. Space
1316 Science Reviews 96**,** 165-194.
1317 Hartmann, W. K., Neukum, G., Werner, S., 2008. Confirmation and utilization of the
1318 "production function" size-frequency distributions of Martian impact craters.
1319 Geophysical Research Letters 35, L02205, doi:10.1029/2007GL031557.
1320 Hartmann, W. K., Werner, S. C., 2010. Martian Cratering 10. Progress in use of crater counts to
1321 interpret geological processes: Examples from two debris aprons. Earth and Planetary
1322 Science Letters 294**,** 230-237.
1323 Harvey, A. M., 1999 The occurrence and role of arid zone alluvial fans. In: D. S. G. Thomas,
1324 (Ed.), Arid Zone Geomorphology. Halstead Press, New York, pp. 136-158.
1325 Hooke, R. L., 1967. Processes on arid-region alluvial fans. Journal of Geology. 75**,** 438-460.
1326 Houston, J., 2002. Groundwater recharge through an alluvial fan in the Atacama Desert, northern
1327 Chile: mechanisms, magnitudes and causes. Hydrological Processes. 16, 3019-3035.
1328 Houston, J., 2006. The great Atacama flood of 2001 and its implications for Andean hydrology.
1329 Hydrological Processes 20**,** 591-610.
1330 Howard, A. D., 1980 Thresholds in river regimes. In: D. R. Coates, J. D. Vitek, (Eds.),
1331 Thresholds in geomorphology. George Allen & Unwin, London, pp. 227-258.

1332 Howard, A. D., 1994. A detachment-limited model of drainage-basin evolution. Water Resources
1333 Research 30**,** 2261-2285.
1334 Howard, A. D., 2009, Badlands and gullying. In: A. J. Parsons, A.D. Abrahams, (Eds.),
1335 Geomorphology of Desert Environments. Springer Verlag, pp. 233-263.
1336 Howard, A. D., Moore, J. M., 2011. Late Hesperian to early Amazonian midlatitude Martian
1337 valleys: Evidence from Newton and Gorgonum basins. Journal of Geophysical Research.
1338 116**,** E05003, doi:10.1029/2010JE003782.
1339 Howard, A. D., Moore, J. M., Irwin, R. P., III, 2005. An intense terminal epoch of widespread
1340 fluvial activity on early Mars: 1. Valley network incision and associated deposits. Journal
1341 of Geophysical Research 110**,** doi:10.1029/2005JE002459.
1342 Hunt, C. B., Robinson, T. W., Bowles, W. A., Washburn, A. L., 1966. General geology of Death
1343 Valley, California; Hydrologic Basin. U. S. Geological Survey Professional Paper.
1344 Report: P 0494-B.
1345 Hynek, B.M., Beach, M., Hoke, M.R.T., 2010. Updated global map of martian valley networks
1346 and implications for climate and hydrologic processes. Journal of Geophysical Research
1347 115, E09008, doi:10.1029/2009JE003548.
1348 Irwin, R. P. I., Tanaka, K. L., Robbins, S. J., 2013. Distribution of Early, Middle, ad Late
1349 Noachian cratered surface in the Martian highlands: Implications for resurfacing events
1350 and processes. Journal of Geophysical Research 118, 278-291, doi:10.1002/jgre.20053.
1351 Ivanov, B. A., 2001. Mars/Moon cratering rate ratio estimates. Space Science Reviews 96**,** 87-
1352 104.
1353 Jerolmack, D. J., Mohrig, D., Grotzinger, J. P., Fike, D. A., Watters, W. A., 2006. Spatial grain
1354 size sorting in eolian ripples and estimation of wind conditions on planetary surfaces:

1355 Application to Meridiani Planum, Mars. Journal of Geophysical Research 111**,** E12S02,
1356 10.1029/2005je002544.
1357 Jerolmack, D. J., Mohrig, D., Zuber, M. T., Byrne, S., 2004, A minimum time scale for
1358 formation of Holden Northeast fan, Mars, Geophysical Research Letters 31, L21701,
1359 doi:10.1029/2004GL021326.
1360 Johnson, A. M., 1984 Debris Flow. In: D. Brunsden, D. B. Prior, (Eds.), Slope Instability. John
1361 Wiley & Sons, Chichester, pp. 257-361.
1362 Kiefer, E., Dörr, M. J., Ibbeken, H., and Götze, H. J., 1997. Gravity-based mass balance of an
1363 alluvial fan giant: the Arcas Fan, Pampa del Tamarugal, Northern Chile. Revista
1364 Geológica de Chile. 24, 165-185.
1365 Kite, E. S., Halevy, I., Kahre, M. A., Wolff, M. J., Manga, M., 2013. Seasonal melting and the
1366 formation of sedimentary rocks on Mars, with predictions for the Gale Crater mound.
1367 Icarus 223**,** 181-210.
1368 Kleinhans, M. G., 2005. Flow discharge and sediment transport models for estimating a
1369 minimum timescale of hydrological activity and channel and delta formation on Mars.
1370 Journal of Geophysical Research 110**,** E12003, doi:10.1029/2005JE002521.
1371 Knighton, A. D., 1998. Fluvial Forms and Processes: A New Perspective. Arnold, London.
1372 Korteniemi, J., Kreslavsky, M. A., 2012. Patterned ground in martian high northern latitudes:
1373 Morphology and age constraints. Icarus, doi:10.1016/j.icarus.2013.09.032, in press.
1374 Kraal, E. R., Asphaug, E., Moore, J. M., Howard, A., Bredt, A., 2008. Catalogue of large alluvial
1375 fans in martian impact craters. Icarus 194**,** 101-110.

1376 Lamb, M. P., Dietrich, W. E., Sklar, L. S., 2008. A model for fluvial bedrock incision by
1377 impacting suspended and bed load sediment. Journal of Geophysical Research 113**,**
1378 F03025, doi:10.1029/2007JF000915.
1379 Langer, A. M., Kerr, P. F., 1966. Mojave Playa crusts; physical properties and mineral content.
1380 Journal of Sedimentary Petrology 36**,** 377-396.
1381 Laskar, J., Correia, A. C. M., Gastineau, M., Joutel, F., Levrard, B., Robutel, P., 2004. Long term
1382 evolution and chaotic diffusion of the insolation quantities of Mars. Icarus 170**,** 343-364.
1383 Lasue, J. et al., 2013. Quantitative assessments of the Martian hydrosphere. Space Science
1384 Reviews, 174. 155-212.
1385 Levy, J., Head, J., Marchant, D., 2009. Thermal contraction crack polygons on Mars:
1386 Classification, distribution, and climate implications from HiRISE observations. Journal
1387 of Geophysical Research 114, E01007, doi:10.1029/2008JE003273.
1388 Lewis, K.W., and Aharonson, O., 2006. Stratigraphic analysis of the distributary fan in
1389 Eberswalde crater using stereo imagery. Journal of Geophysical Research 111, E06001,
1390 doi:10.1029JE002558.
1391 Malin, M. C., and Carr, M. H., 1999. Groundwater formation of Martian valleys. Nature 397,
1392 589-591.
1393 Malin, M. C., et al., 2007. Context Camera Investigation on board the Mars Reconnaissance
1394 Orbiter. Journal of Geophysical Research E: Planets 112**,** Article Number E05S04,
1395 doi:10.1029JE002808.
1396 Malin, M. C. and Edgett, K. S., 2000. Evidence of recent groundwater seepage and surface
1397 runoff on Mars. Science 288, 2330-2335.

1398 Malin, M. C., Edgett, K. S., 2003. Evidence for persistent flow and aqueous sedimentation on
1399 early Mars. Science 302**,** 1931-1934.
1400 Mangold, N., Forget, F., Maurice, S., Feldman, W. C., Costard, F., 2004. Spatial relationships
1401 between patterned ground and ground ice detected by the Neutron Spectrometer on Mars.
1402 Journal of Geophysical Research E: Planets. 109**,** E08001, doi:10.1029/2004JE002235.
1403 Mangold, N., 2012. Fluvial valleys on fresh impact ejecta on Mars. Planetary and Space
1404 Sciences. 62, 69-85.
1405 Mangold, N., Adeli, S., Conway, S., Ansan, V., Langlais, B., 2012a. A chronology of early Mars
1406 climatic evolution from impact crater degradation. Journal of Geophysical Research 117,
1407 E04003, doi:10,1029/2011JE004005.
1408 Mangold, N., et al., 2012b. The origin and timing of fluvial activity at Eberswalde crater, Mars.
1409 Icarus 220**,** 530-551.
1410 Marchant, D. R., and Head, J. W., 2007. Antarctic dry valleys: Microclimate zonation, variable
1411 geomorphic processes, and implications for assessing climate change on Mars. Icarus
1412 182, 187-222.
1413 Matsubara, Y., Howard, A. D., Burr, D. M., Williams, R. M., Moore, J. M.,2012. Meandering
1414 channels in a non-vegetated area: Quinn River, NV as a martian analog. 43rd Lunar and
1415 Planetary Science Conference, Abstract 2534, the Woodlands, Texas.
1416 McEwen, A. S. and Bierhaus, E. B., 2006b The importance of cecondary cratering to age
1417 constraints on planetary surfaces. Annual Review of Earth and Planetary Science, 34,
1418 535-567.
1419 McEwen, A., et al., 2005. The rayed crater Zunil and interpretations of small impact craters on
1420 Mars. Icarus 176**,** 351-381.

McEwen, A. S., et al., 2007. Mars reconnaissance orbiter's high resolution imaging science experiment (HiRISE). Journal of Geophysical Research E: Planets. 112**,** Article Number E05S02, doi:10.1029/2005JE002605.

Mellon, M. T., 1997. Small-scale polygonal features on Mars: Seasonal thermal contraction cracks in permafrost. Journal Geophysical Research 102**,** 25617-25628.

Michael, G. G., Neukum, G., 2010. Planetary surface dating from crater size–frequency distribution measurements: Partial resurfacing events and statistical age uncertainty. Earth and Planetary Science Letters 294**,** 223-229.

Moore, J., M., Howard, A. D., 2005. Large alluvial fans on Mars. Journal of Geophysical Research 110**,** E04005, doi:10.1029/2004JE002352.

Moore, J. M., Howard, A. D., Dietrich, W. E., Schenk, P. M., 2003. Martian layered fluvial deposits: Implications for Noachian climate scenarios. Geophysical Research Letters 30**,** 2292, doi:10.1029/2003GL019002.

Morato, Z. M., Broxton, M. J., Beyer, R. A., Lundy, M., Husmann, K., 2010. Ames Stereo Pipeline, NASA's open source automated stereogrammetry software. Lunar and Planetary Science Conference 41. Abstract 2364.

Morgan, A.M., Beyer, R.A., Howard, A.D., Moore, J.M., (2012a) The Alluvial Fans of Saheki Crater. Abstract #2815, 43rd Lunar and Planetary Science Conference, The Woodlands, TX.

Morgan, A.M., Howard, A.D., Moore, J.M., Hobley, D. E. J., Beyer, R.A. (2012b) Episode(s) of intense alluvial deposition during an era of drought on Mars: Evidence from fans at Saheki (and Gale?). Abstract P11B-1830, 2012 Fall Meeting, AGU, San Francisco, CA, 3-7 Dec.

1443 Morgan, G. A., Head, J. W. III, 2009. Sinton crater, Mars: Evidence for impact into a plateau
1444 icefield and melting to produce valley networks at the Hesperian–Amazonian boundary.
1445 Icarus 202, 39-59.
1446 Murchie, S., et al., 2007. Compact Reconnaisance Imaging Spectrometer for Mars (CRISM) on
1447 Mars Reconnaissance Orbiter (MRO). Journal of Geophysical Research 112**,** E05S03,
1448 doi:10.1029/2006JE002682.
1449 Neal, J. T., Langer, A. M., Kerr, P. F., 1968. Giant dessication polygons of Great Basin playas.
1450 Geological Society of America Bulletin 79**,** 69-90.
1451 Parker, G., 1978. Self-formed straight rivers with equilibrium banks and mobile bed. Part 2. The
1452 gravel river. Journal of Fluid Mechanics 89**,** 127-146.
1453 Pondrelli, M., Rossi, A. P., Marinagleli, L., Hauber, E., Gwinner, K., Baliva, A., Di Lorenzo, S.,
1454 2008, Evolution and depositional environments of the Eberswalde fan delta, Mars, Icarus
1455 197, 429-451
1456 Pondrelli, M., Rossi, A. P., Platz, T., Ivanov, A., Marinangeli, L., Baliva, A., 2011, Geological,
1457 geomorphological, facies and allostratigraphic maps of the Eberswalde fan delta.
1458 Planetary and Space Science 59, 1166-1178.
1459 Pueyo, J. J., Chong, G., Jensen, A., 2001. Neogene evaporites in desert volcanic environments:
1460 Atacama Desert, northern Chile. Sedimenology 48**,** 1411-1431.
1461 Rickenmann, D., Recking, A., 2011. Evaluation of flow resistance in gravel-bed rivers through a
1462 large field data set. Water Resources Research 47**,** W07538,
1463 doi:10.1029/2010WR009703.

1464 Roering, J. J., Kirchner, J. W., Dietrich, W. E., 1999. Evidence for nonlinear, diffusive sediment
1465 transport on hillslopes and implications for landscape morphology. Water Resources
1466 Research. 35**,** 853-870.
1467 Roering, J. J., Kirchner, J. W., Dietrich, W. E., 2001. Hillslope evolution by nonlinear, slope-
1468 dependent transport; steady state morphology and equilibrium adjustment timescales.
1469 Journal of Geophysical Research, B, Solid Earth and Planets 106**,** 16,499-16,513.
1470 Servicio Nacional de Geologia y Mineria, G. d. C., 2003. Mapa Geologico de Chile: Version
1471 Digital. Publication Geologica Digital, No. 4.
1472 Shaw, P. A., Thomas, D. S. G., 1989. Playas, pans and salt lakes. In: D. S. G. Thomas, (Ed.),
1473 Arid Zone Geomorphology. John Wiley & Sons, New York, pp. 184-205.
1474 Smith, G. I., 1957. Core logs from Owens, China, Searles and Panamint basins, California. U.S.
1475 Geological Survey Bulletin 1045-A.
1476 Smith, G. I., 1974. Subsurface stratigraphy and geochemistry of Late Quaternary evaporites,
1477 Searles Lake, California. U.S. Geological Survey Professional Paper 1043. 1-130.
1478 Smoot, J. P., Castens-Seidel, B., 1995 Sedimentary features produced by efflorescent salt crusts,
1479 Saline Valley and Death Valley, California. Sedimentology and Geochemistry of Modern
1480 and Ancient Saline Lakes. Society for Sedimentary Geology, pp. 73-90.
1481 Spötl and Wright, 1992., Groundwater Dolocretes from the Upper Triassic of the Paris Basin,
1482 France: a Case Study of an Arid, Continental Diagenetic Facies. Sedimentology. 36,
1483 1119-1136.
1484 Stock, J. D., 2013 Waters divided: A history of alluvial fan research and a view of its future. In:
1485 J. Shroder, E. Wohl, (Eds.), Treatise on Geomorphology. Academic Press, San Diego,
1486 CA, pp. in press.

1487 Stock, J. D., Schmidt, K. M., Miller, D. M., 2008. Controls on alluvial fan long-profiles.
1488 Geological Society of America Bulletin 120**,** 619-640.
1489 Stoertz, G. E., Ericksen, G., E., 1974. Geology of Salars in Northern Chile. U. S. Geological
1490 Survey. Professonal Paper 811**,** 65 p.
1491 Sullivan, R., et al., 2008. Wind-driven particle mobility on Mars: Insights from Mars Exploration
1492 Rover observations at "El Dorado" and surroundings at Gusev Crater. Journal of
1493 Geophysical Research. 113**,** E06S07, doi:10.1029/2008JE003101.
1494 Talling, P. J., 2000. Self-organization of river networks to threshold states. Water Resources
1495 Research 36**,** 1119-1128.
1496 Tanaka, K. L., 1986. The stratigraphy of Mars. Journal Geophysical Research 91(B13)**,** E139-
1497 E158.
1498 Ward, W. R., 1979. Present obliquity oscillations of Mars - Fourth-order accuracy in orbital E
1499 and I. Journal Geophysical Research 84**,** 237-241.
1500 Weinberger, R., 1999. Initiation and growth of cracks during dessication of stratified muddy
1501 sediments. Journal of Structural Geology 21**,** 379-386.
1502 Wentworth, C. K., 1922. A scale of grade and class terms for clastic sediments. Journal of
1503 Geology. 30, 377-392.
1504 Werner, S. C., Ivanov, B. A., Neukum, G., 2009. Theoretical analysis of secondary cratering on
1505 Mars and an image-based study on the Cerberus Plains. Icarus 200**,** 406-417.
1506 Werner, S. C., Tanaka, K. L., 2011. Redefinition of the crater-density and absolute-age
1507 boundaries for the chronostratigraphic system of Mars. Icarus 215**,** 603-607,
1508 doi:10.1016/j.icarus.2011.07.024.

1509 Williams, K., Toon, O., Heldmann, J., McKay, C., Mellon, M., 2008a. Stability of mid-latitude
1510 snowpacks on Mars. Icarus 196**,** 565-577.
1511 Williams, K., Toon, O., Heldmann, J., Mellon, M., 2009a. Ancient melting of mid-latitude
1512 snowpack on Mars as a water source for gullies. Icarus 200**,** 418-425.
1513 Williams, R. M. E., et al., 2011. Evidence for episodic alluvial fan formation in far western Terra
1514 Tyrrhena, Mars. Icarus 211**,** 222-237.
1515 Williams, R. M. E., et al, 2013. Martian fluvial conglomerates at Gale crater. Science. 340, 1068-
1516 1072.
1517 Williams, R. M. E., Irwin, R. P., Zimbelman, J. R., 2009b. Evaluation of paleohydrologic models
1518 for terrestrial inverted channels: Implications for application to martian sinuous ridges.
1519 Geomorphology. 107**,** 300-315.
1520 Williams, R. M. E., Malin, M. C., 2008b. Sub-kilometer fans in Mojave Crater, Mars. Icarus 198**,**
1521 365-383.
1522 Wilson, L., Ghatan, G. J., Head, I. J. W., Mitchell, K. L., 2004. Mars outflow channels: A
1523 reappraisal of the estimation of water flow velocities from water depths, regional slopes,
1524 and channel floor properties. Journal of Geophysical Research E: Planets 109**,** E09003 1-
1525 10.
1526 Wilson, S. A. and J. R. Zimbelman, 2004, Latitude-dependent nature and physical characteristics
1527 of transverse aeolian ridges on Mars, Journal of Geophysical Research E: Planets 109,
1528 E10003, doi: 10.1029/2004JE002247.
1529 Wilson, S. A., Grant, J. A., Howard, A. D., 2013. Inventory of alluvial fans and deltas on Mars.
1530 Lunar and Planetary Sci. Conf. XLIV. Abstract 2710.

1531 Wilson, S. A., Howard, A. D., Moore, J. M., Grant, J. A., 2007. Geomorphic and stratigraphic
1532 analysis of Crater Terby and layered deposits north of Hellas basin, Mars. Journal of
1533 Geophysical Research E: Planets 112**,** E08009, doi:10.1029/2006JE002870.
1534 Wordsworth, R., Forget, F., Millour, E., Head, J. W., Madeleine, J.-B., Charnay, B., 2013.
1535 Global modeling of the early martian climate under a censer CO_2 atmosphere: Water
1536 cycle and ice evolution. Icarus 222**,** 1-19.
1537 Yechieli, Y., Wood, W. W., 2002. Hydrogeologic processes in saline systems: Playas, sabkhas,
1538 and saline lakes. Earth-Science Reviews 58**,** 343-365.
1539 Zimbelman, J. R., Irwin, R. P. I., Williams, S. H., Bunch, F., Valdez, A., Stevens, S., 2009. The
1540 rate of granule ripple movement on Earth and Mars. Icarus 203**,** 71-76.
1541 Zuber, M. T., et al., 1992. The Mars Observer laser altimeter investigation. Journal of
1542 Geophysical Research 97**,** 7781-7797.
1543

Figure Captions

Figure 1. Regional digital elevation location map of the northern Hellas rim. Image extends from 15°S to 30°S and 65°E to 85°E, Mercator projection. Letters in parentheses indicate crater designation in *Moore and Howard* (2005). "@" symbols show craters hosting fans identified by *Kraal et al*. (2008) and *Wilson et al*. (2007, 2013). Box shows location of Figure 2. Topographic scale is in meters to Mars datum. North is up in this and all following figures (excluding photographs).

Figure 2. Close up of boxed area of Fig. 1. Saheki crater exhibits poorly expressed proximal crater ejecta, a total floor to rim relief of ~2.5 km, and a central peak that rises approximately one kilometer above the crater floor. Crater "L" is 20 km to the southwest of Saheki. Individual fans and source basins are outlined in white and are marked with asterisks and arrows, respectively. Small fans denoted by "@". Fan notation follows Moore and Howard (2005). Scale is in meters to Mars datum.

Figure 3. Interpretive map of southern portion of the Saheki crater K2 fan and related features. The central peak and degraded interior rim are in the upper right and lower left, respectively. Also along the southern edge of the fan are slumps sourced from the crater walls which pre-date the fan material. Numbers indicate locations of additional figures. Purple lines and areas are raised ridges and platforms interpreted to be fluvial distributaries radiating from the fan apex at the upper left. Where the linear ridges or paired ridges are less than about 100 m in width they are shown as purple lines, but broader ridges and level platforms are portrayed as purple areas. Aeolian erosion has raised these into varying degrees of inverted relief. Red areas are crater floor

materials interpreted to be megabreccia. Cyan features along southern margin of fan are flat-topped benches interpreted to be lacustrine or playa deposits contemporaneous with the fan. Uncolored areas on the fan are discontinuous distributaries and low areas partially mantled by transverse aeolian ridges (TARs). Mosaic of ~6 m/pixel CTX images P17_007543_1586, P19_008545_1576, and B09_007543_1586 centered at 21.96°S, 72.81°E.

Figure 4. Detail of inverted ridges and interbedded fine sediment exposed on subjacent slopes Sediment capping ridge crests have yellowish cast relative to fine sediment. Fine aeolian sediment concentrated on north side of ridges has distinct bluish tone. Note scalloped indentations on ridge crests, presumably due to wind scour. Part of IRB color ~.3 m/pixel HiRISE image PSP_007688_1575 centered on 22.092°S, 72.966°E, with colors stretched for clarity. Portions of low areas are occupied by TAR ridges.

Figure 5. Radial topographic profiles through Saheki crater. Saheki crater is approximately circular and the eastern half of the crater floor is nearly flat, making radial profiles A through E nearly coincident, whereas F to I cross the K1 and K2 fans permitting depth estimates assuming a symmetrical initial crater. Difference between the two sets of profiles provides an estimate of fan deposit thickness, reaching a maximum of about 850 m near the fan apices. Profiles H and I approximately follow the main valley axes of the source basins upstream from the K1 and K2 fans. Topography from interpolated MOLA PEDR data.

Figure 6. Down-fan transition from a linear depression (D) through a U-shaped trough (delimited by black arrows) to a linear ridge (R) delimited by white arrows. Feature is interpreted

as a fluvial channel with increasing degree of exposure and inversion down-fan due to increasing depth of aeolian deflation. Parallel ridges (black arrows) may be narrow natural levees. Part of ~.3 m/pixel HiRISE image ESP_029788_1575, centered at 22.123°S, 72.906°E.

Figure 7. Flat platforms on the K2 fan. We interpret the ridges to be mantled with gravelly sediment deposited by low-sinuosity meandering or braiding streams during deposition. An interpreted meander bend is shown by dashed white lines, and possible point-bar deposits interior to the bend occur near the asterisks, with black arrows pointing in the direction of inferred meandering. Paired white arrows on right hand of image shows ridges representative of those sampled to determine original widths. Paired black arrows show paired narrow ridges interpreted to be natural levees exposed through partial aeolian distributary exposure. Part of ~.3 m/pixel HiRISE image PSP_007588_1675, centered at 22.016°S and 72.936°E.

Figure 8. Splay-like inverted platforms. White arrows show outer limits of splay. Ridges on surface of ridge suggest a spreading, possibly avulsive set of channels. Splays generally terminate down-fan in multiple finger-like ridges, separated by incised linear depressions (black arrows point upstream). All images at same scale. These structures are interpreted as fluvial deposits generally fed by a single channel upstream that spread into local depressions on the fan surface, or as autogenic transverse bars causing upstream deposition. Flows across the splay deposit eventually incise into the distal end of the deposit (black arrows). Images are part of ~6 m/pixel CTX image P14_006686_1579. (a) Centered at 21.927°S 72.634°E, (b) at 22.019°S, 72.811°E, and (c) at 22.141°S, 72.863°E.

Figure 9. Shaded relief image of the distal end of the Saheki K2 fan from ~3 m DEM constructed from HiRISE stereo image pair PSP_7688_1575 and PSP_008545_1575, centered at 22.10°S, 72.97°E. A plane fit to the overall dip (0.03 ESE) and strike (NNE) of the fan surface was subtracted from the DEM, and elevations (in meters) relative to that plane are indicated in color shading. Portions of the fan surface at approximately equal stratigraphic level have the same relative elevation. This indicates that the depth of aeolian erosion increases towards the distal end of the fan, which is accordant with higher ridge inversion near the distal end of the fan. Axis labels in degrees North and East. Portions of image not mantled with fan deposits are uncolored.

Figure 10. Detail of inverted ridge showing gravelly sediment and wind scoured surface. Inset is magnified 3x. Layered sediments exposed on slopes below ridge. Part of ~.3 m/pixel HiRISE image PSP_007688_1575 centered at 22.049°S and 72.944°E.

Figure 11. Distribution of coarse-grained deposits on part of the Saheki K2 fan. These occurrences were mapped on 0.25 m/pixel HiRISE images PSP_007686_1575 (lower red outlined area) and PSP_006686_1580 (upper left red area). Mapping additionally included the remainder of these images and HiRISE image PSP_007899_1580 near the apex of the K2 fan (not shown). Visible coarse deposits and characteristic mottling or speckling in HiRISE images indicated by solid and hollow diamonds, respectively. These are interpreted as deposits of gravel just below the limit of resolution of individual boulders. Image base is CTX image P19_008545_1576 centered at 22.02°S, 92.96°E.

Figure 12. Histogram of measured channel widths. Average width of segments is 38 meters.

Figure 13. Layered deposits exposed on slope below narrow ridge. (a) Exposed layers. Note thick, medium toned layers about 2-3 m thick separated by thin, light-toned layers with nodular or discontinuous presentation. (b) Interpretation of layering in (a), showing layer pinch-out locations indicated with an asterisk. (c) Contours from a 3 m/pixel DEM (pink) from HiRISE stereo pair PSP_7688_1575 and PSP_008545_1575 DEM superimposed on layer drawing. Ten meter contour interval. Note very shallow dip of layers broadly to the SE. Box at lower right indicates location of Fig. 14. Image scale is reduced in (c) relative to (a) and (b). Part of HiRISE image PSP_007688_1575, centered at 22.007°S, 72.975°E.

Figure 14. Detail of thin, light-toned layers interbedded with thicker, massive layers (see Fig. 13 for context). Note the discontinuous appearance of the layers and indications of concave-upward layer cross-section. Part of HiRISE image PSP_007688_1575, centered at 22.008°S, 72.982°E.

Figure 15. Thick sequence of beds in eastern wall of a 5.3 km diameter crater superimposed onto fan deposits adjacent to Saheki central peak. Finest visible beds are ~2 m thick. Thicker blobs, as near "1" may be channel deposits. Circular features 2 and 3, obscuring bedding, may be scars of small impacts into interior crater wall. Note faulting in near left and right side of image, presumably due to impact deformation. Bottom of layer sequence at lower left of image where coarse crater floor or central peak materials are exposed. Image DN highly stretched to emphasize layering. Part of HiRISE image ESP_013226_1580, centered at 21.762°S, 73.046°E.

Figure 16. Flat-topped benches at boundary between southern K2 fan deposits and Saheki crater wall. Note multiple levels and irregular terrace edges. Arrow points to location where inverted fan ridge may be at the same elevation at the adjacent terrace. Box shows location of Figure 17. Part of CTX image P19_008545_1576_XI_22S287W centered at 22.216°S and 72.946°E.

Figure 17. Benches at two levels (see Fig. 16 for context). Note pitted surface, interpreted to be the result of impact gardening. The bench surface is mantled with coarse blocks, which are mass-wasted onto slopes at terrace edges. Fine, layered sediment that is largely conformable with overlying benches is exposed on slopes below benches. Benches are interpreted to be chemically-cemented lacustrine or playa deposits. Part of HiRISE image PSP_007688_1575.

Figure 18. Rough-textured, nearly level surface in the interior of "L" crater (red outlining), located at the point of convergence of several fans. Surface of deposit as well as ridges on surrounding fans are slightly inverted due to aeolian erosion. Deposit is interpreted as cemented playa or shallow lacustrine sediments sourced from runoff from the adjacent fans. Note the similarity in morphology to benches in Figs. 16 and 17 in Saheki crater. Part of map-projected CTX image P3_002295_1568, centered at 23.060°S, 74.030°E.

Figure 19. Crater age determination plots. N-H and H-A indicate Noachian-Hesperian and Hesperian-Amazonian boundaries. Absolute age determination used craters greater than 500 meters in diameter to avoid errors arising from aeolian erosion (see text for discussion). **Red:** K1 fan. **Black:** Aggregate of four fans in "L" Crater. **Green:** K2 fan. The young age and large error bars for the K2 fan can likely be attributed to high amount of aeolian modification.

Figure 20. Overview of geographic setting of fine grained fans in the Pampa del Tamarugo region of northern Chile, centered at 20.87°S, 69.55°W. Arrow shows lateral extent of fan complexes. Numbers show approximate location of other figures. Light-toned regions on fans have received recent deposition, whereas dark-toned areas are inactive and have accumulated a granule surface layer die to aeolian deflation. City of Iquique indicated. Base map from Yahoo! Maps.

Figure 21. Fan distributary, showing fine-grained cohesive banks and extensive overbank deposits. Bank crest to bank crest about 3 m. Photo by A. Howard. Location at about 21.097°S, 69.486°W.

Figure 22. Atacama fan flood deposits. Red-toned deposits deposited by an early 2012 flood sourced from the Andes foothills to the east. Deposits radiate from the end an entrenched channel section at left boundary. Broad sheet deposits source from overflow of main distributary channels. Earliest deposits are darkest red, with later overflows and channelized flow being lighter pink. Main distributary averages about 12m wide. Flooding and sediment deposition continued for 25 km downstream, spanning the length of the alluvial fan. Center of image at 20.765°S, 69.311°W. North is up. Iconos 0.8 m/pixel Image, taken 12/27/2012.

Figure 23. Wind-scoured surface of an Atacama fan. Reddish and light-toned surfaces expose fine-grained overbank sediments, scoured by winds directed to the right. Rounded balls of mud locally protect the surface from erosion, producing elongated tails. Darker granule-covered

aeolian ripples mantle parts of the surface as well as infilling the channel in the middle distance. Boulders aligned along the margins of the channel were deposited by overbank flows in proximal parts of levees. Photo by A. Howard. Location 21.121°S, 69.527°W.

Figure 24. Channels inverted by aeolian erosion. Arrows point to representative inverted channels. Dark coloration in vicinity of channels is granule deposits winnowed from the channel deposits. Inversion is due to coarser grain size of the channel deposits, protecting them from wind erosion and possibly chemical cementation. Note dirt track crossing image. Recent overbank deposits are pinkish. Older overbank deposits (upper left) are lightly mantled with winnowed granules as in Fig. 21. Maximum inverted channel relief 1-2 m. GeoEye imaging from Google Earth centered at 21.115°S, 69.576°W.

Figure 25. View looking upstream along the Quebrada de Guatacondo channel. Three mudflows are labeled with oldest being number one. Note that mudflows coat steep banks. Channel floor is composed of clean fluvially transported coarse sediment (gravel, cobbles, and occasionally boulders). Photo by A. Howard. Location 21.024°S, 69.367°W.

Figure 26. Complex history of distributary history on part of a fan surface. Numbers indicate sequence of fan activity (1 is oldest). Note that flow 7 has covered the railroad track crossing the image. Inactive parts of fan become darker due to progressive mantling by granule ripples derived from overbank deposits. GeoEye imaging from Google Earth centered at 20.75°S, 69.40°W, taken prior to the 2012 flood deposition.

Figure 27. Cross section of an overbank deposit containing sparse granules. Note mudcracking of overbank sediments in background. Photo by W. E. Dietrich.

Figure 28. Surveys across channel and overbank deposits of distributary shown in Figure 20, showing broad natural levees. Top cross section centered on 21.093°S, 69.478°E, bottom cross section centered on 21.100°S, 69.490°E. The bottom of the channel in the top survey is higher than the surrounding fan surface. Note 25x vertical exaggeration.

Figure 29. Interpretive model of aeolian fan erosion in Saheki crater. A hypothetical along-strike cross section of the fan is pictured, with white being fine-grained, wind-erodible overbank sediment, and blue being randomly seeded channel gravels. Wind erosion starts from the black horizontal upper surface and colored profiles show successive stages of modeled wind erosion. See Section 3.3.1 in text and Appendix A for further discussion.

Figure 30. Effect of image resolution on interpretation of gravel deposits. Images (a) and (e) are snippets from larger images of gravelly sediment. Sediment in (a) is well-sorted gravel and in (e) is poorly sorted. Images (b) and (f) show reduced resolution of full images in which the particles representative of about the 84^{th} percentile size are shown at 2 pixels per particle (for full resolution HiRISE images this would correspond to 50 cm particles). Location of snippets in (a) and (b) are shown as white boxes in (b) and (c), respectively. In (c) and (g) resolution is further reduced to 1 pixel per particle, and to ½ pixel per particle in (d) and (h). In reduced resolution images gravel shows a characteristic mottled texture. Note that scale was not provided for original images. Source for original illustrations:

1751 http://www.texturemate.com/content/free-gravel-texture-19-11-2011-001 (a)-(d)

1752 http://aquaponics.wiki.com/wiki/gravel?file=Gravel_small_stones.jpg (e)-(h)

1753

1754 **Figure 31.** Variability of calculated dominant discharges and associated flow velocities

1755 with sediment concentration in the fluid and grain size. The fields shown correspond to the

1756 effects of varying grain size across the interval $0.125 < D_{84} < 0.25$ m, consistent with

1757 observations from HiRISE (Figs. 10 and 30); higher values of discharge and velocity are derived

1758 from the coarser grain sizes.

1759

Table 1. Properties of Saheki crater fans and terrestrial Atacama Desert fans.

Property	K1 Fan	K2 Fan	Average Mars Fan[a]	Atacama Fan 1	Atacama Fan 2
Catchment Size, km^2	501	319	149	910	328
Catchment Relief, km	1.5	2.3	1.6	3.7	3.0
Catchment Gradient	0.096	0.089	0.118	0.050	0.084
Fan Size, km^2	813	750	251	199	215
Fan Relief, km	1.33	1.22	0.72	0.3	0.38
Overall Fan Gradient	0.030	0.031	0.041	0.0094	0.018
Mid-Fan Gradient	0.038	0.030	---	0.02[b]	0.028[b]
Fan Length, km	44.8	40.1	18.74	30.0	20.5
Fan Concavity[c]	0.0193	0.0045	0.0700	0.048	0.072

[a]Average of 31 large fans reported in Moore and Howard (2005)

[b]Fan gradient near apex

[c]Fan concavity is measured by $-(d^2z/dx^2)/(dz/dx)$, where z is surface elevation (m) and x is distance from the fan apex (km), estimated from measurements at the fan apex, midpoint, and termination (Moore and Howard, 2005).

Table 2. Terminology for grain sizes used in this paper based on the Wentworth (1922) classification.

Particle Size (mm)	Main Class	Subclass	Secondary Class
4096			
		Boulder	
256			
		Cobble	
64	Gravel		
4		Pebble	
			Granule
2			
		Coarse Sand	
0.5			
	Sand	Medium Sand	
0.25			
		Fine Sand	
0.0625			
	Silt[a]		
0.0039			
	Clay[a]		

[a]Silt and clay grouped together are termed “mud”.

Table 3. Grain size characteristics of Atacama fan sediment expressed as percentages with comparative values from the Cucomungo fan of California.

Description	Property	Clay	Silt	Fine-Medium Sand	Coarse Sand	Pebbles
Upstream	Average[a]	16.68	30.75	18.85	12.91	20.81
Mudflows	Minimum	9.99	21.36	11.27	0.00	0.00
	Maximum	27.53	60.95	35.52	29.30	40.01
Channel Bank	Average[b]	15.30	30.92	33.15	11.35	9.28
Deposits	Minimum	1.09	6.25	12.97	0.02	0.00
	Maximum	25.95	55.52	80.61	37.36	53.73
Overbank	Average[c]	16.74	42.53	37.64	3.09	0.00
Sediment	Minimum	12.35	34.12	12.36	0.00	0.00
	Maximum	24.28	63.37	49.27	6.75	0.00
Cucomungo	Average	1.06	8.50	42.11	29.52	18.80
Fan	Minimum	0.60	5.40	24.80	1.30	0.00
Deposits[d]	Maximum	2.20	21.80	74.70	44.50	35.50

[a]Sample size=11; [b]Sample size=22; [c]Sample size=5

[d]Summarized from Table 4 of Blair (2003)

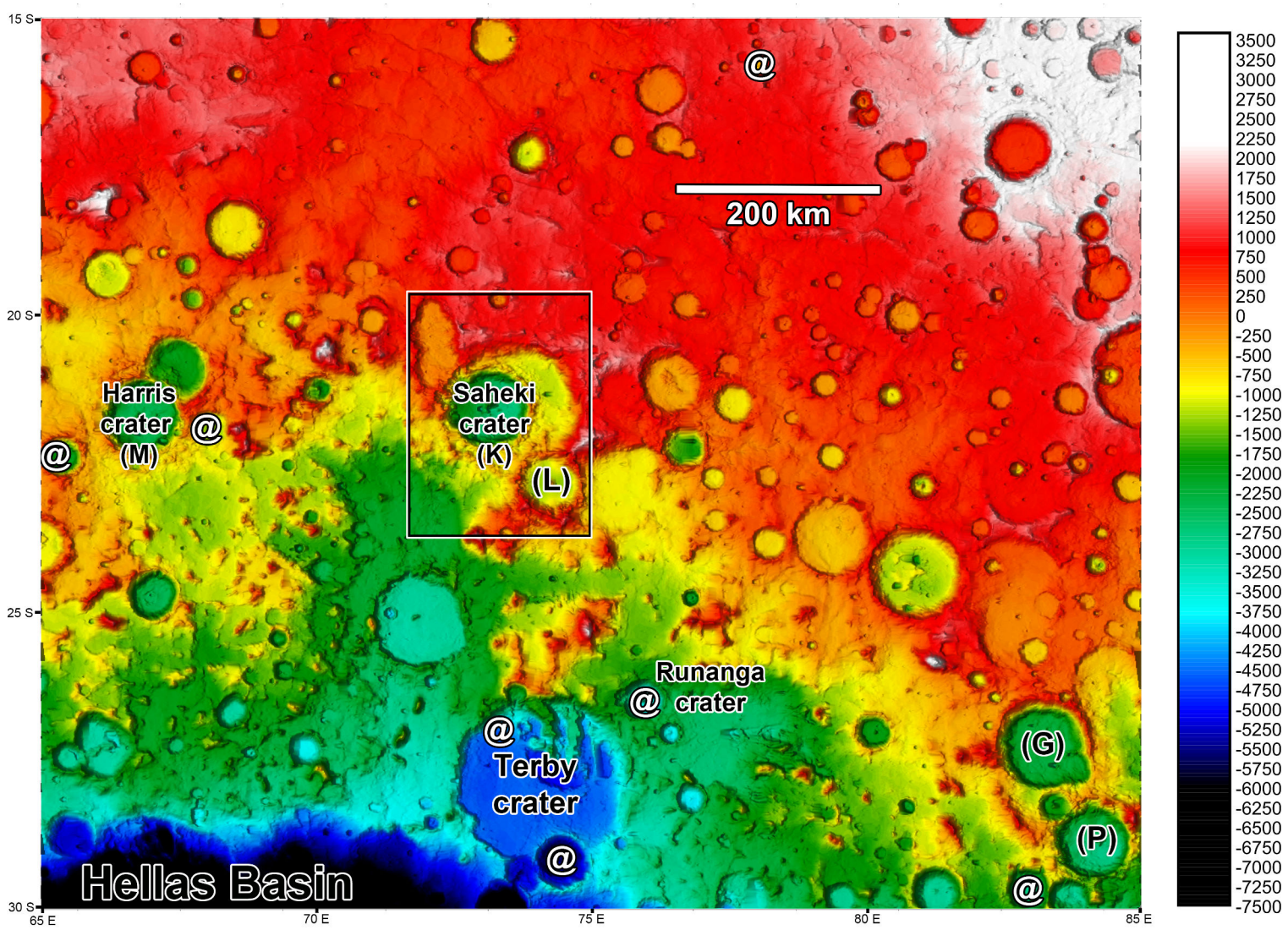
15 S
20 S
25 S
30 S
65 E
70 E
75 E
80 E
85 E
200 km
Harris
crater
(M)
Saheki
crater
(K)
(L)
Runanga
crater
Terby
crater
(G)
(P)
Hellas Basin
3500
3250
3000
2750
2500
2250
2000
1750
1500
1250
1000
750
500
250
0
-250
-500
-750
-1000
-1250
-1500
-1750
-2000
-2250
-2500
-2750
-3000
-3250
-3500
-3750
-4000
-4250
-4500
-4750
-5000
-5250
-5500
-5750
-6000
-6250
-6500
-6750
-7000
-7250
-7500

Fig. 1

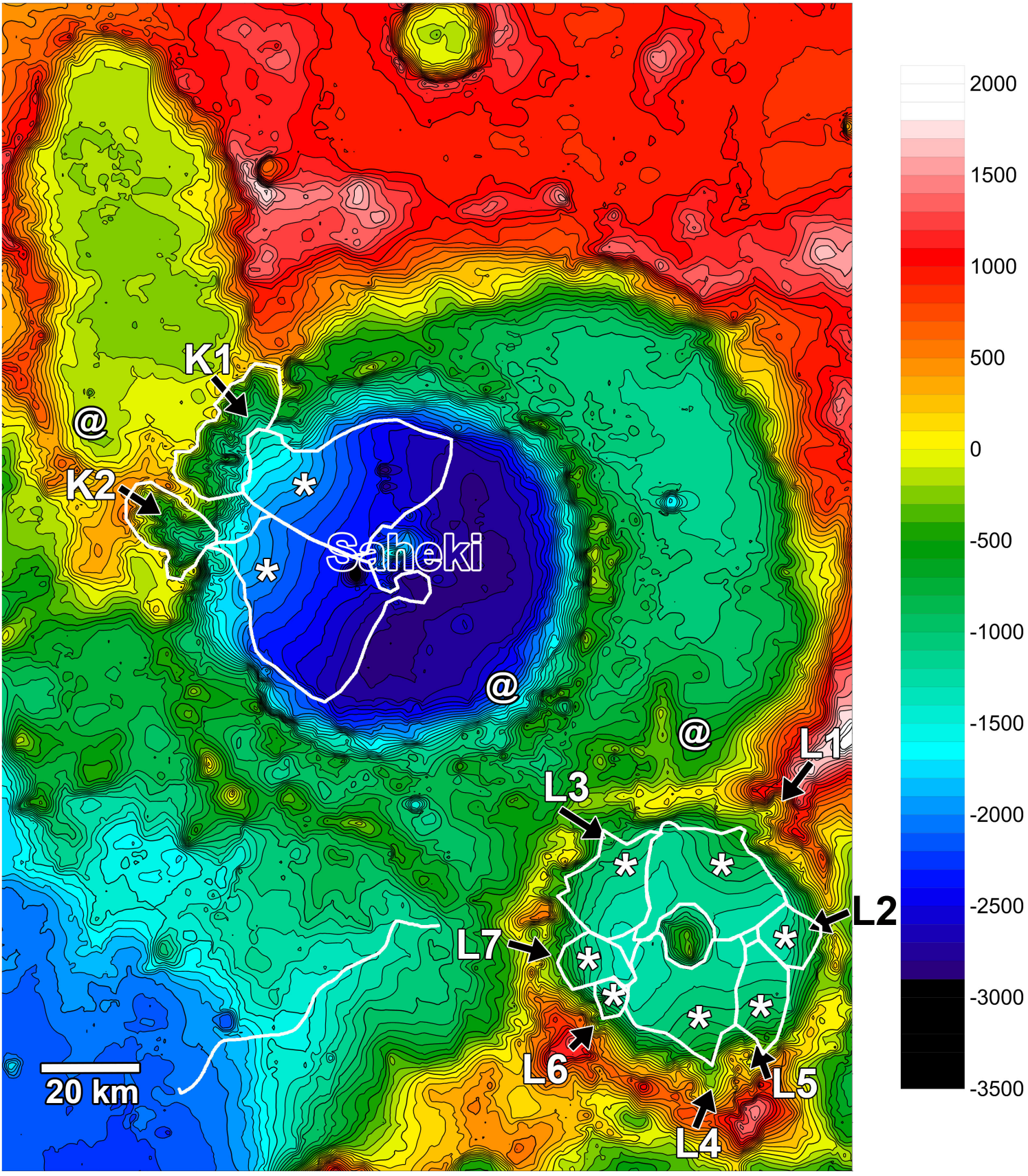
K1
K2
Saheki
L1
L2
L3
L4
L5
L6
L7
20 km
2000
1500
1000
500
0
-500
-1000
-1500
-2000
-2500
-3000
-3500

Fig. 2

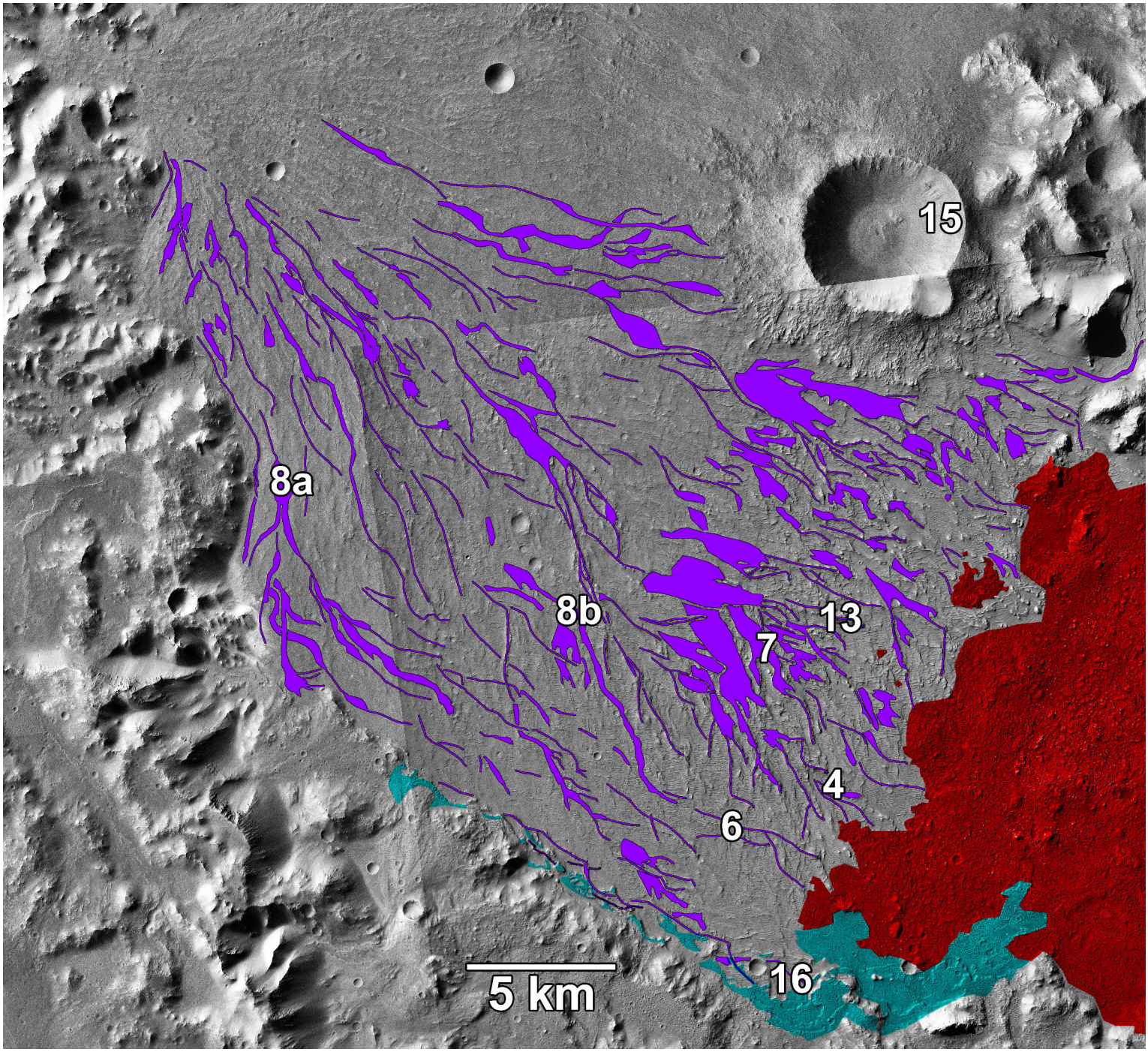

Fig. 3

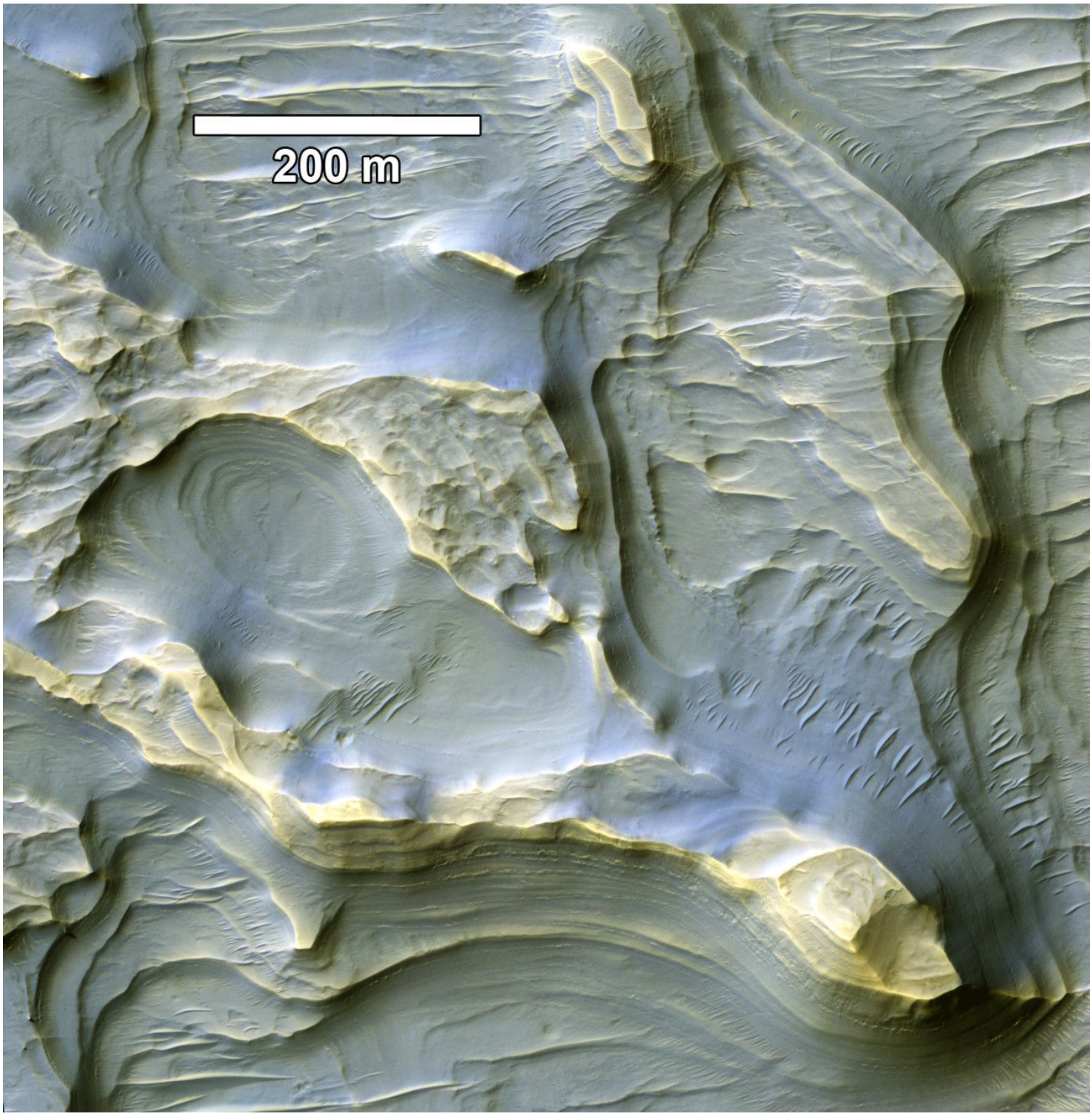

Fig. 4

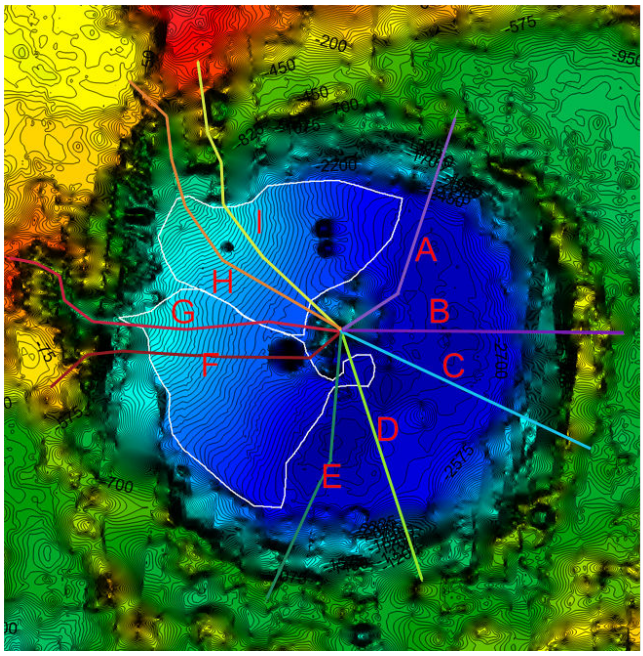

Fig. 5

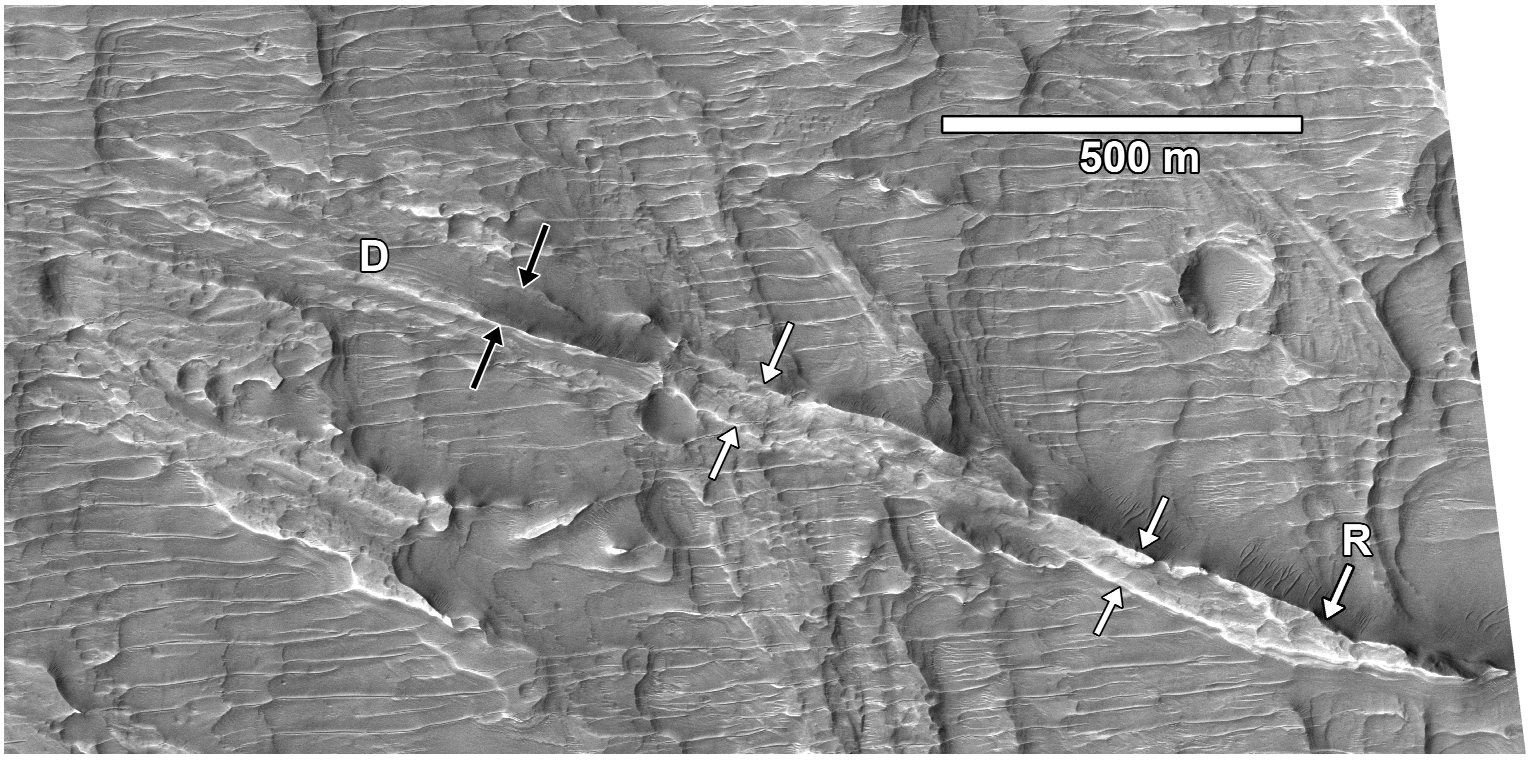

Fig. 6

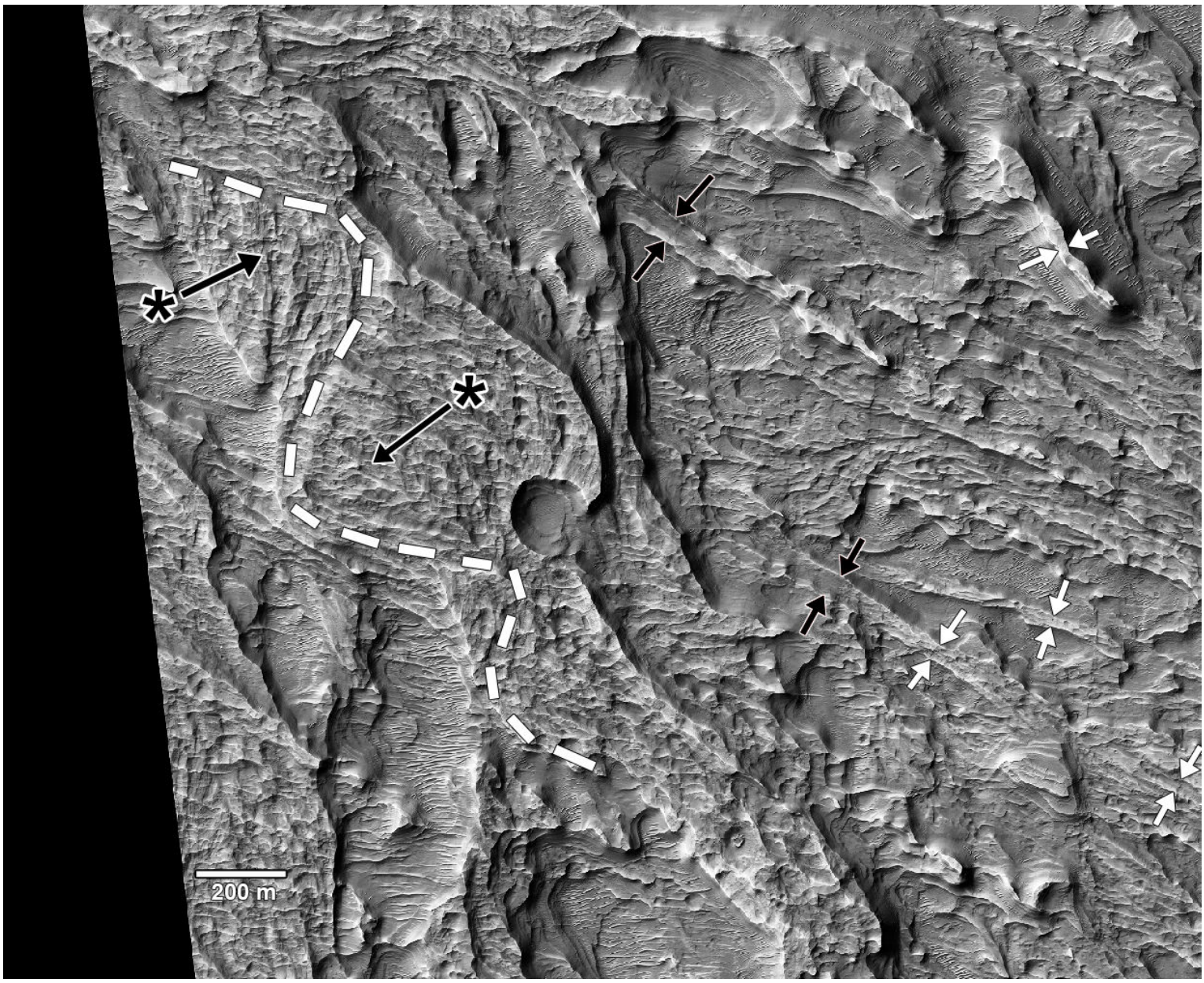

Fig. 7

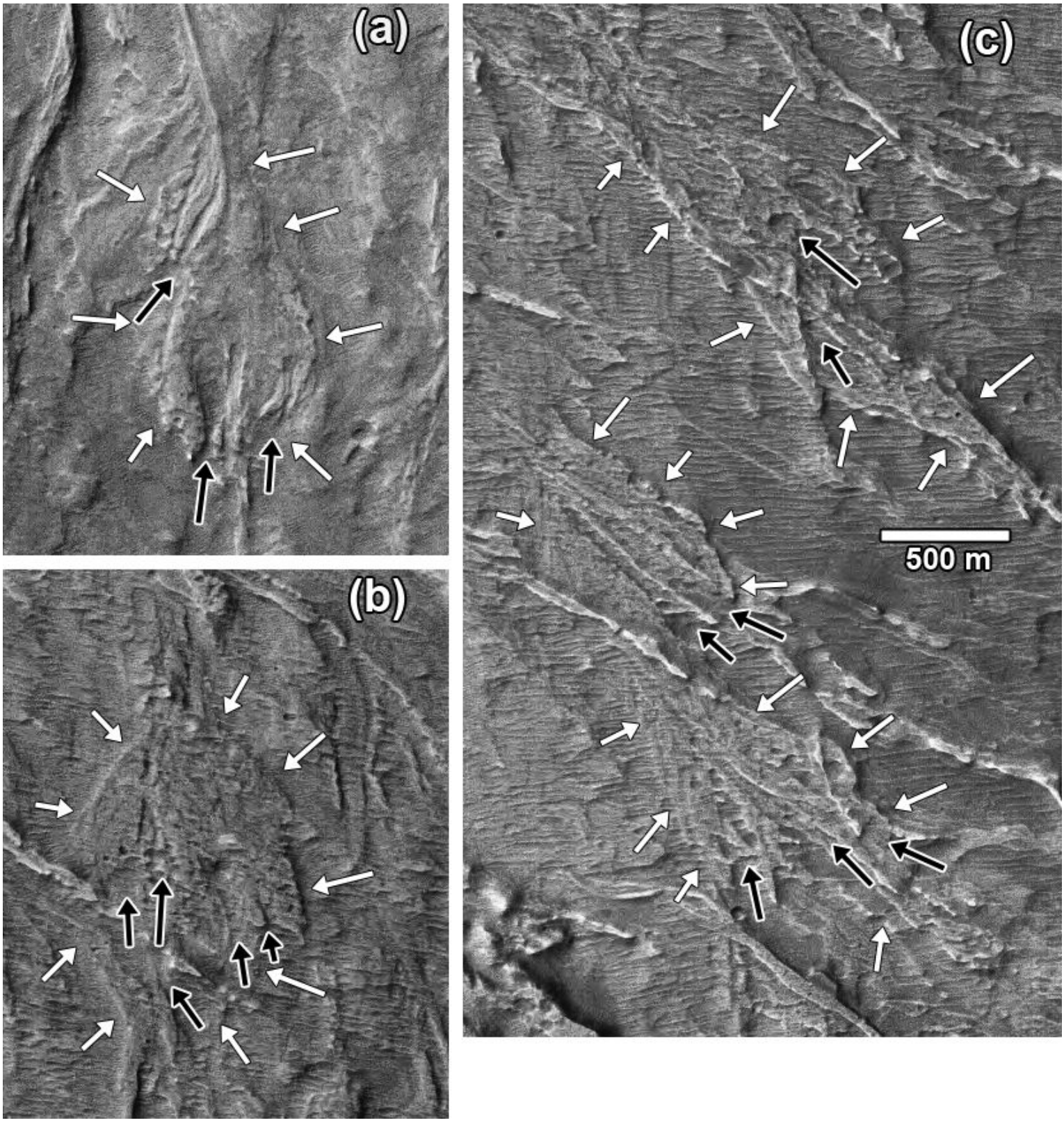

Fig. 8

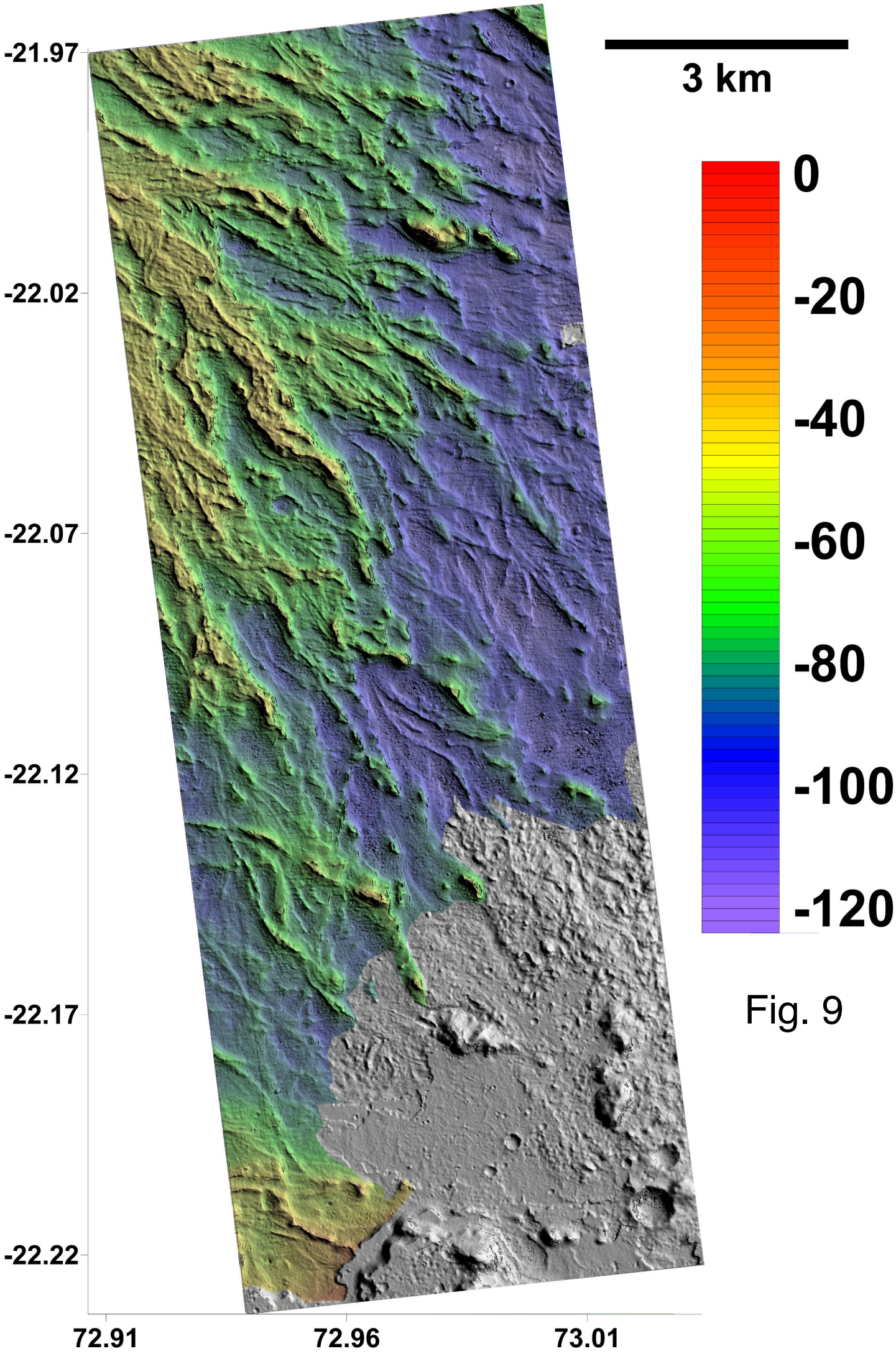
-21.97
-22.02
-22.07
-22.12
-22.17
-22.22
72.91
72.96
73.01
3 km
0
-20
-40
-60
-80
-100
-120

Fig. 9

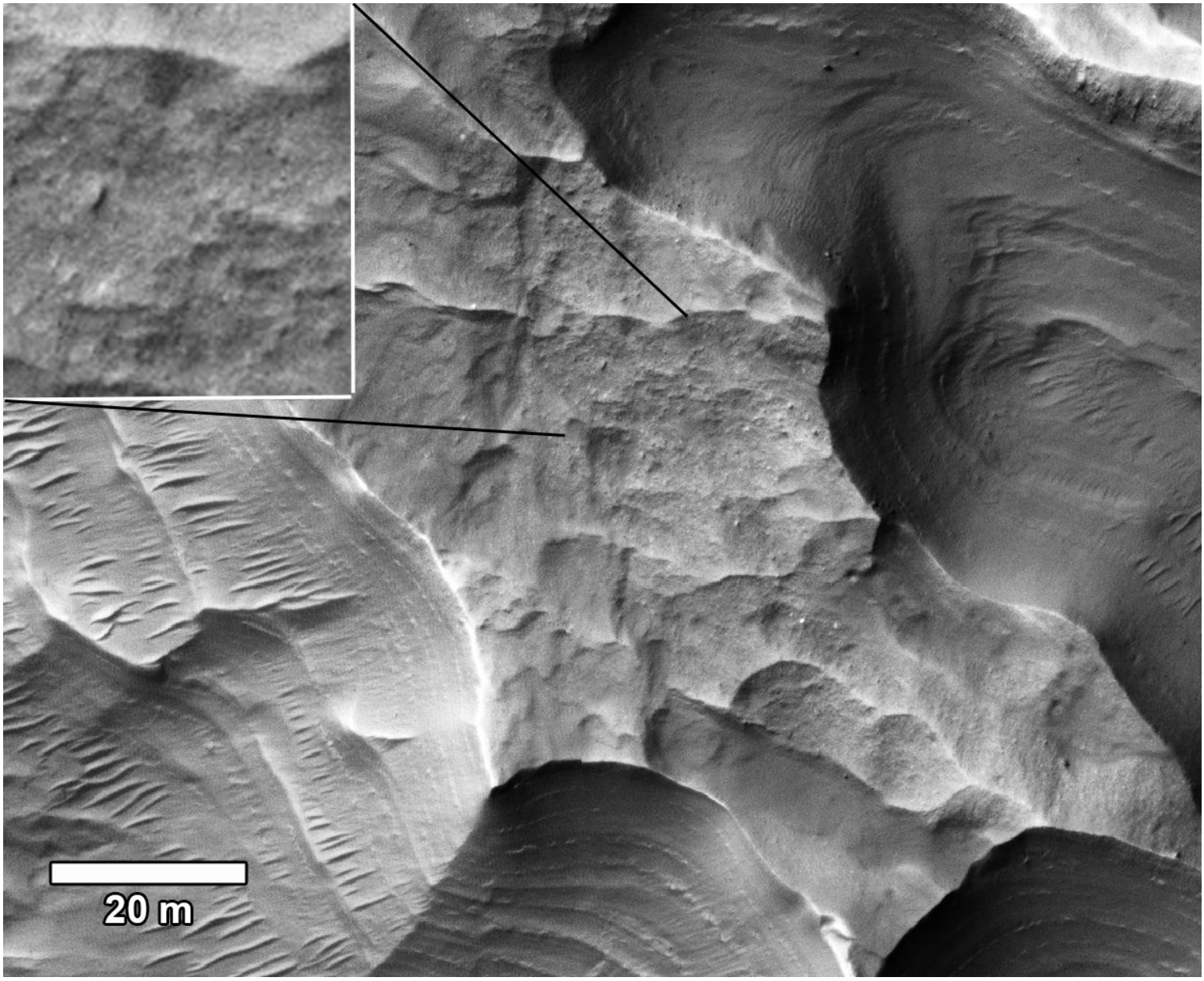

Fig. 10

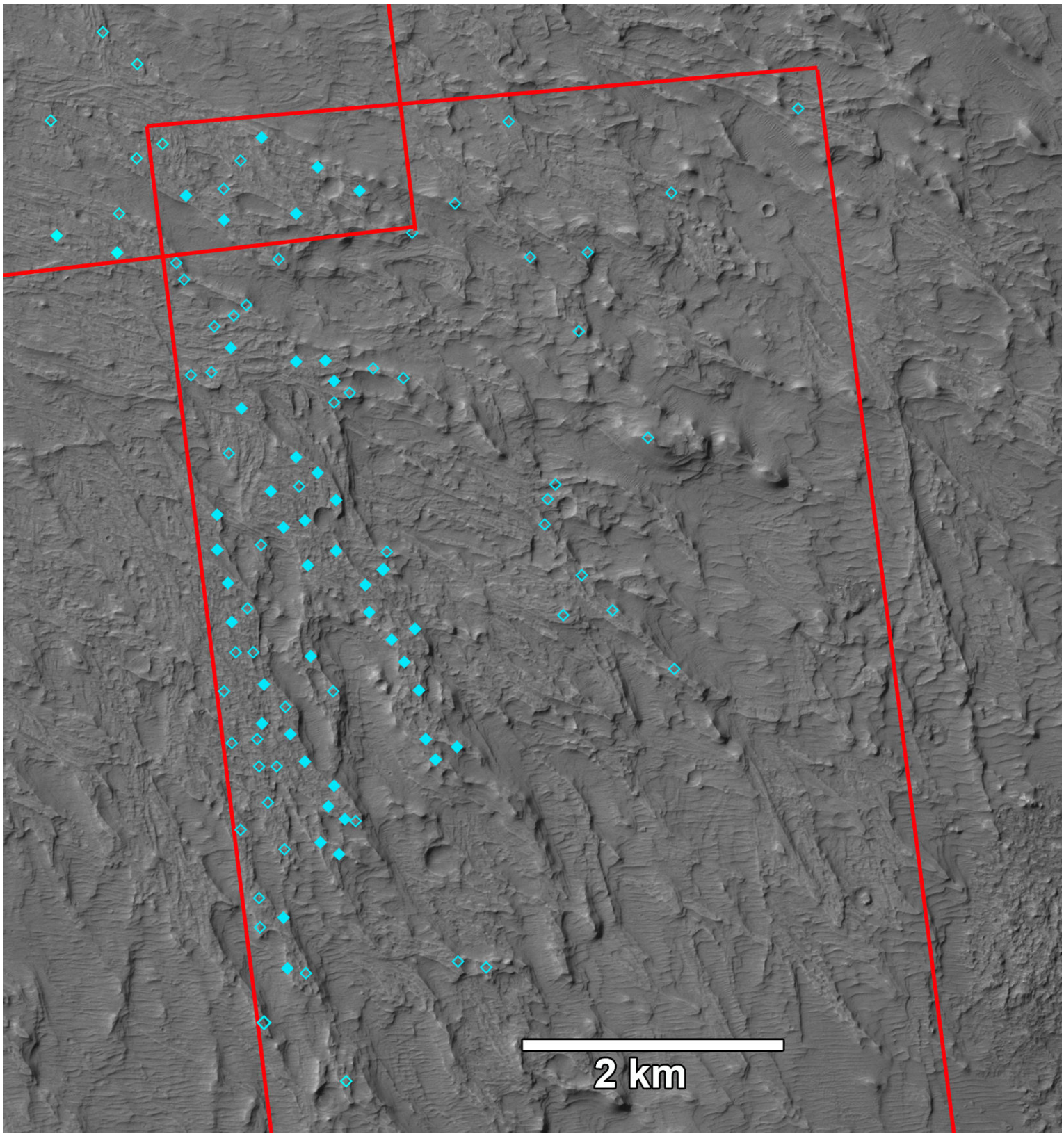

Fig. 11

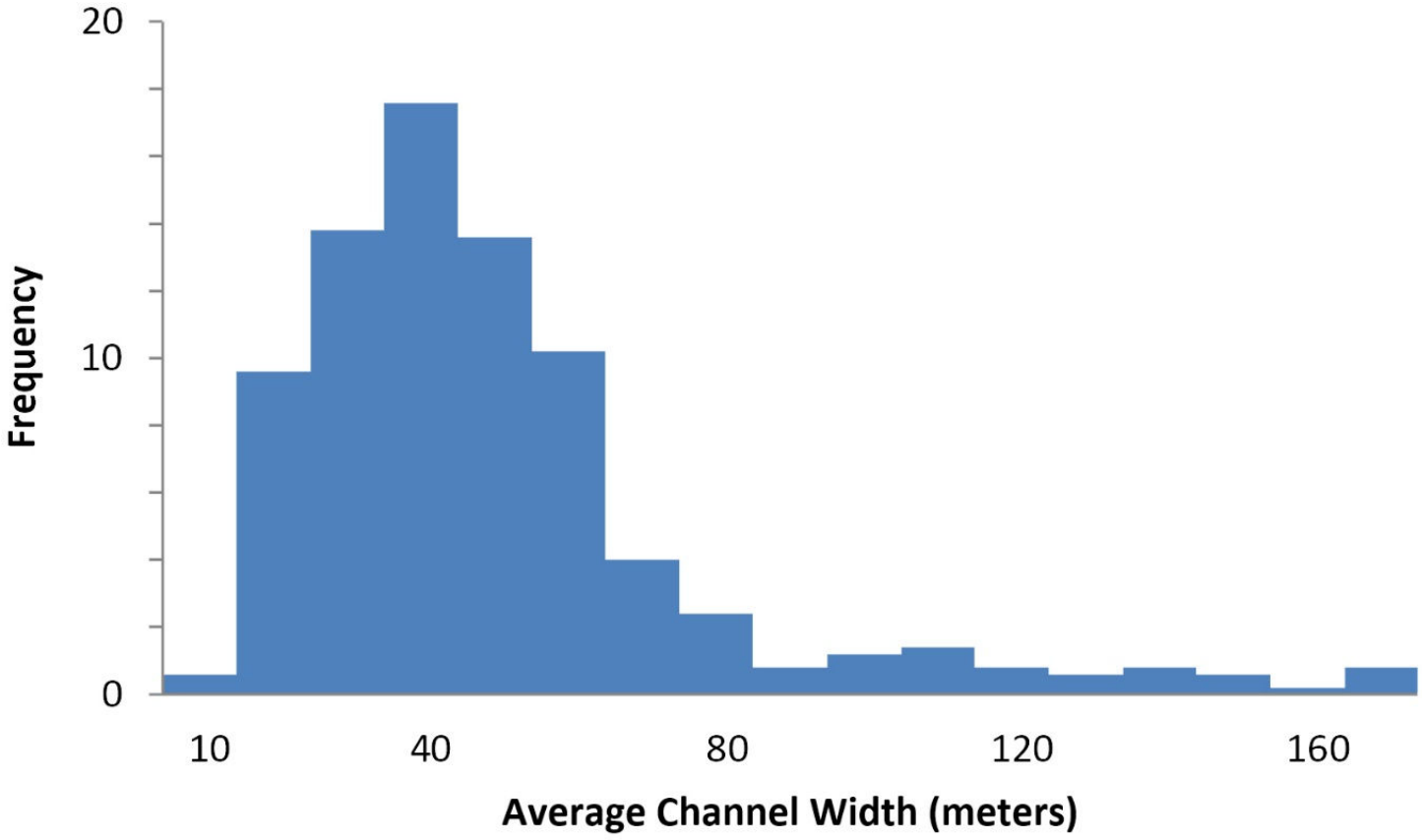
20
10
0
Frequency
10
40
80
120
160
Average Channel Width (meters)

Fig. 12

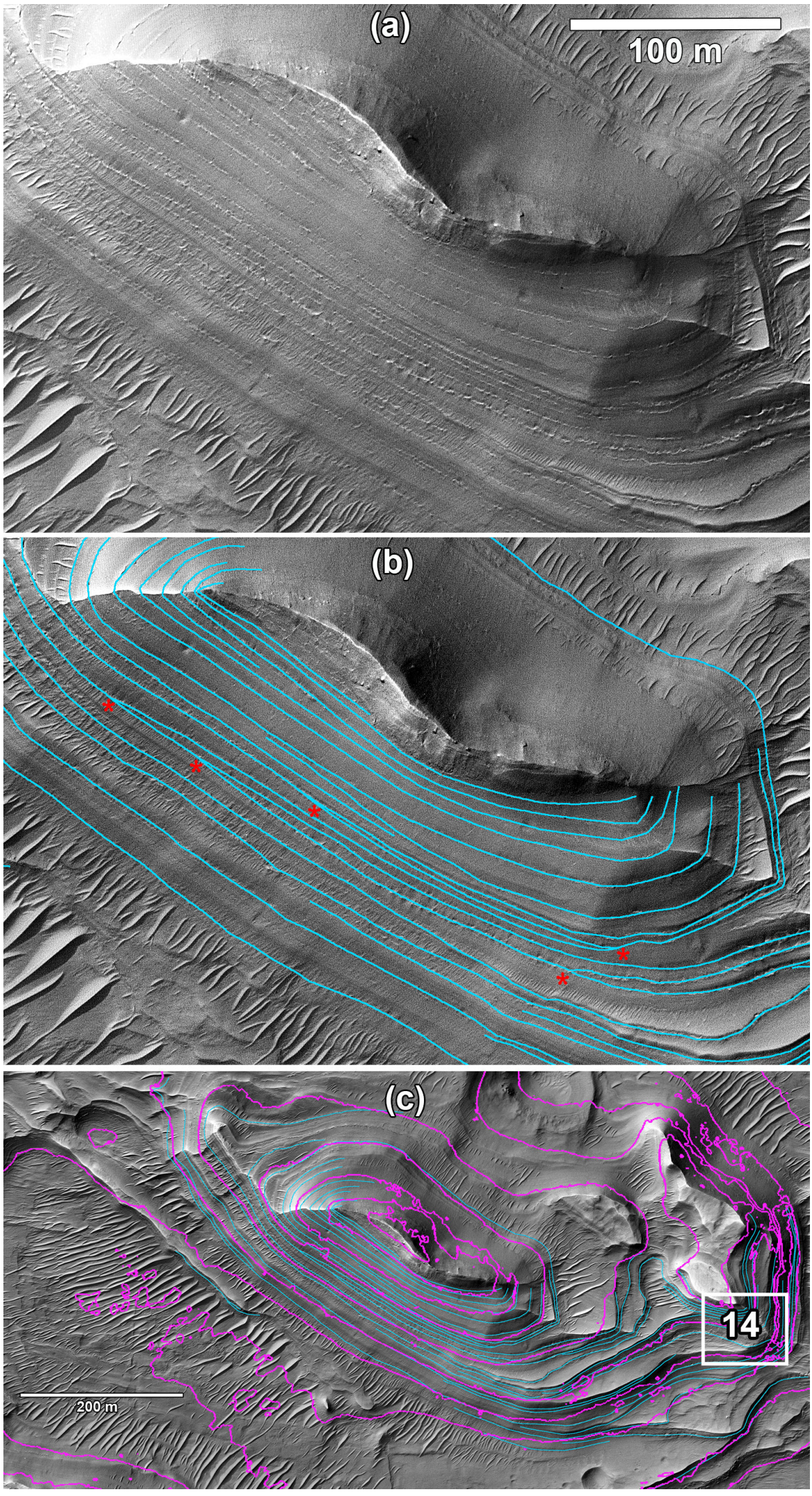

Fig. 13

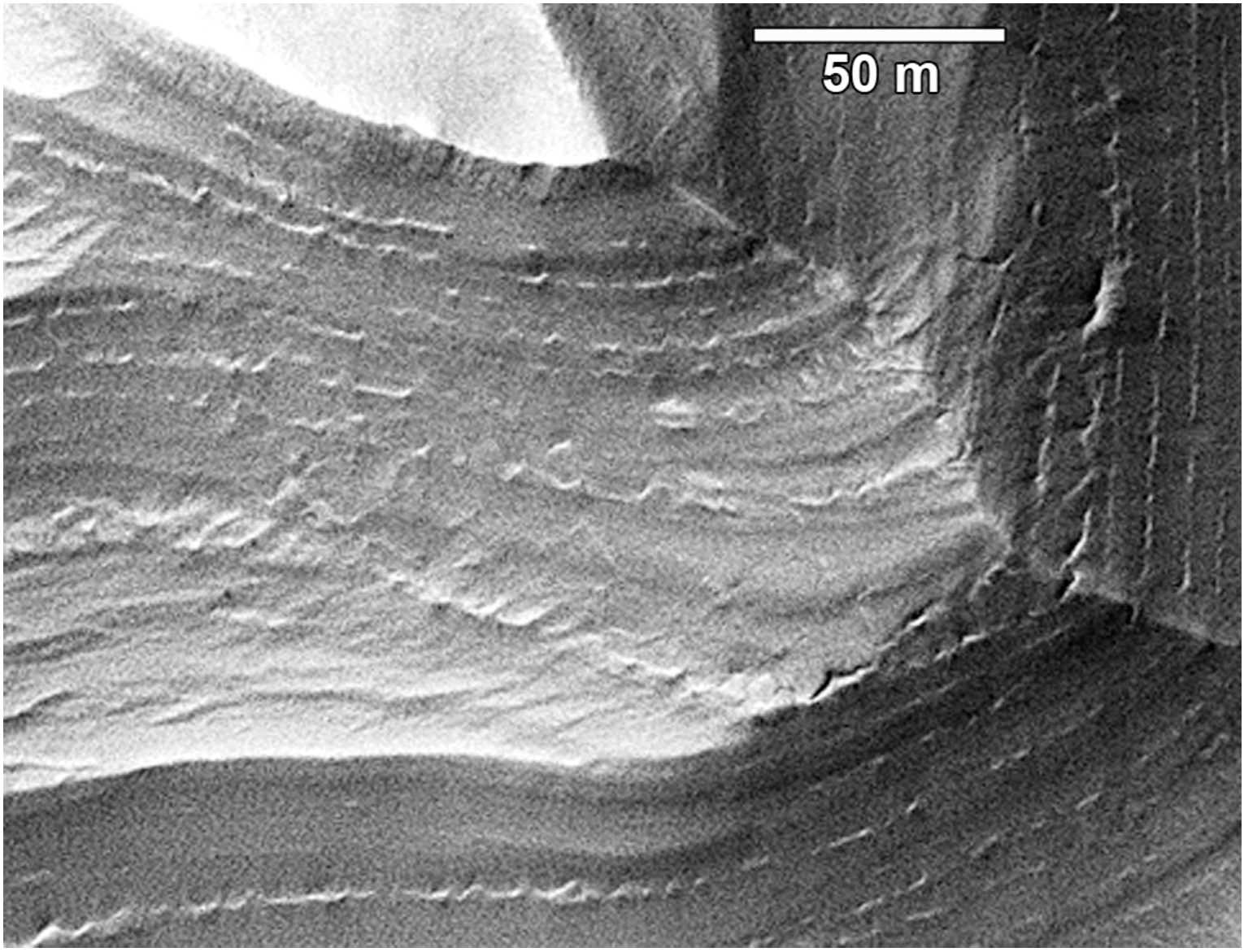

Fig. 14

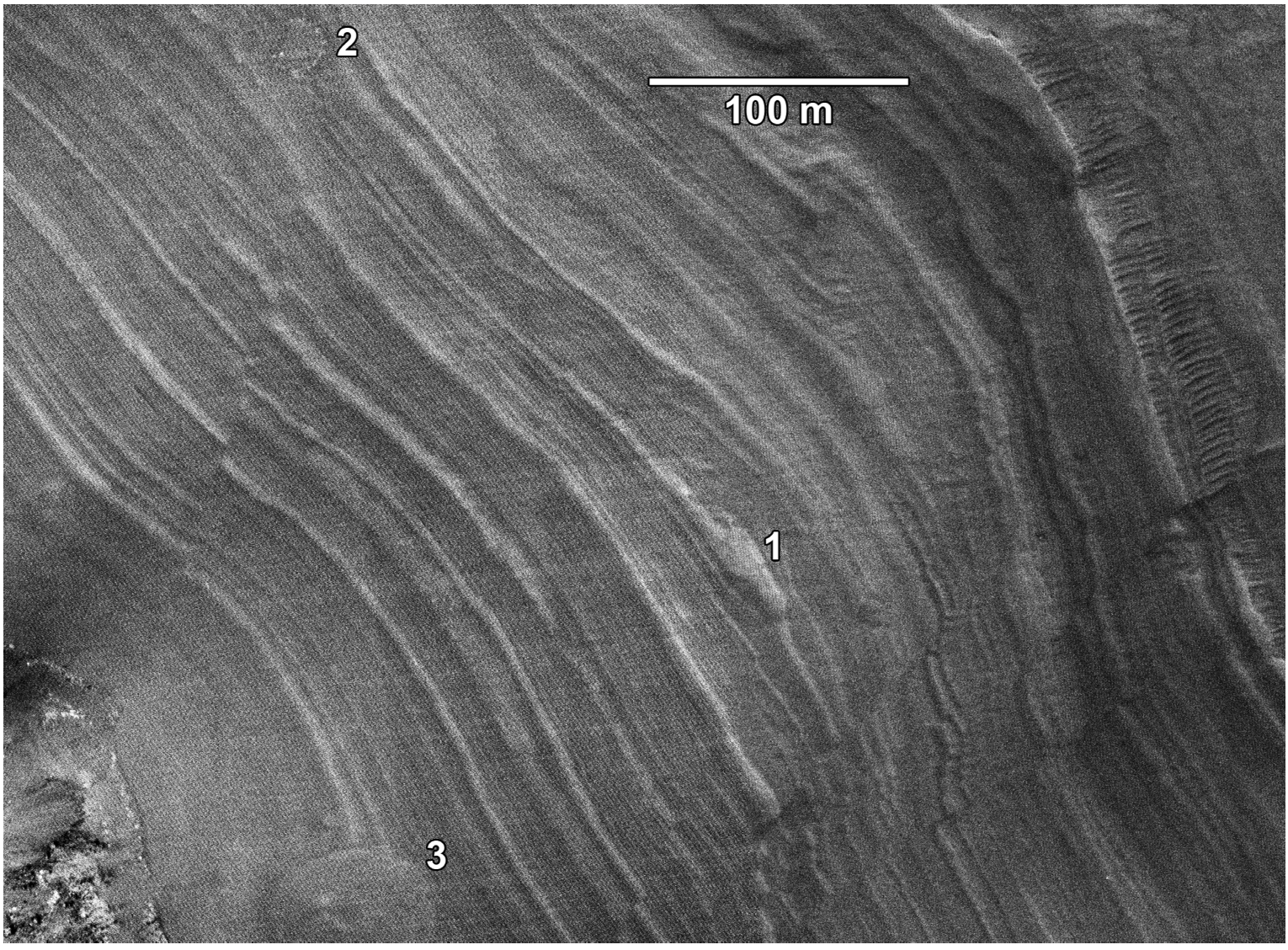

Fig. 15

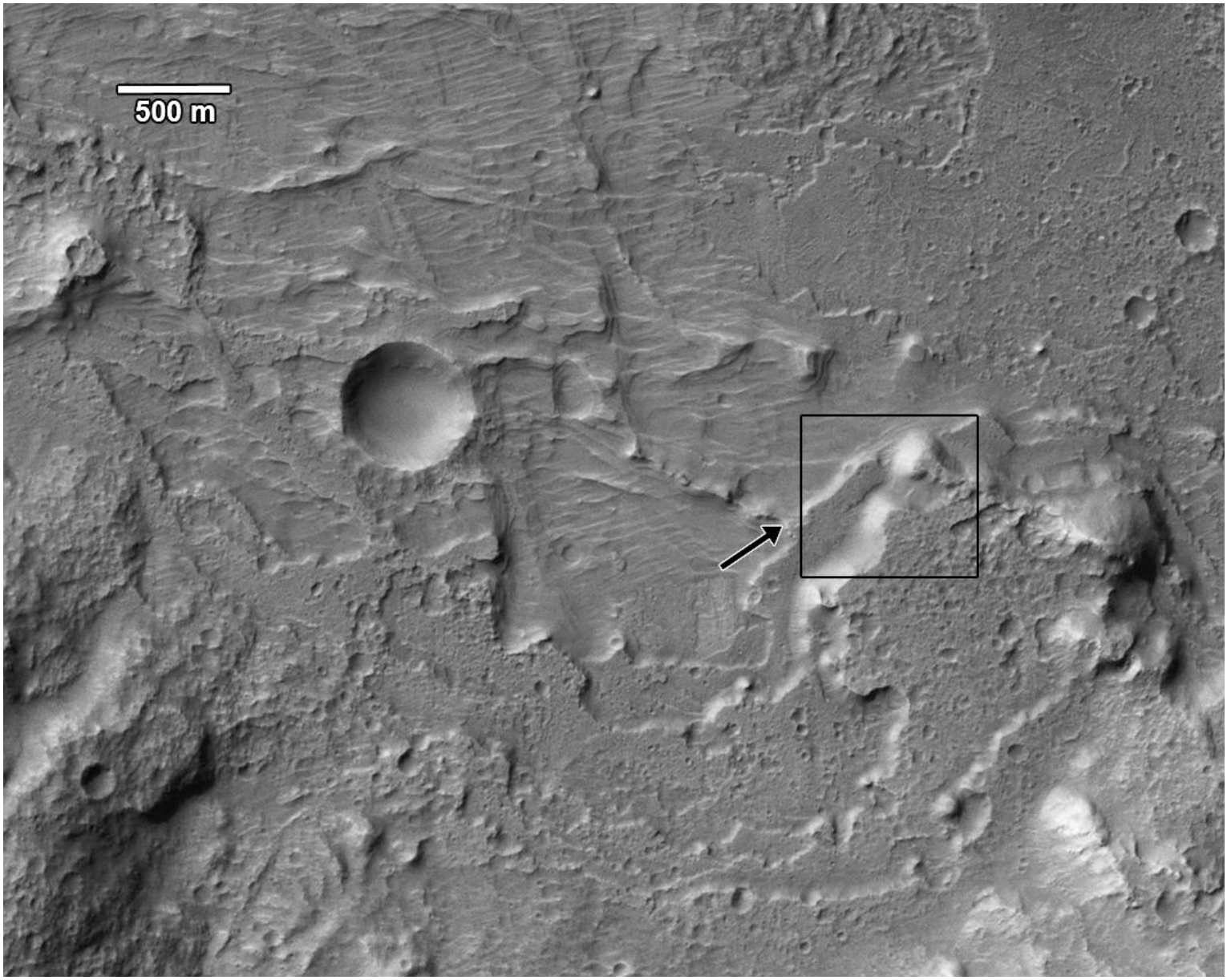

Fig. 16

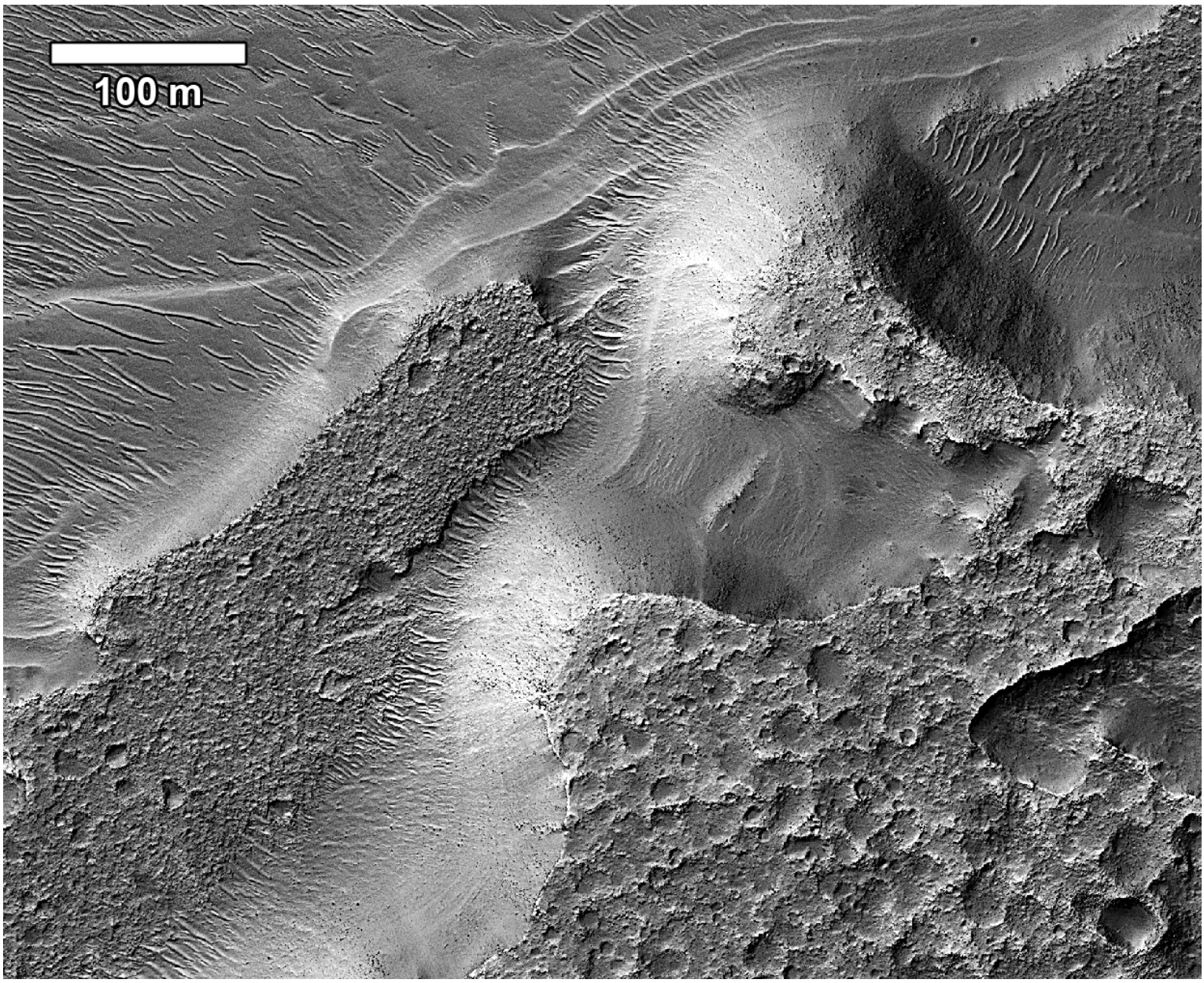

Fig. 17

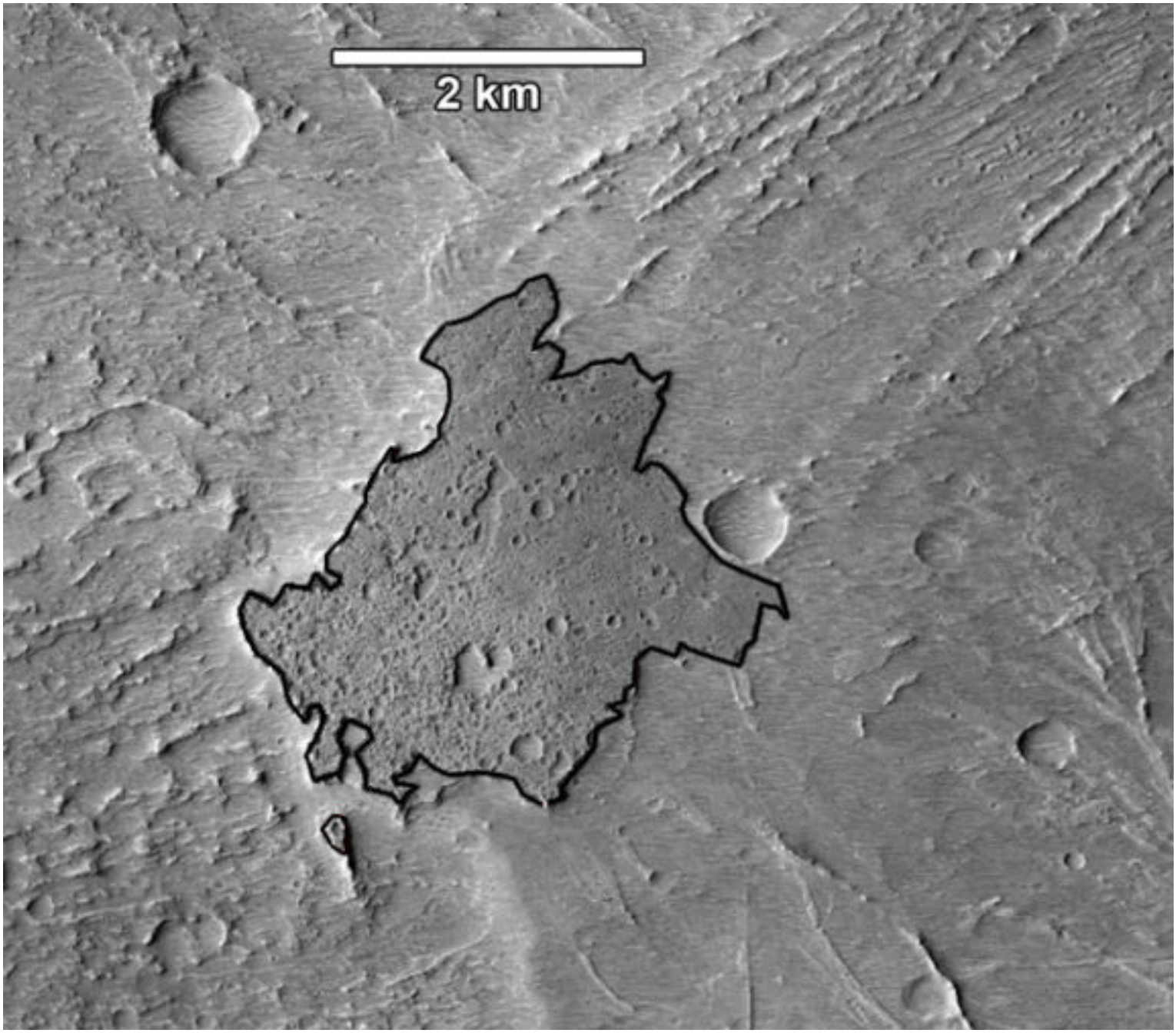

Fig. 18

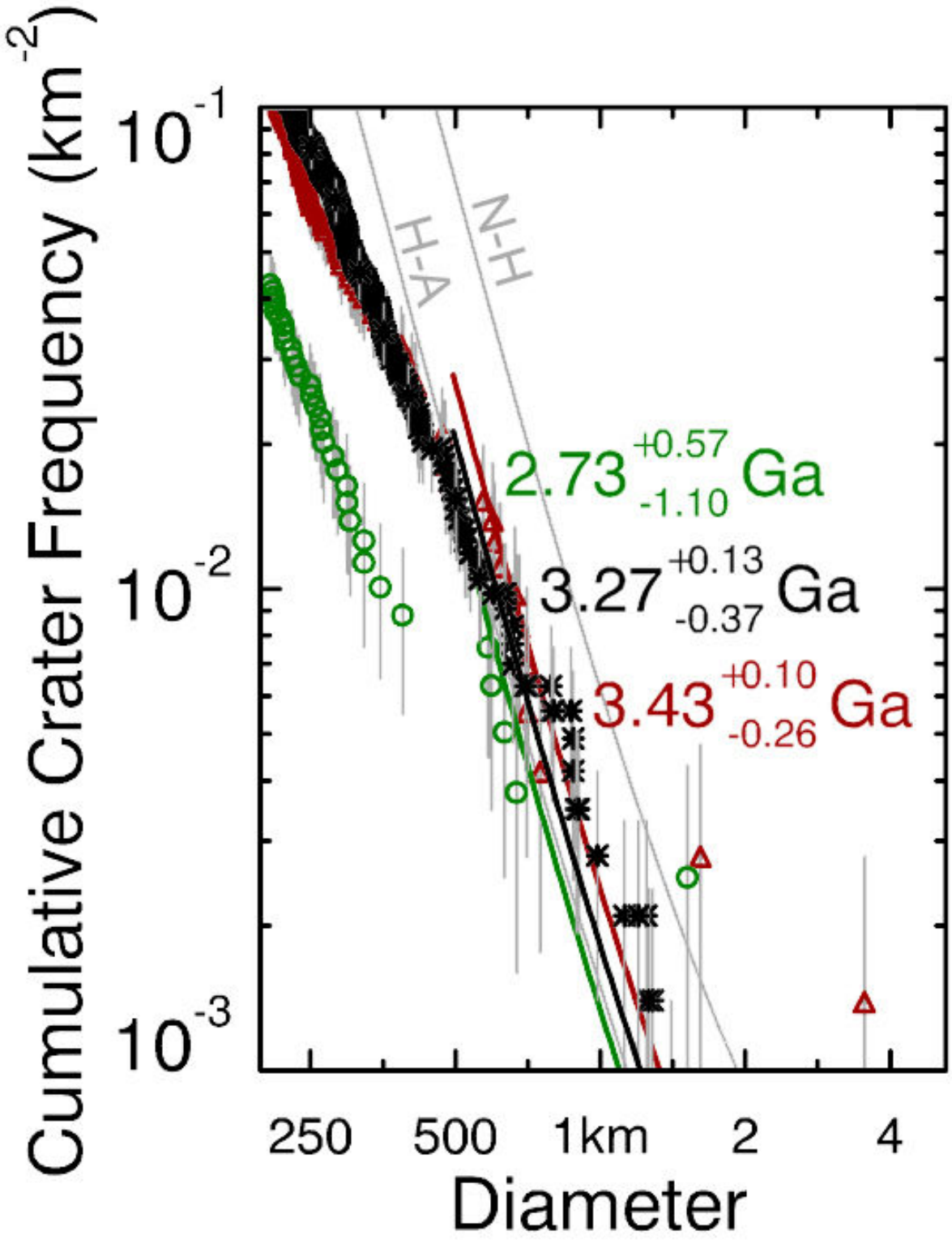
Cumulative Crater Frequency (km-2)
10-1
10-2
10-3
H-A
N-H
2.73 +0.57 -1.10 Ga
3.27 +0.13 -0.37 Ga
3.43 +0.10 -0.26 Ga
250
500
1km
2
4
Diameter

Fig. 19

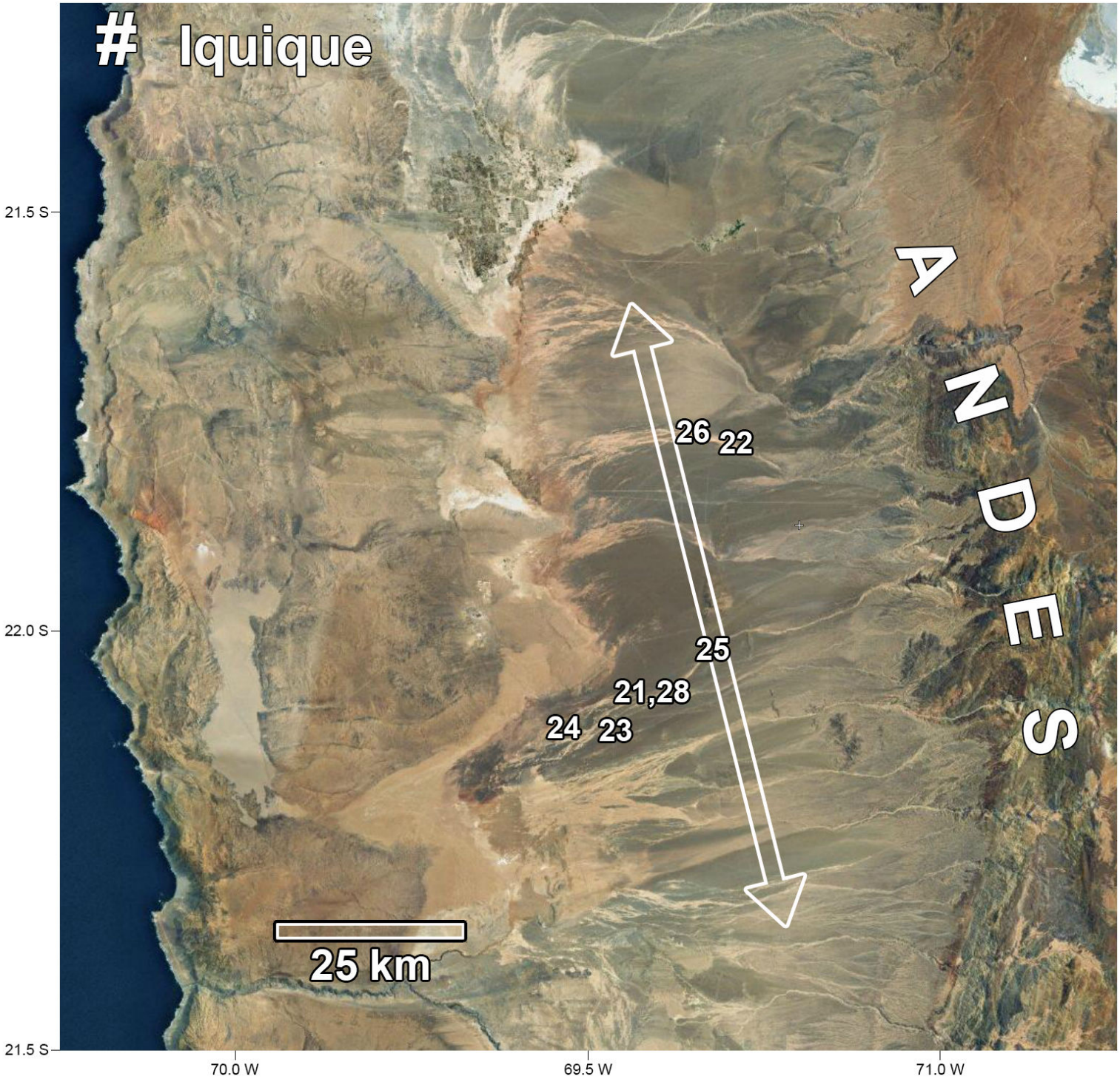
Iquique
ANDES
26
22
25
21,28
24
23
25 km
21.5 S
22.0 S
21.5 S
70.0 W
69.5 W
71.0 W

Fig. 20

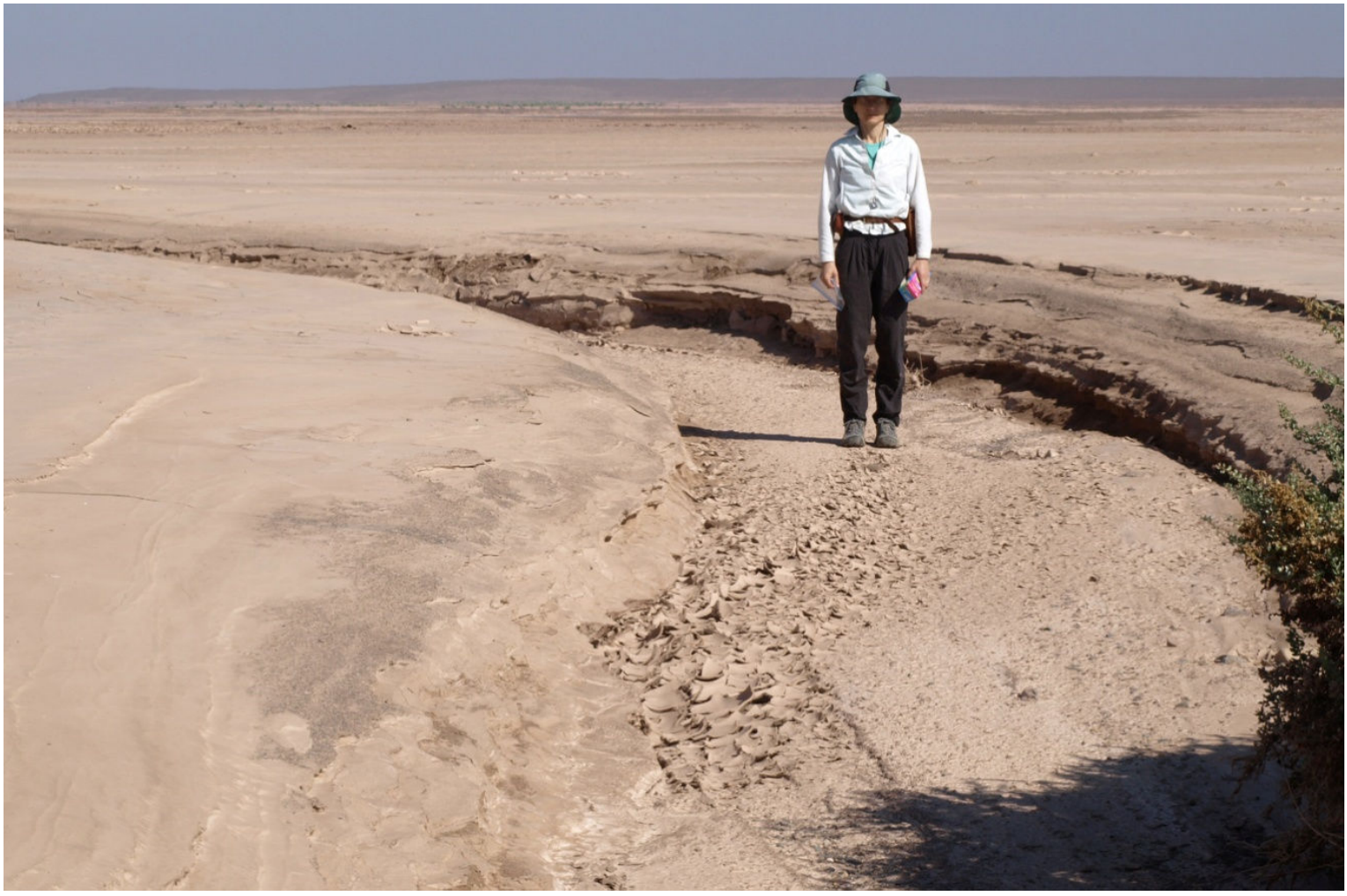

Fig. 21

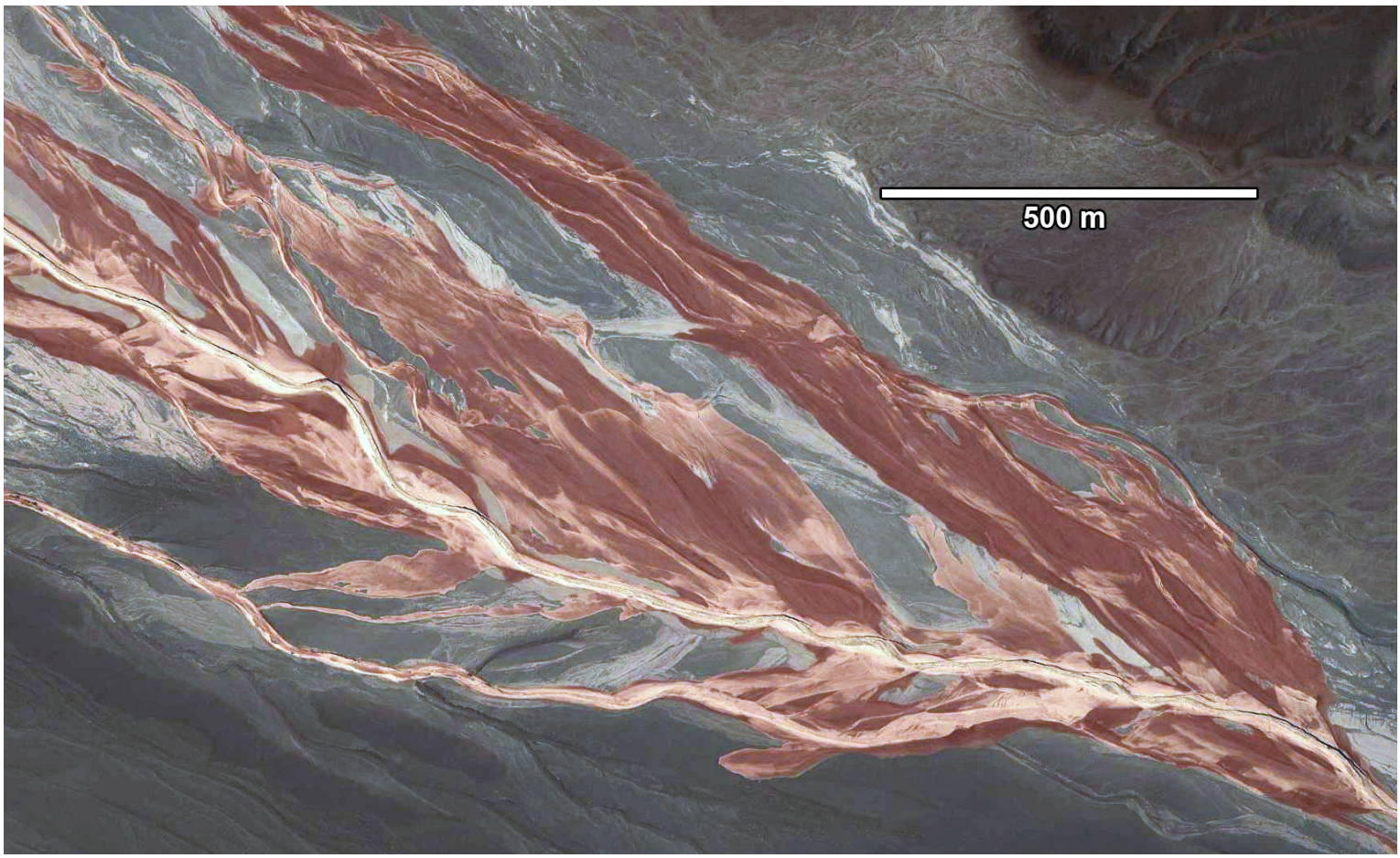

Fig. 22

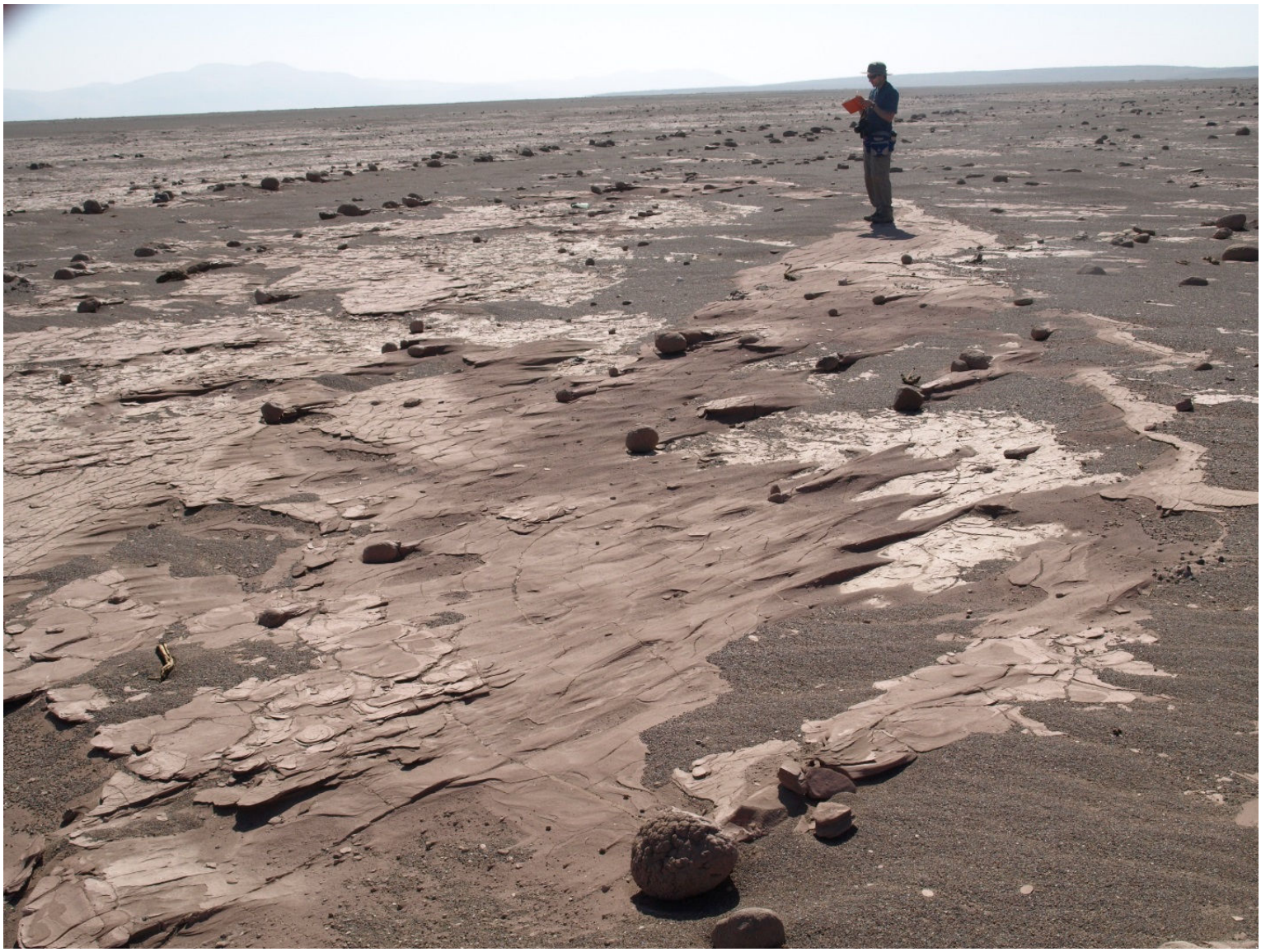

Fig. 23

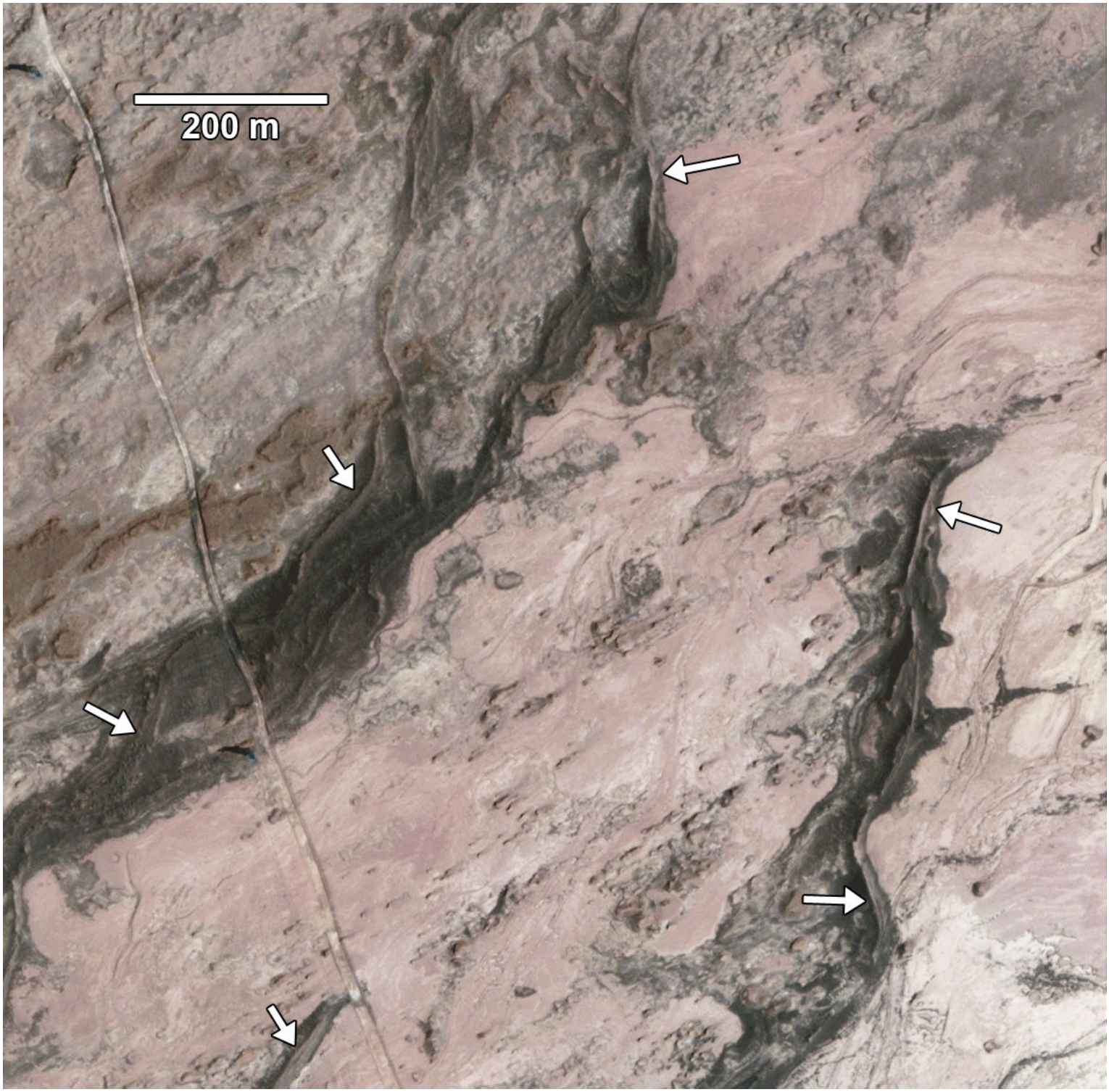

Fig. 24

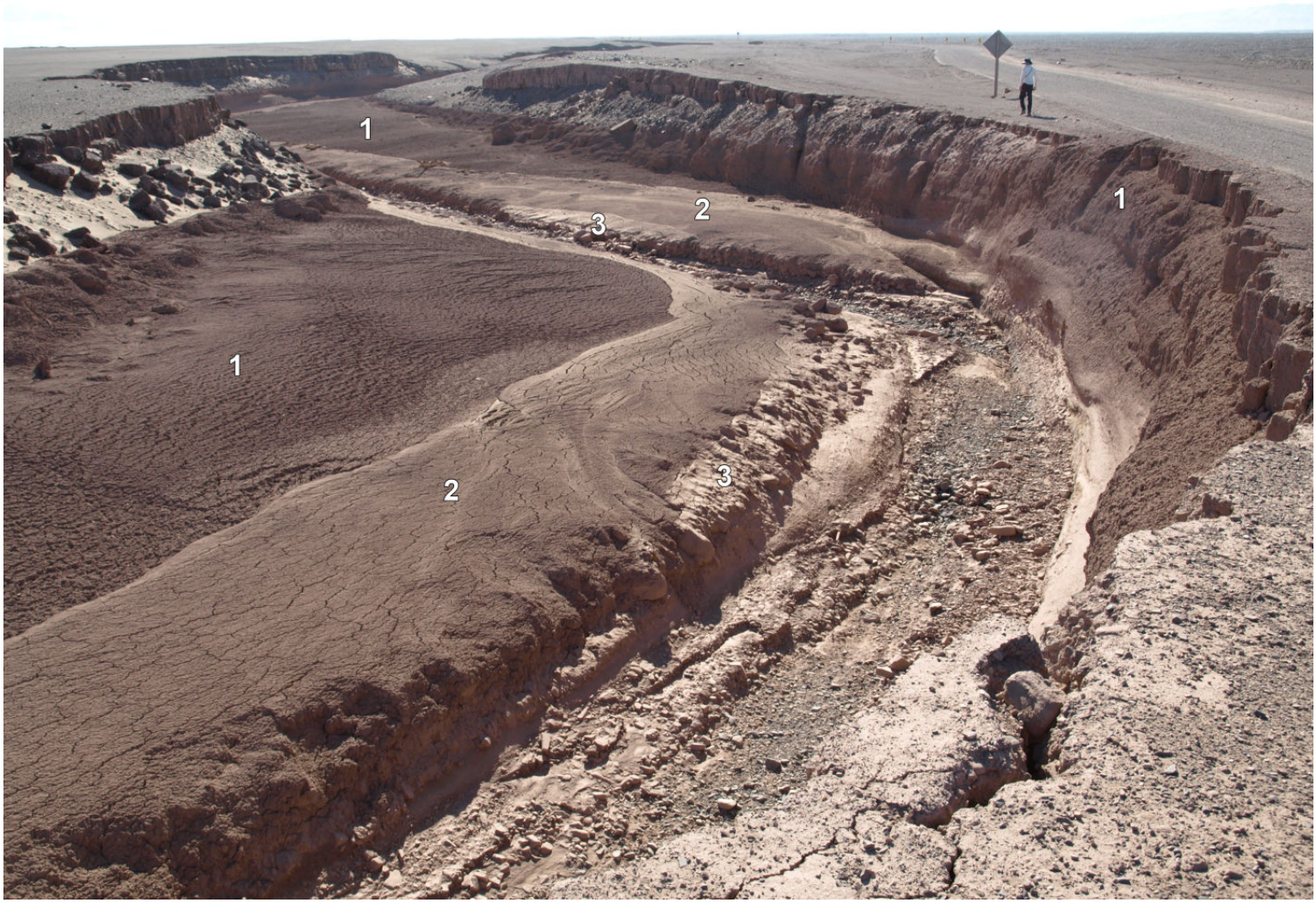

Fig. 25

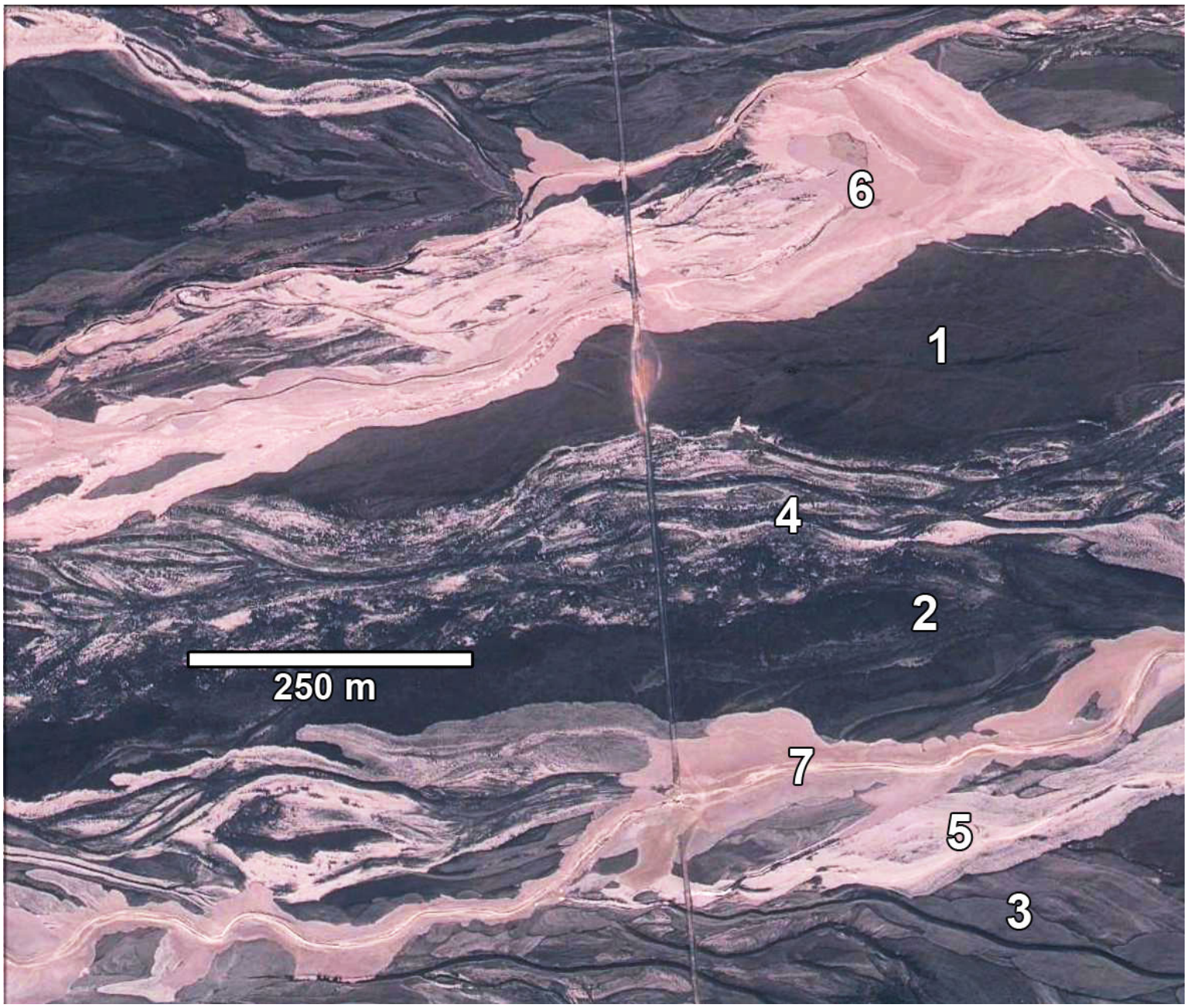

Fig. 26

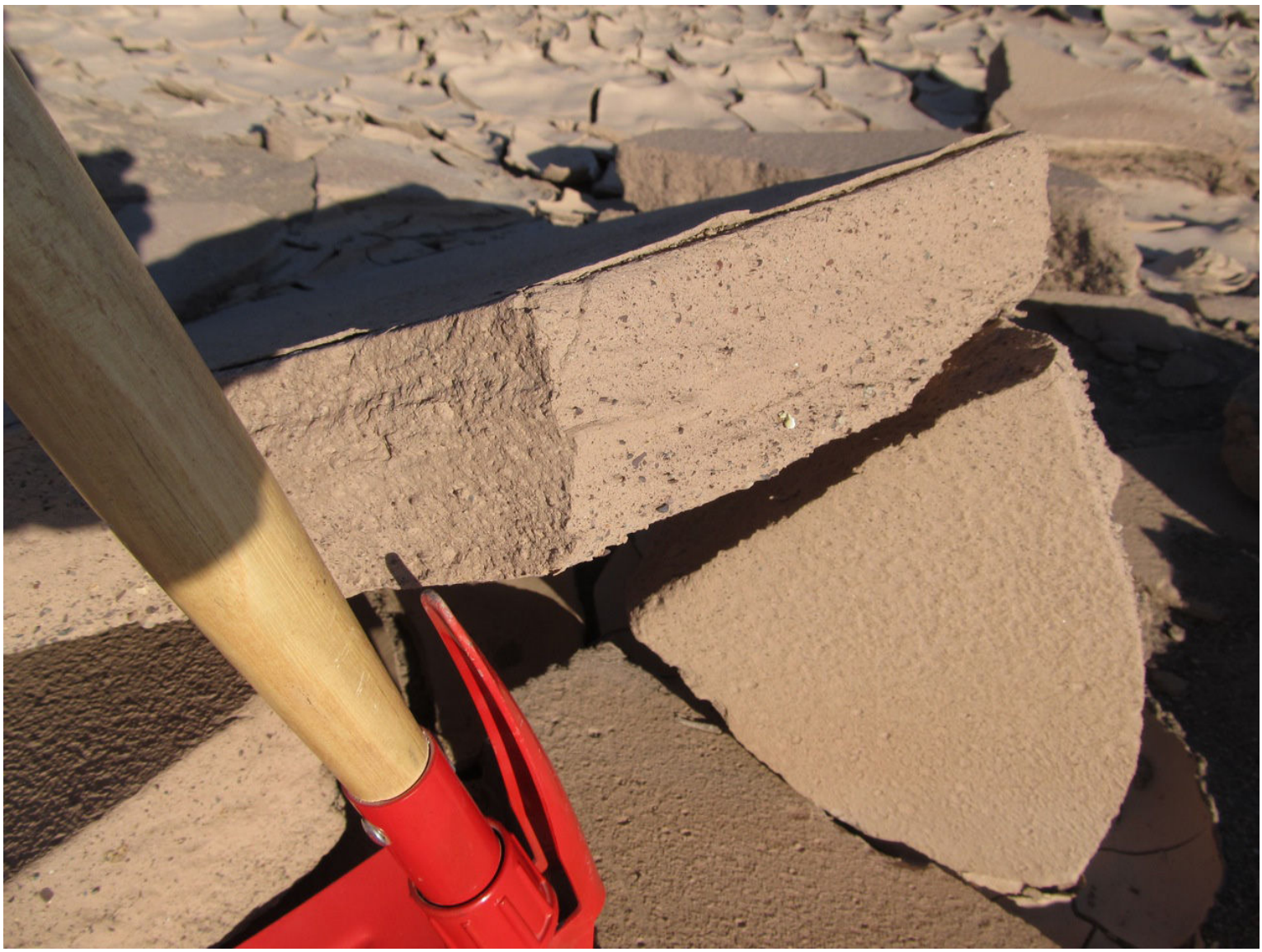

Fig. 27

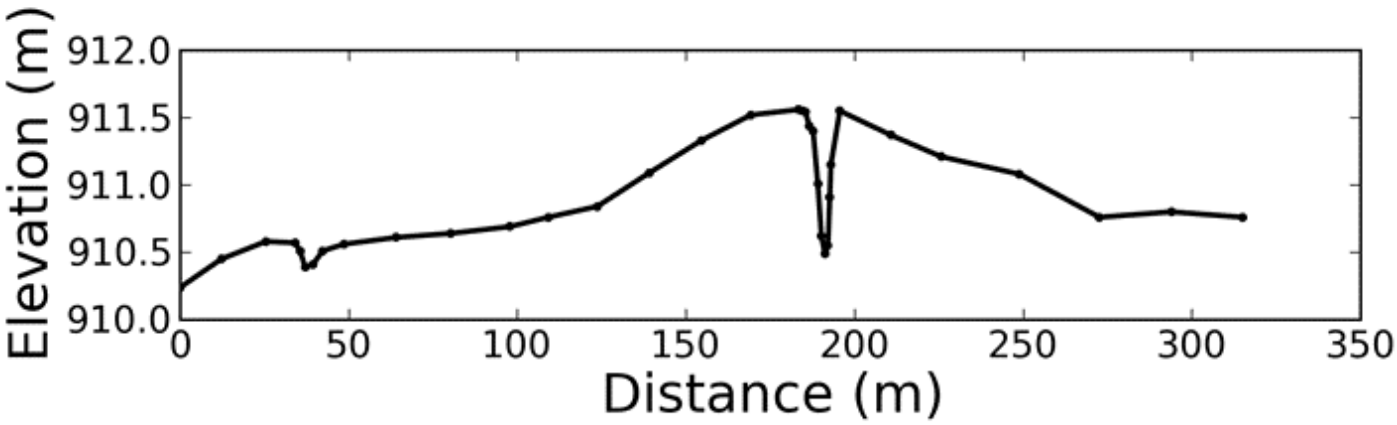
Elevation (m)
912.0
911.5
911.0
910.5
910.0
0
50
100
150
200
250
300
350
Distance (m)

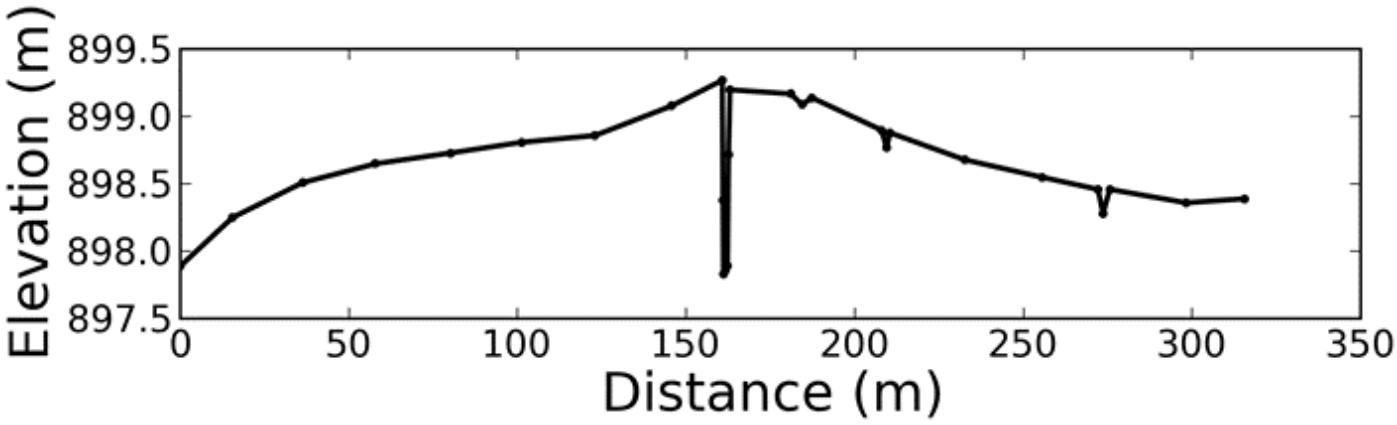
Elevation (m)
899.5
899.0
898.5
898.0
897.5
0
50
100
150
200
250
300
350
Distance (m)

Fig. 28

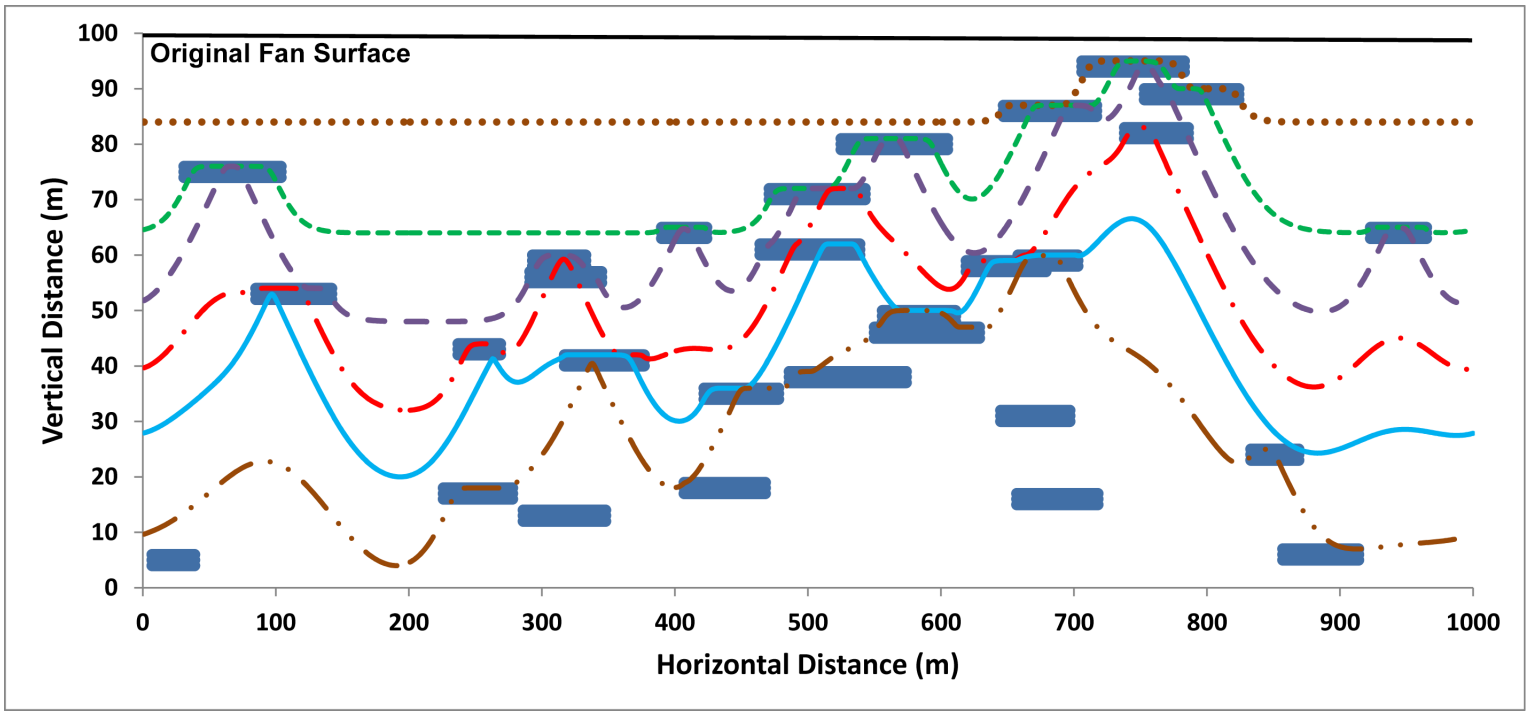
Original Fan Surface
Vertical Distance (m)
Horizontal Distance (m)
0
10
20
30
40
50
60
70
80
90
100
0
100
200
300
400
500
600
700
800
900
1000

Fig. 29

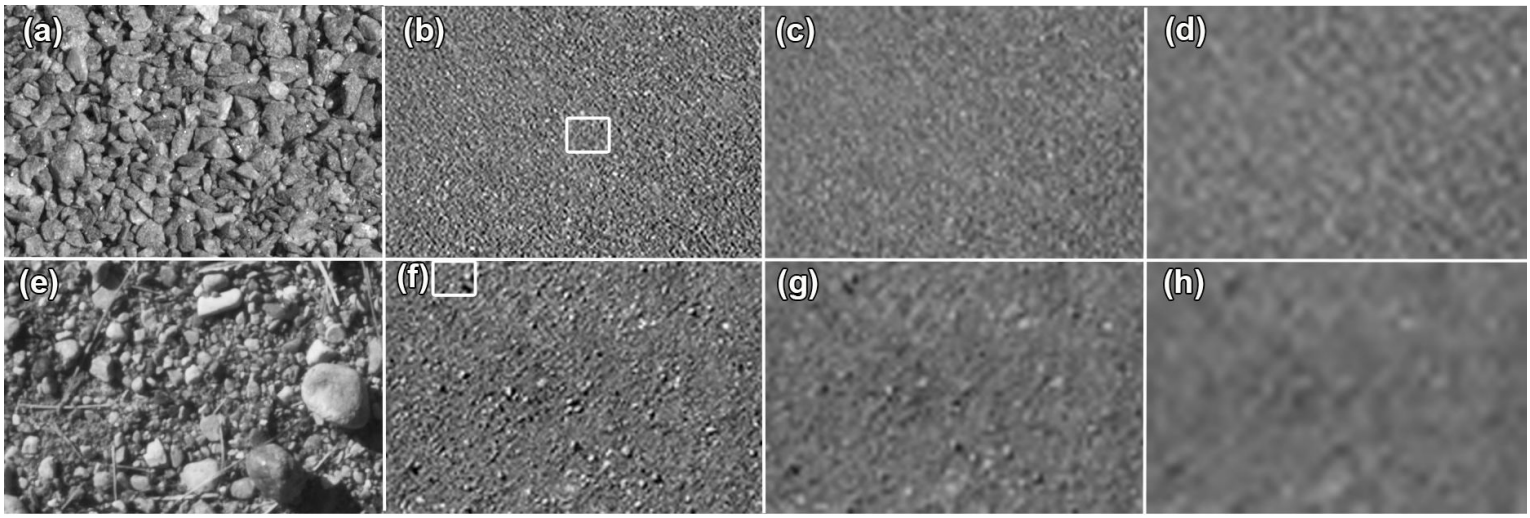

Fig. 30

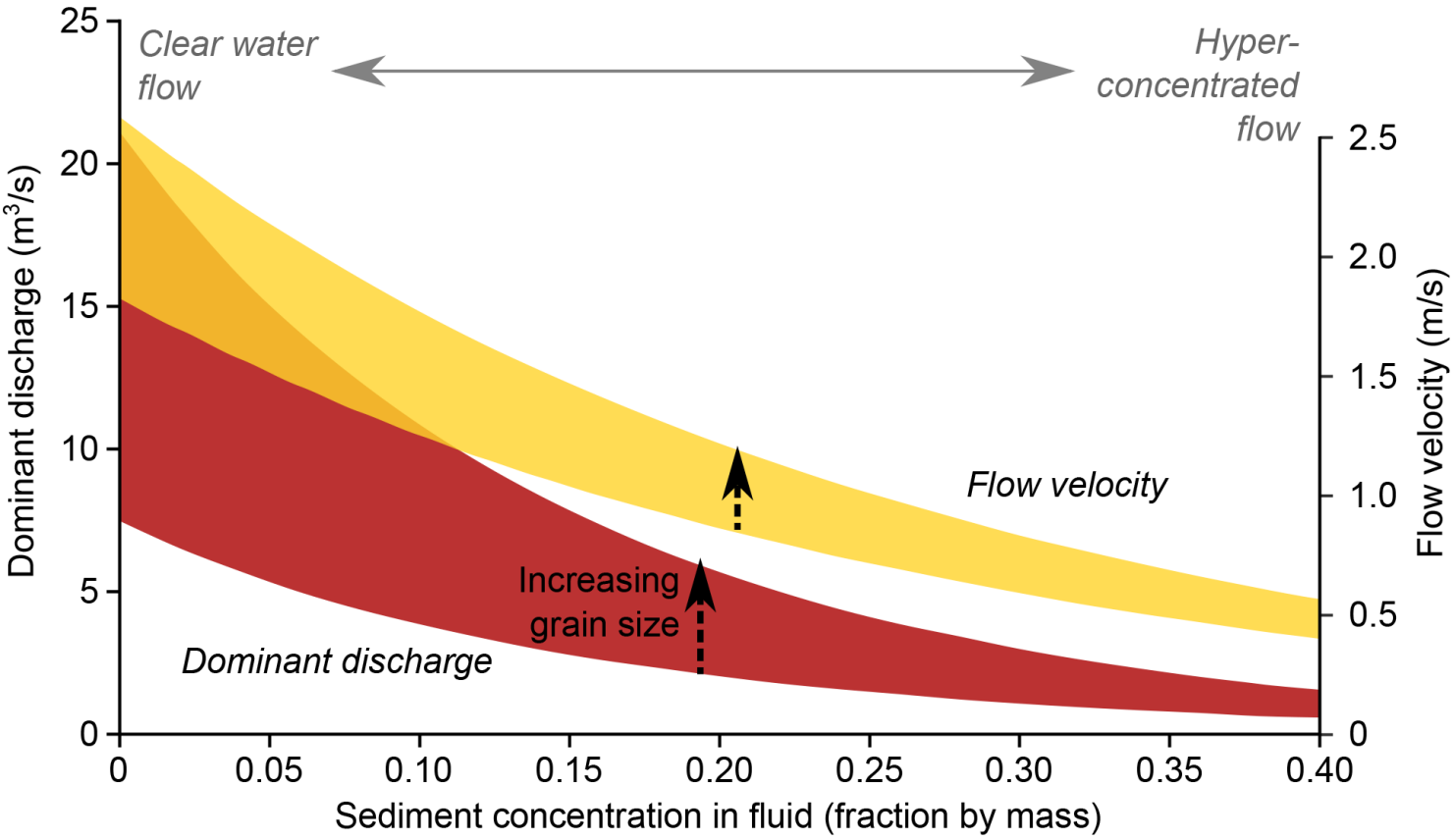
Clear water flow
Hyper-concentrated flow
Flow velocity
Increasing grain size
Dominant discharge
Dominant discharge (m³/s)
Flow velocity (m/s)
Sediment concentration in fluid (fraction by mass)
0
5
10
15
20
25
0
0.5
1.0
1.5
2.0
2.5
0
0.05
0.10
0.15
0.20
0.25
0.30
0.35
0.40

Fig. 31